中国科学院上海营养与健康研究所
SHANGHAI INSTITUTE OF NUTRITION AND HEALTH, CAS

代谢实验技术

翟 琦 巍

Shanghai Institute of Nutrition and Health
Chinese Academy of Science

目 录

代谢研究模型

动物模型

细胞模型

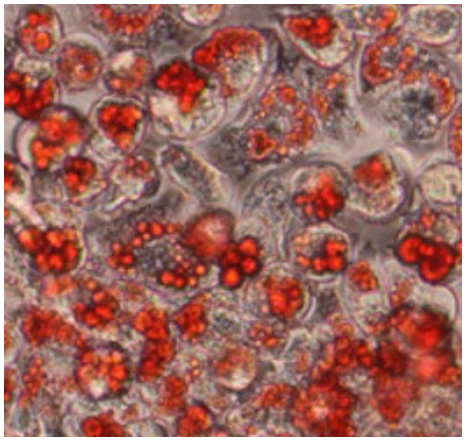

代谢研究动物模型

- **喂养模型**（不同饮食模型）
- **人工干预模型**（药物处理、手术等模型）
- **遗传模型**（自发模型与人为构建模型）
- **表观遗传模型**（获得性代谢性状的代际传递）

喂养模型

- **以正常实验动物，遗传或人为干预模型为研究对象，通过特殊饮食喂养使其发生代谢异常。**
- **常见的饮食模型：**
- ✓ **营养组分限制饮食**(高/低脂、(果)糖、蛋白等饮食、卡路里限制饮食、特定营养素缺乏饮食)
- ✓ **时间限制饮食**(限时饮食、隔天限制饮食等间歇性节食、限时特定营养素过量或缺乏)

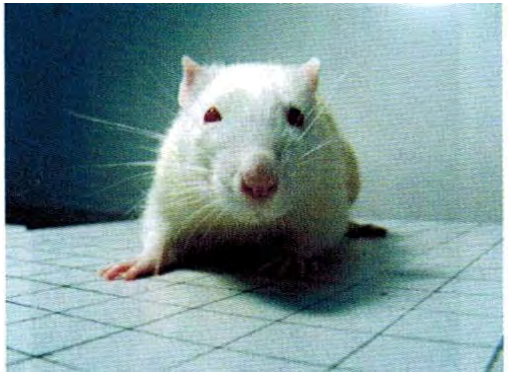

正常和高脂饮食组分

蛋白一般保持不变

脂肪含量高

➢ 正常和高脂小鼠饮食成分对比

Caloric Information Physiological Fuel Values	D12450K	D12492
Protein:	**20** % Kcal	**20** % Kcal
Fat:	**10** % Kcal	**60** % Kcal
Carbohydrate:	**70** % Kcal	**20** % Kcal
Energy density:	**3.82** Kcal/g	**5.21** Kcal/g

Formulation D12450K

Class description	Ingredients	Grams
Protein	Casein, Lactic, 30 Mesh	200.00 g
Protein	Cystine, L	3.00 g
Carbohydrate	Starch, Corn	550.00 g
Carbohydrate	Lodex 10	150.00 g
Carbohydrate	Sucrose, Fine Granulated	4.00 g
Fiber	Solka Floc, FCC200	50.00 g
Fat	Soybean Oil, USP	25.00 g
Fat	Lard	20.00 g
Mineral	S10026B	50.00 g
Vitamin	Choline Bitartrate	2.00 g
Vitamin	V10001C	1.00 g
Dye	Dye, Blue FD&C #1, Alum. Lake 35-42%	0.03 g
Dye	Dye, Red FD&C #40, Alum. Lake 35-42%	0.03 g
	Total:	1055.05 g

Formulation D12492

Class description	Ingredients	Grams
Protein	Casein, Lactic, 30 Mesh	200.00 g
Protein	Cystine, L	3.00 g
Carbohydrate	Lodex 10	125.00 g
Carbohydrate	Sucrose, Fine Granulated	72.80 g
Fiber	Solka Floc, FCC200	50.00 g
Fat	Lard	245.00 g
Fat	Soybean Oil, USP	25.00 g
Mineral	S10026B	50.00 g
Vitamin	Choline Bitartrate	2.00 g
Vitamin	V10001C	1.00 g
Dye	Dye, Blue FD&C #1, Alum. Lake 35-42%	0.05 g
	Total:	773.85 g

researchdiets.com

高脂饮食的代谢表型

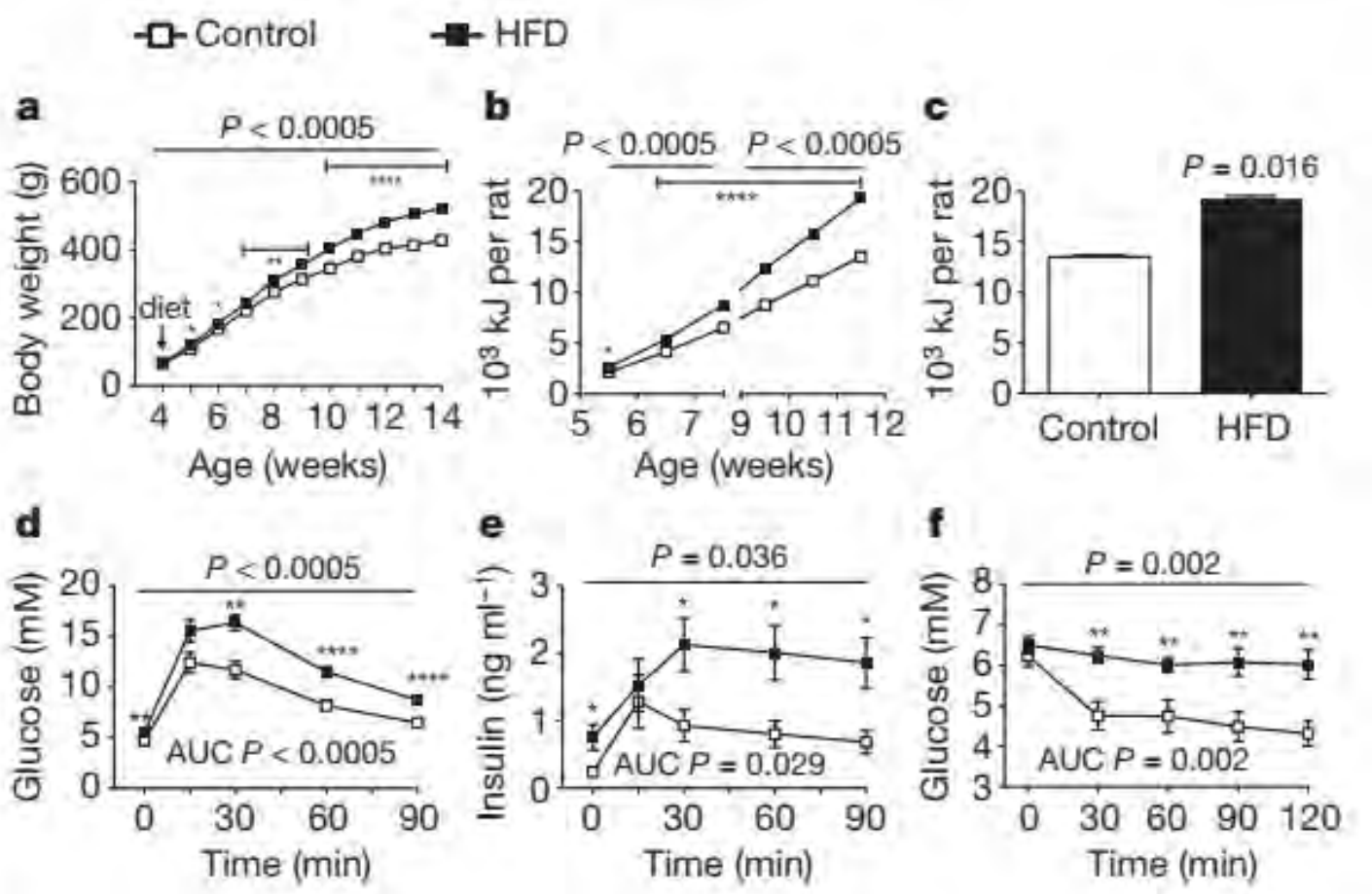

60%高脂饮食小鼠出现胰岛素抵抗和葡萄糖耐受。

Nature. 2010 ;**467**(7318):963-6.

60%高蛋白饮食组分

特定饮食有时候才能诱导产生特定的表型

TABLE 1 Diet formulations and macronutrient composition

	NPC	HPC	HPS	HPM	Chow
Ingredients (g/1000 g)					
Cornstarch[a]	396	174	183	157	
Casein (87% protein)[b]	174	395	-	-	
Soy protein (87% protein)[b]	-	-	406	100	
Wheat gluten (76% protein)[b]	-	-	-	115	
Complete milk protein (89% protein)[b]	-	-	-	100	
Egg white (82% protein)[b]	-	-	-	106	
Dextrinized cornstarch	132	132	132	132	
Sucrose	100	100	100	100	
Soybean oil with TBHQ[c]	98	96	82	93	
Cellulose	50	50	50	50	
AIN-93M mineral mix	35	35	35	35	
AIN-93VX vitamin mix	10	10	10	10	
L-cystine	3	6	-	-	
Choline bitartarate	3	3	3	3	
Macronutrient composition					
Protein (% energy)	15	35	35	35	20
Carbohydrate (% energy)	64	44	44	44	70
Fat (% energy)	21	21	21	21	10

Abbreviations: NPC = normal protein casein; HPC = high protein casein; HPM = high protein mixed; HPS = high protein soy; TBHQ = *tert*-Butylhydroquinone.

Obesity. 2016, **24**, 123-131.

高蛋白饮食的代谢表型

注意高蛋白也会变瘦

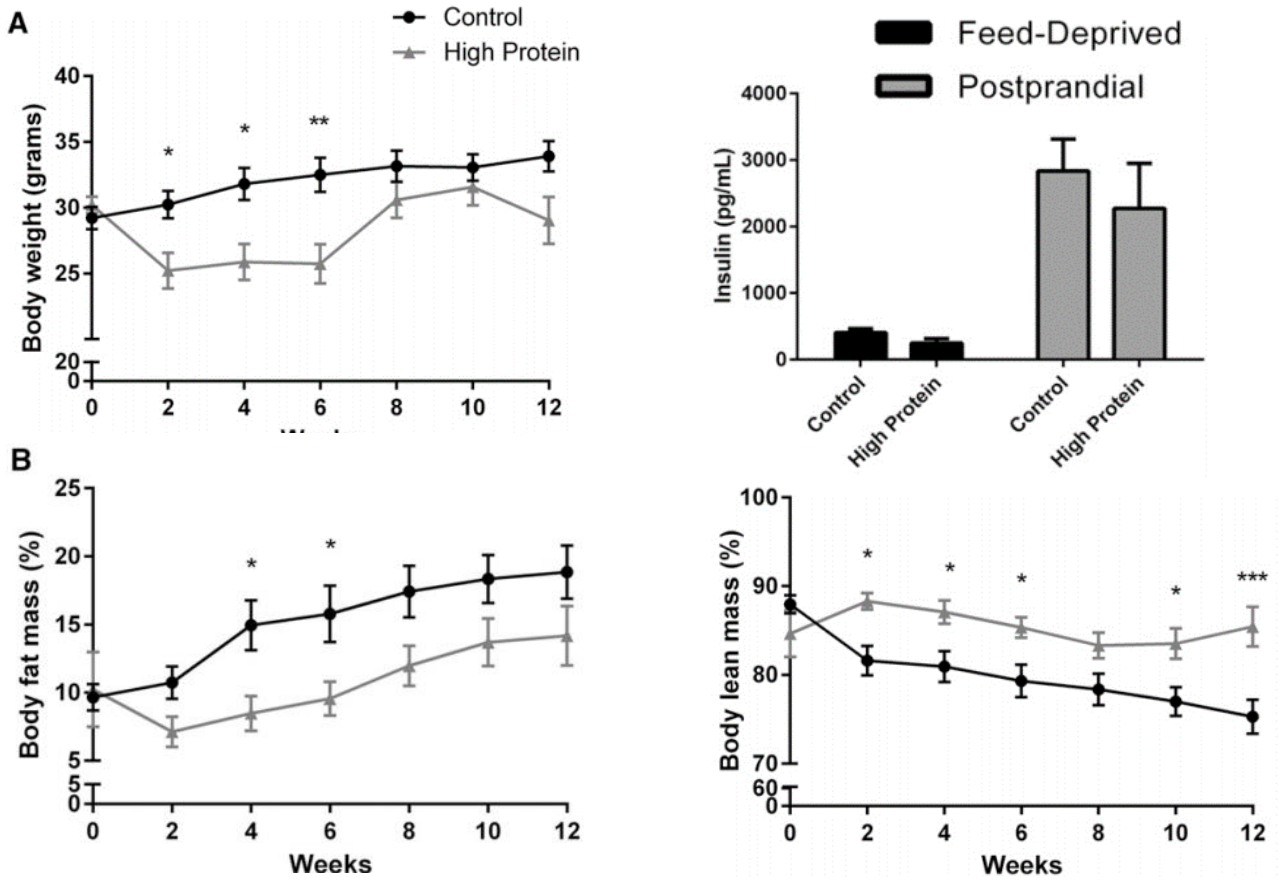

60%高蛋白膳食下C57小鼠体重和体脂显著降低。

J Nutr. 2017;**147**(12):2243-2251.

10%低蛋白饮食组分

Ingredient	Control	Low Protein
Cornstarch	39.75% (w/w)	39.75%
Casein	20%	10.90%
Maltodextrin	13.20%	13.20%
Sucrose	10%	19.10%
Soybean Oil	7%	7%
Cellulose	5%	5%
Mineral Mix	3.50%	3.50%
Vitamin Mix	1%	1%
L-Cystine	0.30%	0.30%
Choline Bitartrate	0.25%	0.25%
Tert-butyl hydroquinone	0.00%	0.00%

Cell. 2010, **143**, 1084–1096.

低蛋白饮食代谢表型

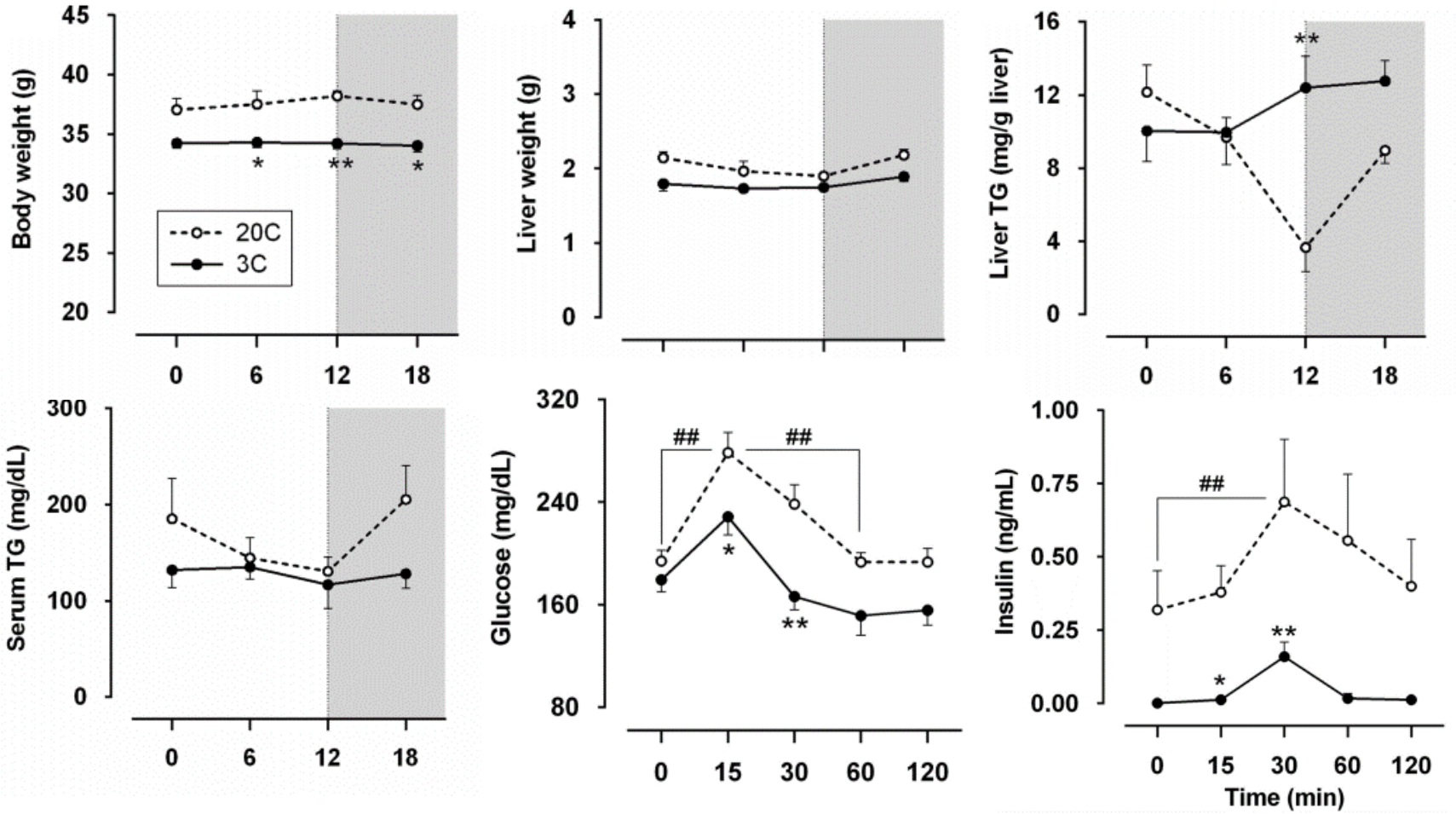

低蛋白饮食(3C)体重、肝脏重量降低，出现胰岛素抵抗。

Nutr Biochem. 2019 ;**63**:177-185.

特定营养素缺乏饮食

- **特定氨基酸缺乏饮食**（例如Leu缺乏饮食等）

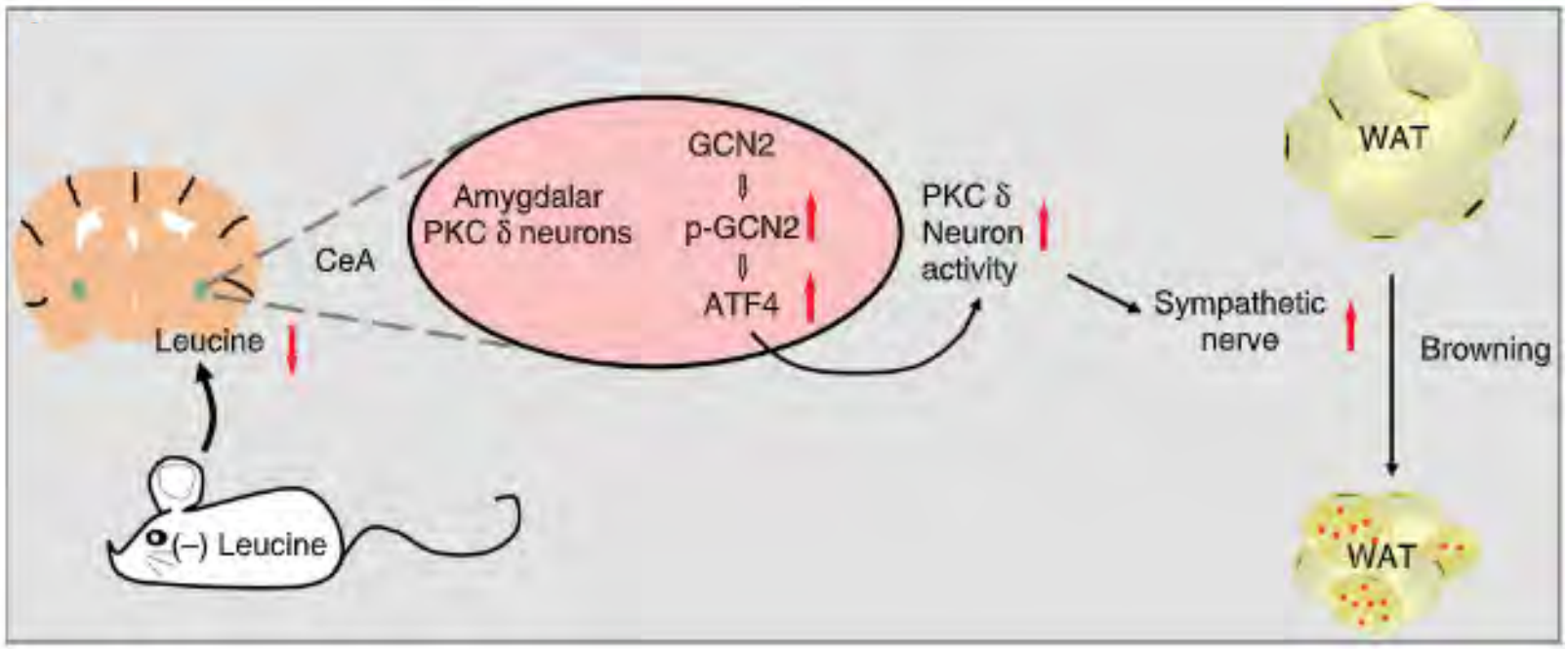

氨基酸在信号转导和代谢调控中起关键作用。
特定氨基酸缺乏对糖脂代谢有重要调控作用。

Nat Commun. 2020 ;**11**(1):2847.

时间限制饮食

➢ 每日限时饮食

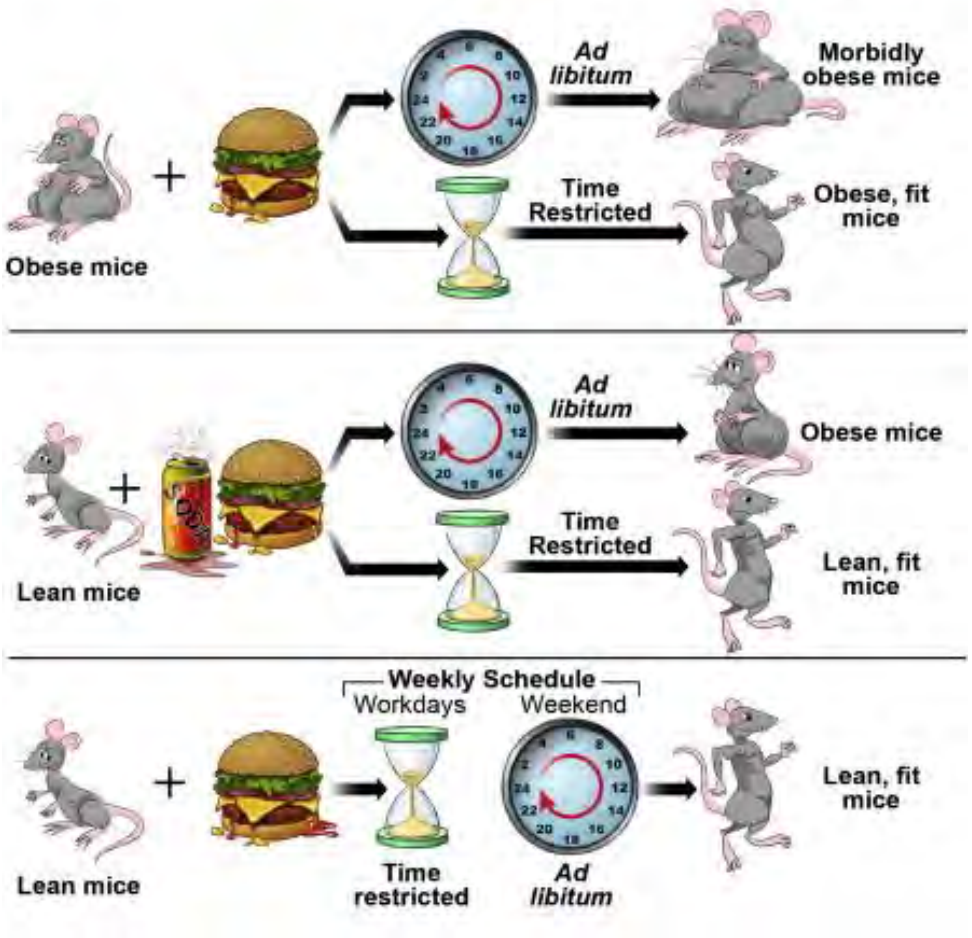

Time-restricted feeding (TRF) confines food access to 9–12 hr during the active phase.

TRF is effective against high-fat, high-fructose, and high-sucrose diets

Cell Metab. 2014, **20**, 991-1005.

时间限制饮食

➢ 每日限时饮食

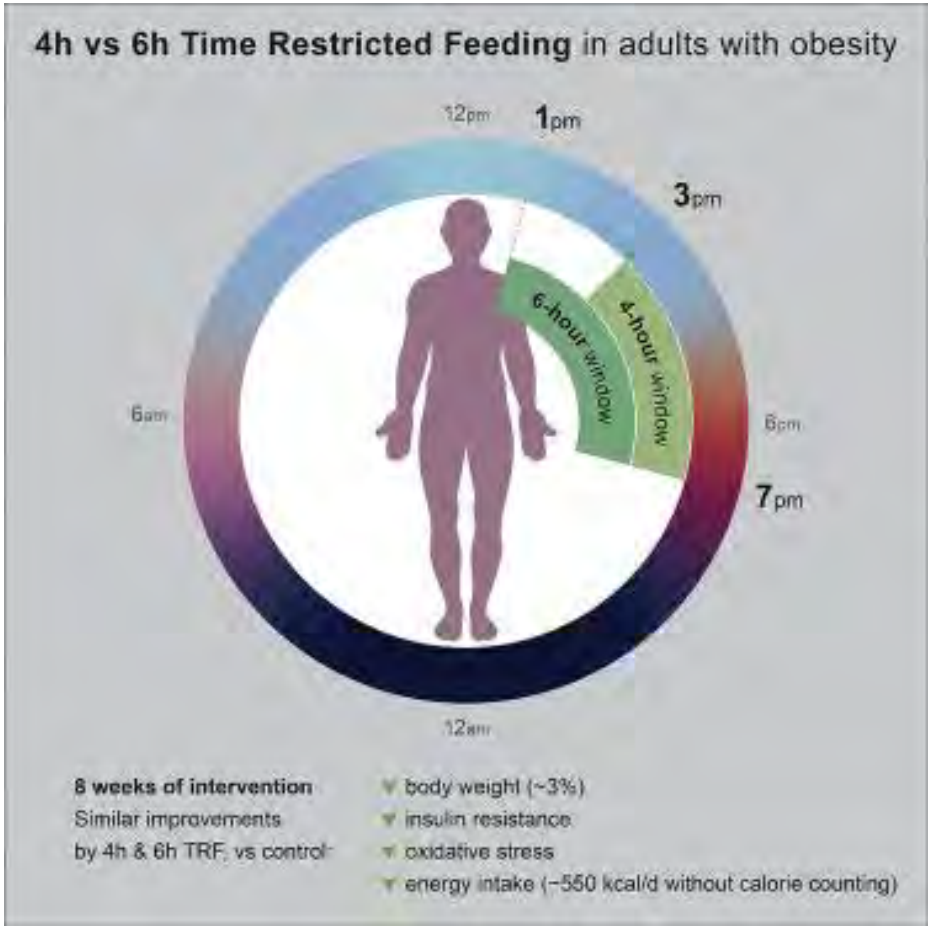

4- and 6-h time-restricted feeding regimens were tested in adults with obesity

Both regimens produce similar weight loss over the 2 months of the study

Both regimens reduce energy intake by ~550 kcal per day without calorie counting

Cell Metab. 2020, **32**, 366-378.

时间限制饮食

- 隔天禁食(Every-Other-Diet-Feeding)

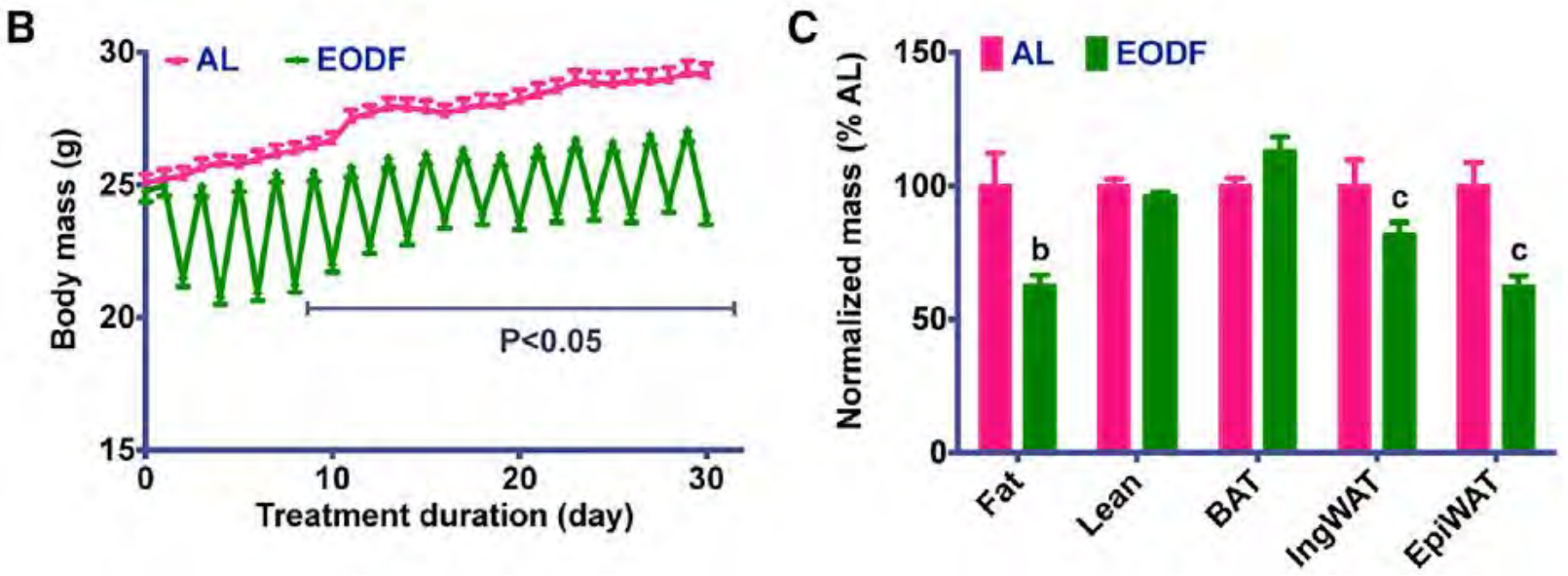

(**B**) Body weight. AL, ad libitum; EODF every-other-day fasting; (**C**) Normalized mass of body depots.

EODF可逆转高脂饮食引起的肥胖症和相关的代谢异常。

Cell Metab. 2017, **26**, 672–685.

时间限制饮食

- 隔天禁食(Every-Other-Diet-Feeding)

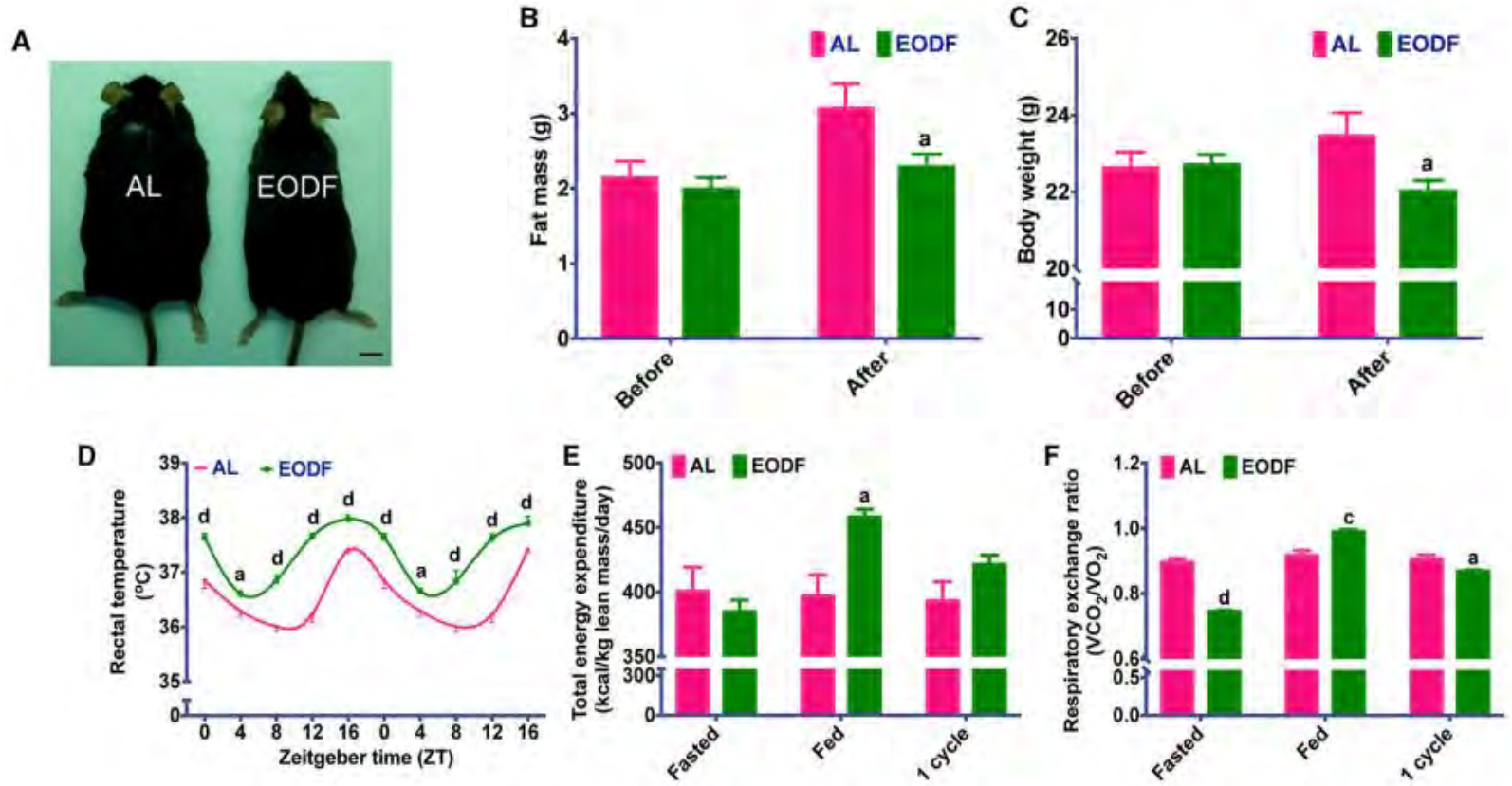

EODF可逆转高脂饮食引起的肥胖症和相关的代谢异常。

Cell Metab. 2017, **26**, 672–685.

代谢研究动物模型

- **喂养模型**（不同饮食模型）
- **人工干预模型**（药物处理、手术等模型）
- **遗传模型**（自发模型与人为构建模型）
- **表观遗传模型**（获得性代谢性状的代际传递）

人工干预模型

- **链脲佐菌素(Streptomycin, STZ)注射诱导1型糖尿病模型**
- ✓ STZ破坏胰岛β细胞，诱导形成1型糖尿病模型。可以和高脂饮食等组合诱导糖尿病模型。

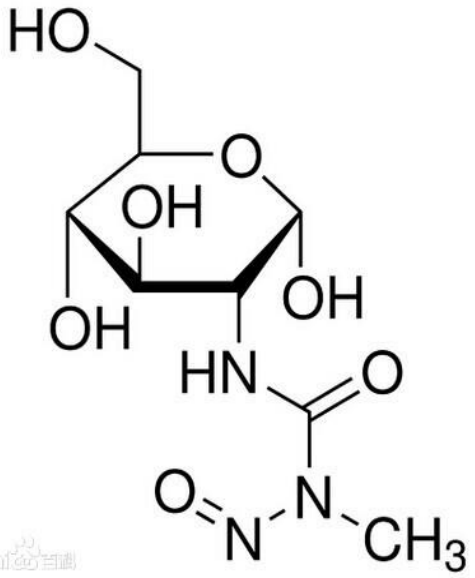

STZ诱发小鼠产生I型糖尿病

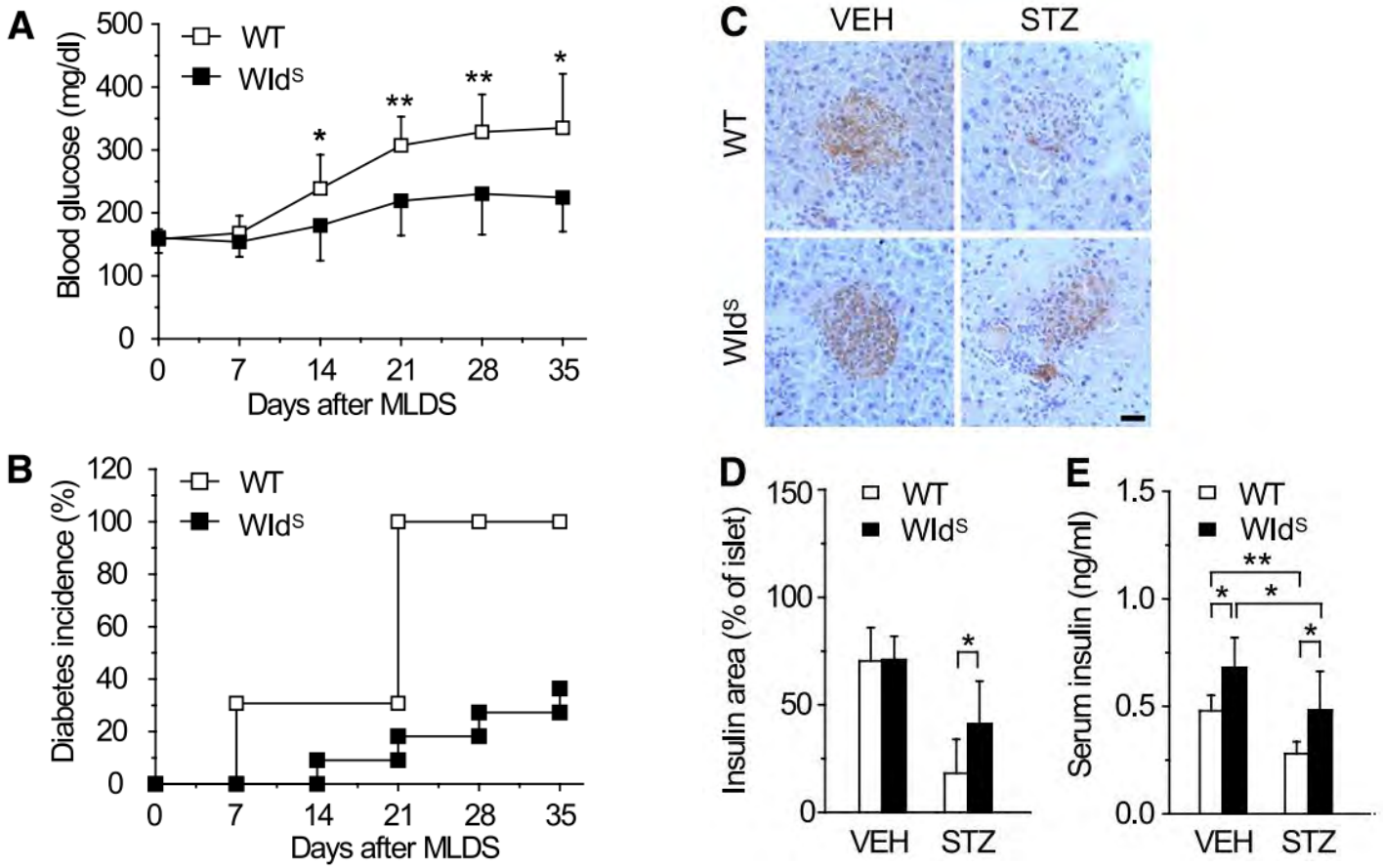

注射STZ后血糖升高、胰岛细胞和血清胰岛素显著减少。

Diabetes. 2011; **60**:3197-207.

代谢研究动物模型

- **喂养模型**（不同饮食模型）
- **人工干预模型**（药物处理、手术等模型）
- **遗传模型**（自发模型与人为构建模型）
- **表观遗传模型**（获得性代谢性状的代际传递）

遗传模型

- **自发基因突变模型**（ob/ob小鼠、db/db小鼠、肥胖Zuker大鼠、Wistar-Kyoto肥胖大鼠等）
- **人工遗传操作模型**（例如全身或组织特异性或诱导性的基因敲除、转基因、基因编辑等）

ob/ob自发突变小鼠

- Leptin基因纯合突变小鼠(ob/ob小鼠)

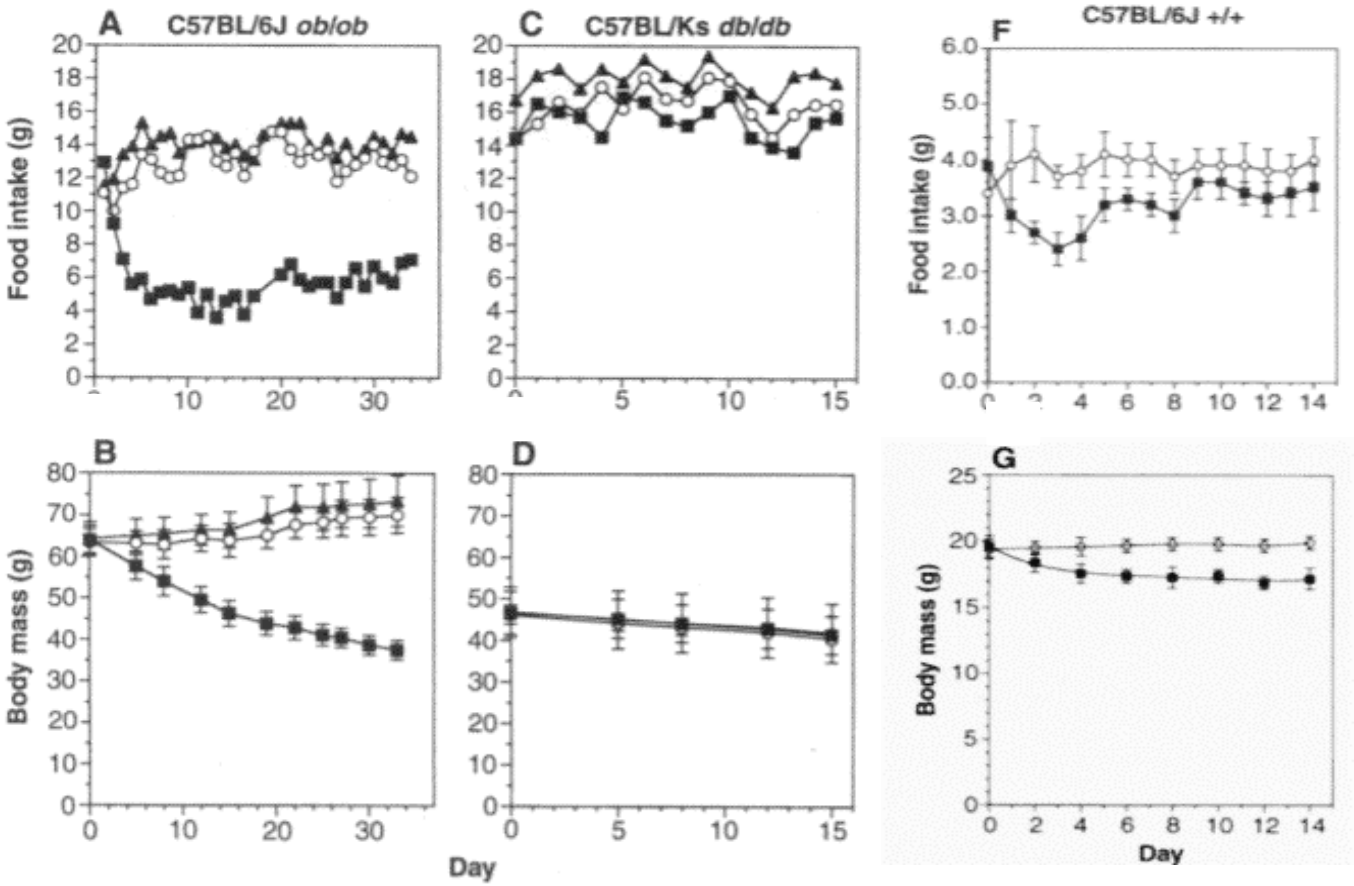

特征：肥胖、多食、高血糖和胰岛素抵抗。

Science. 1995; **269**:543-6.

db/db自发突变小鼠

➢ Leptin受体基因纯合突变小鼠(db/db小鼠)

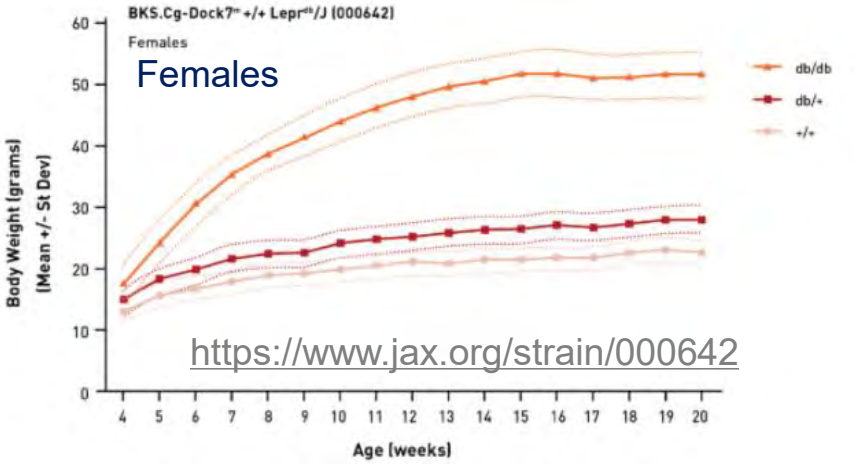

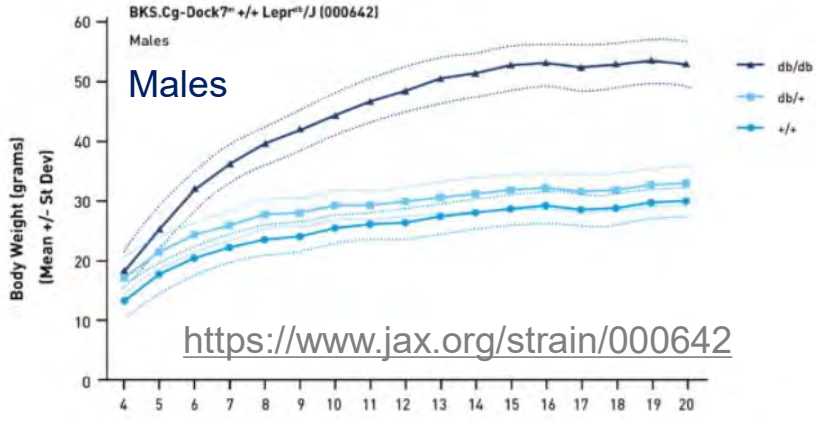

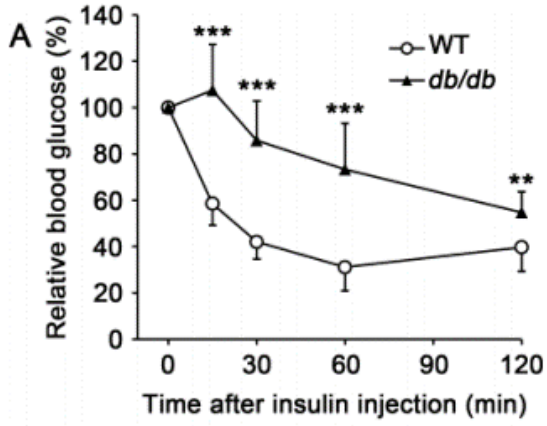

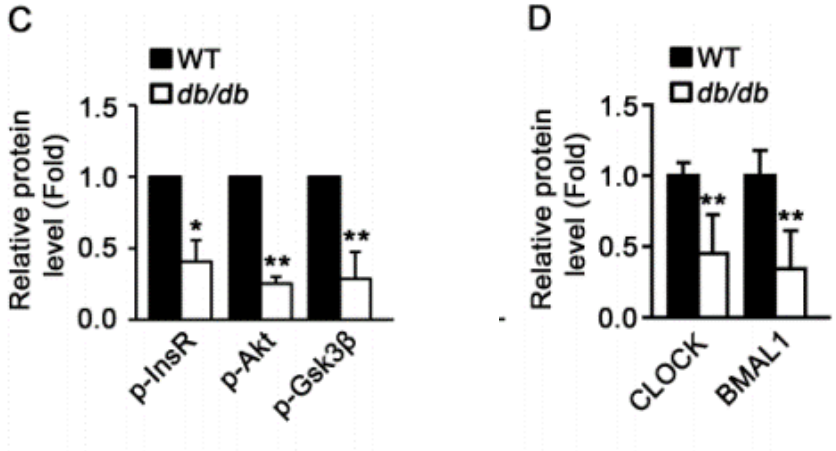

特征：小鼠肥胖且存在葡萄糖不耐受、胰岛素抵抗的现象

代谢研究动物模型

- **喂养模型**（不同饮食模型）
- **人工干预模型**（药物处理、手术等模型）
- **遗传模型**（自发模型与人为构建模型）
- **表观遗传模型**（获得性代谢性状的代际传递）

表观遗传代谢模型

- 代谢记忆、获得性性状代际传递

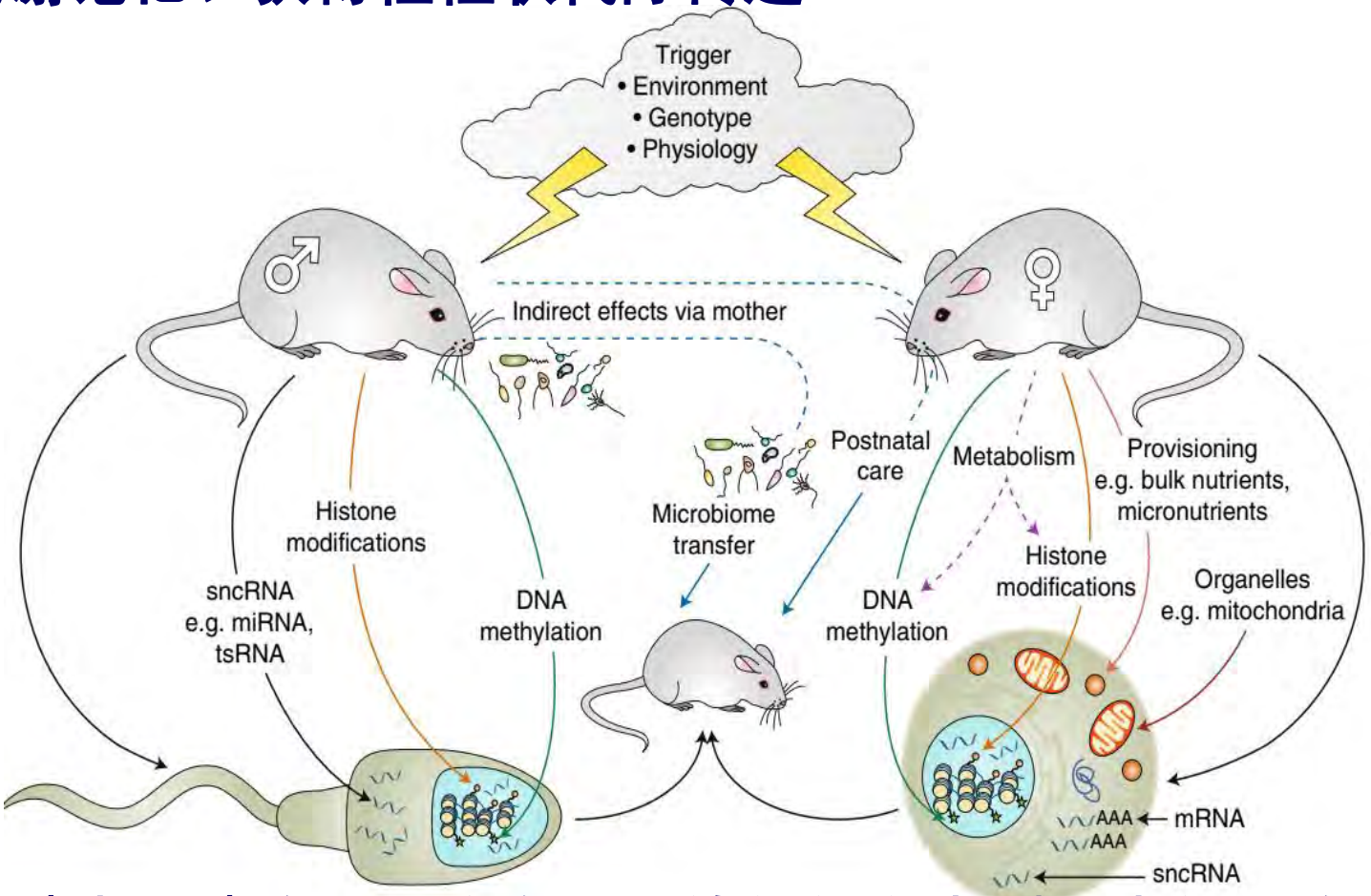

多种表观遗传因素均有可能使得代谢表型发生代际传递。

Nature Cell Biology. 2019. **56.** 135-156.

高脂饮食导致的表型代际传递

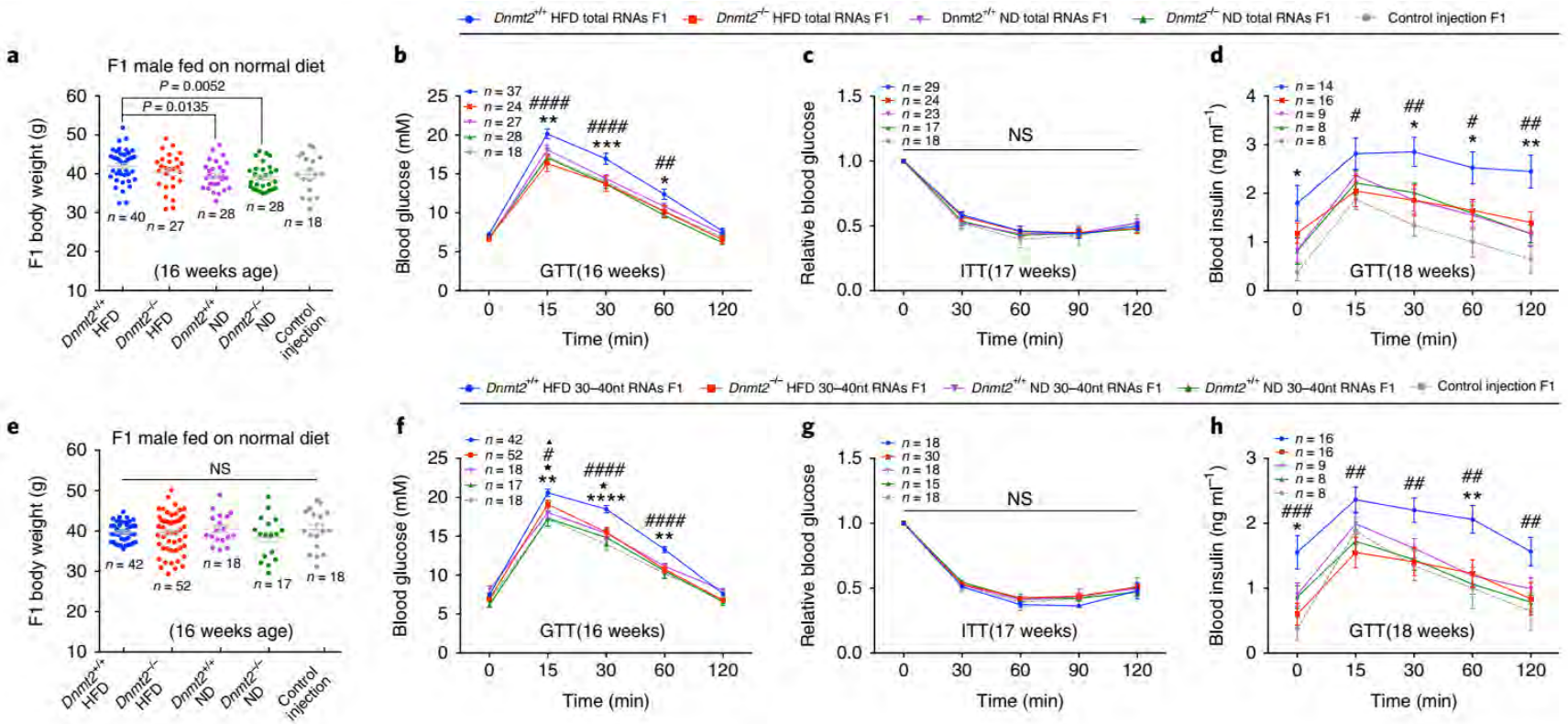

高脂饮食小鼠下的代谢异常表型可通过精子发生代际传递。

Nat Cell Biol. 2018 ;**20**(5):535-540.

低蛋白饮食与表型代际传递

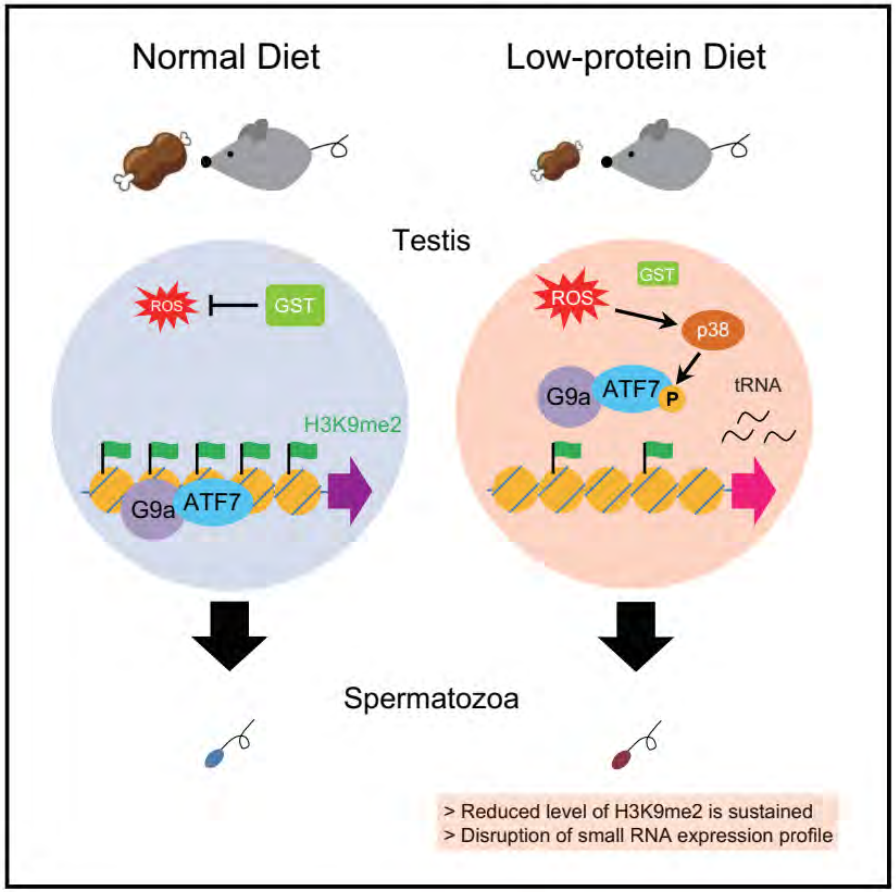

ATF7-Dependent Epigenetic Changes Are Required for the Intergenerational Effect of a Paternal Low-Protein Diet

Molecular Cell. 2020; **78**:1–14.

代谢研究模型

动物模型

细胞模型

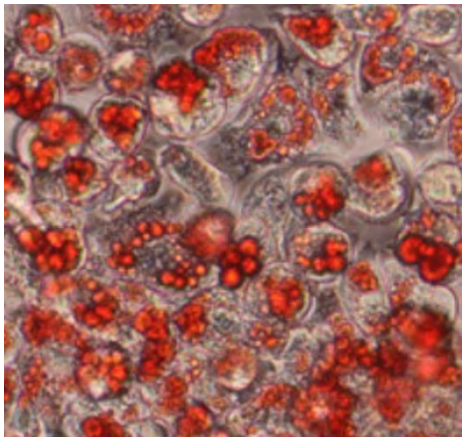

脂肪细胞模型

➢ 3T3-L1分化形成的脂肪细胞模型

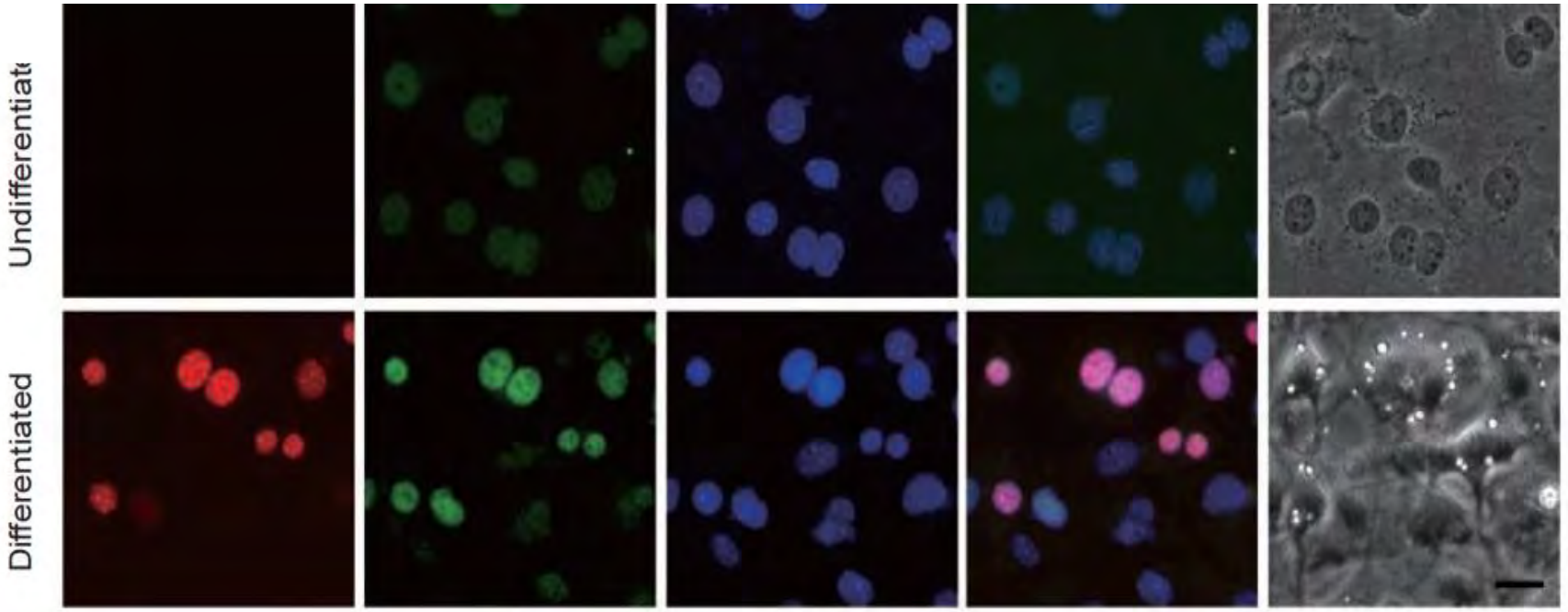

To differentiate 3T3-L1 cells：the cells were allowed to grow for 2 days, and then exposed to fresh differentiation medium containing DMEM, 10% FBS, 1 μM dexamethasone, 0.5mM 3-isobutyl-1 methylxanthine, 10 μM troglitazone and 1 μg/ml insulin. After 2 days, the cells were refed with fresh DMEM containing 10% FBS, 10 mM troglitazone and 1 μg/ml of insulin for another 2 days. Then, the cells were cultured in DMEM with 10% FBS.

Cell Research 2010; 20:470-9.

肌肉细胞模型

➢ C2C12分化形成的肌肉细胞模型

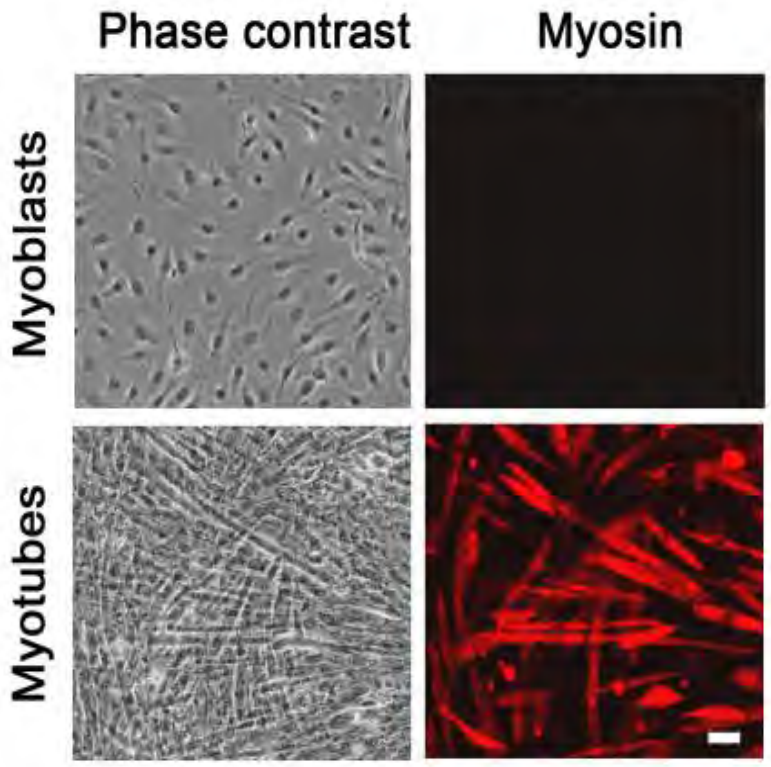

Mouse myoblast cell line C2C12 was maintained in DMEM containing 10% fetal bovine serum and differentiated in DMEM supplemented with 2% horse serum after growing to 60%–80% confluent.

C2C12成肌细胞分化成C2C12肌细胞前后的细胞形态
及肌管标志蛋白Myosin的表达情况

肝细胞模型

➢ 小鼠原代肝细胞

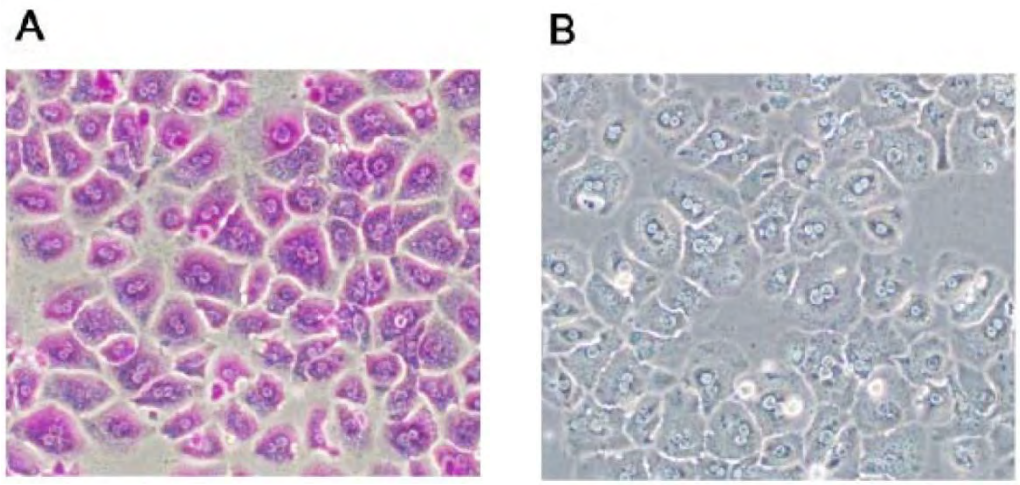

The puritity and viability of isolated primary hepatocytes. *A*: The purity of isolated primary hepatocytes was verified by PAS staining to stain glycogen. *B*. The viability of isolated primary hepatocytes was verified by trypan blue staining.

1. Liver was perfused with Krebs-Ringer buffer with glucose (120 mM NaCl, 4.8 mM KCl, 1.2 mM MgSO4, 1.2 Mm KH2PO4, 24 mMNaHCO3, 20 mM glucose, and 5 mM HEPES, pH 7.45) containing 100 EGTA.
2. Then Krebs-Ringer buffer with glucose containing 5 mM CaCl2,1.2% BSA and 140 U/mL Type I collagenase.
3. Livers were removed and cut into small pieces,gently agitated in DMEM containing 25 mM glucose to release the hepatocytes, and then filtered through a 70 m cell strainer.
4. Then resuspended in about 4 mL DMEM containing 25 mM glucose and mixed with an equal volume of 90% percoll in PBS followed by centrifugation at 50 g for 10 min at4 C.
5. Then the cells were seeded in 12-well plates precoated overnight with 20 g/Ml Collagen Type I.

胰岛β细胞模型

- 小鼠原代胰岛细胞分离培养，Min6、Ins-1细胞系

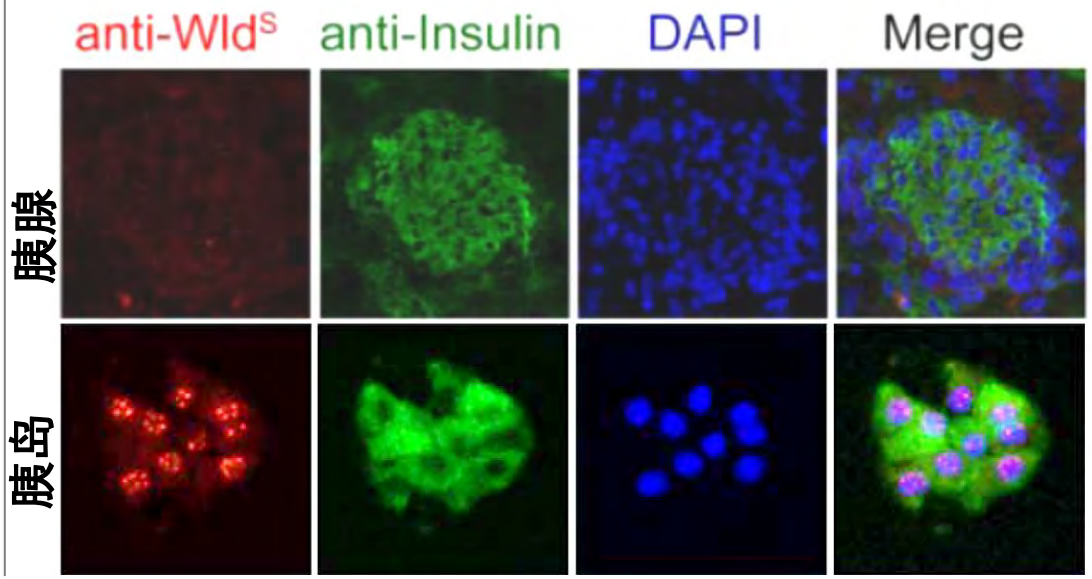

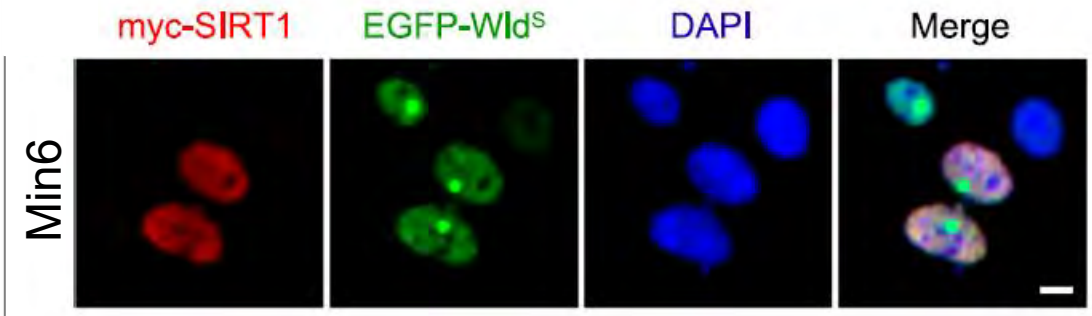

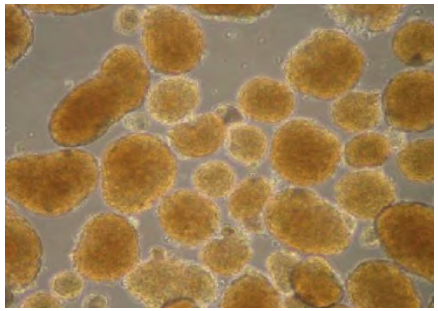

小鼠胰腺用胶原酶P消化：

1. 从小鼠的胆总管处灌入含有1mg/ml 胶原酶P 的分离液(10x HBSS, 10 mM HEPES, 1 mM MgCl2, 5 mM Glucose, pH 7.4) 38℃消化11-15分钟。
2. 用HBSS洗数次，然后通过一个70μm细胞筛，过滤掉杂细胞。细胞筛上面的就是胰岛。
3. 冲洗和重悬胰岛于1640完全培养液中。

Diabetes. 2011; **60**:3197-207.

目 录

活体代谢表型分析

- 体重、摄食和饮水(不同时间段摄食和饮水)、体脂含量(Fat mass)、瘦体重(Lean mass)

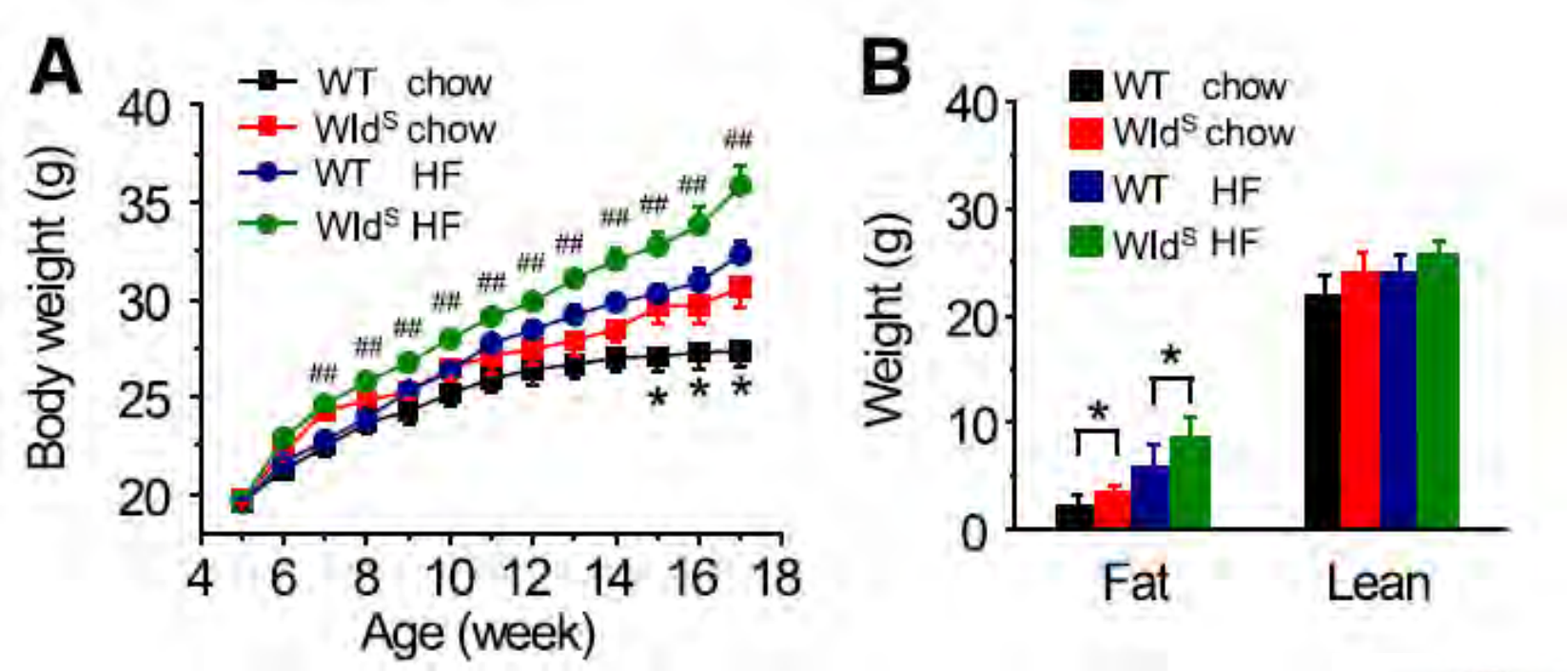

Diabetes 60:3197–3207, 2011

活体代谢表型分析

➢ 核磁共振(NMR)检测fat mass和lean mass

小鼠放置在此Holder进行检测

核磁共振活体组织分析仪
Whole body composition analyzer (EchoMRI)

EchoMRI-100体成分分析仪能够对100g重量以下的活体小动物提供脂肪、瘦体重、游离水和总水量的精确测量。
根据精度选项，扫描时间约0.5-3.2分钟。
活体动物在测量之前不需要麻醉和特殊的准备。

NMR检测原理

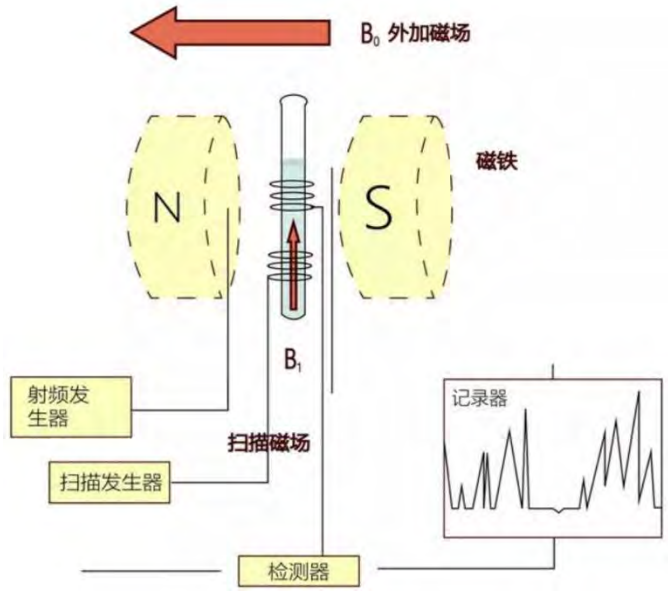

核磁共振谱仪工作原理
核磁共振谱来源于原子核能级间的跃迁。只有置于强磁场中的某些原子核才会发生能级分裂，当吸收的辐射能量与核能级差相等时，就发生能级跃迁而产生核磁共振信号。
用一定频率的电磁波对样品进行照射，可使特定化学结构环境中的原子核实现共振跃迁，在照射扫描中记录发生共振时的信号位置和强度，就得到核磁共振谱。核磁共振谱上的共振信号位置反映样品分子的局部结构（如官能团，分子构象等），信号强度则往往与有关原子核在样品中存在的量有关。

活体代谢表型分析

➢ 微型CT (microCT)

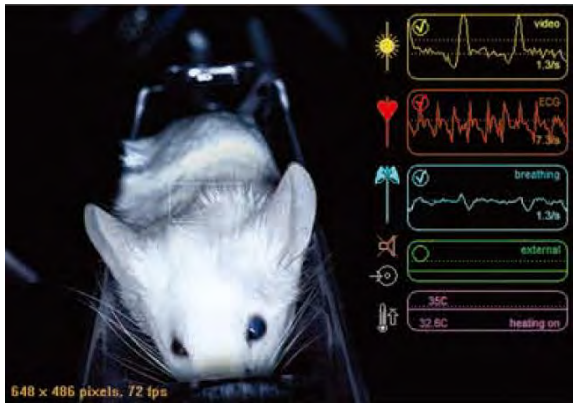

microCT检测原理

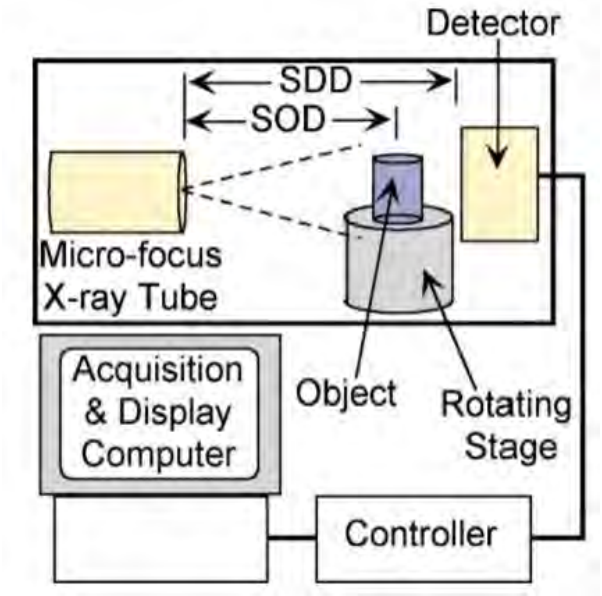

Schematic diagram of the micro-CT scanner

Micro-CT成像原理是采用微焦点X射线球管对小动物各个部位的层面进行扫描投射，由探测器接受透过该层面的X射线，转变为可见光后，由光电转换器转变为电信号，再经模拟/数字转换器转为数字信号，输入计算机进行成像。

Med Phys. 2003; 30(11):2869-77.

活体代谢表型分析

- **微型CT (microCT)**

  使用micro-CT检测小鼠脂肪分布与对应体积

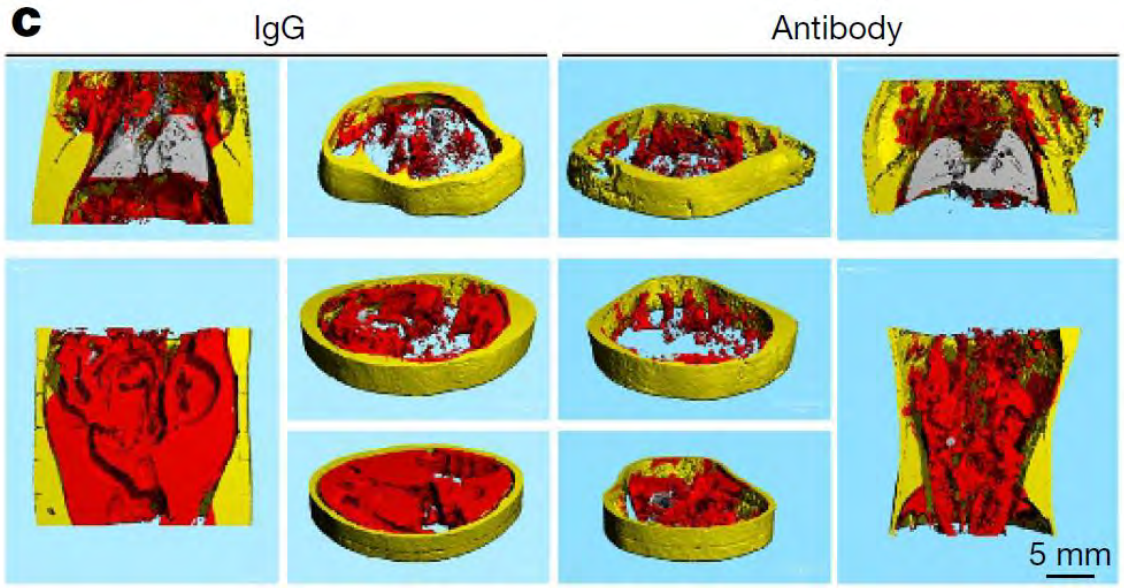

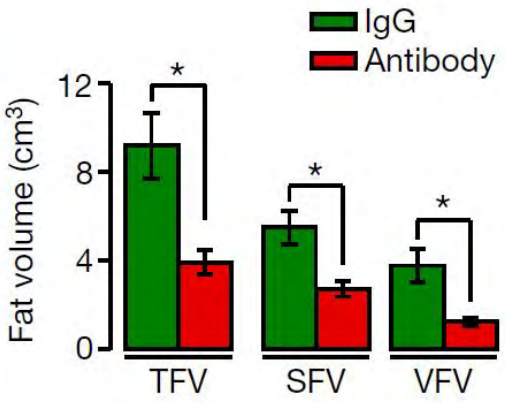

Fsh antibody reduces obesity in mice on a high-fat diet. c, TFV, SFV and VFV measured by micro-CT (representative coronal and transverse sections from the same experiment; visceral, red; subcutaneous, yellow). TFV, total fat volume; SFV, subcutaneous fat volume; VFV, visceral fat volume.

Nature. 2017 Jun 1;546(7656):107-112.

活体代谢表型分析

- **PET/CT和SPECT/CT**

  [^{18}F]Fluorodeoxyglucose-PET/CT (^{18}F-FDG-PET/CT)

  [$^{123/125}$I]-β-methyl-p-iodophenyl-pentadecanoic acid-SPECT/CT

  检测同位素的三维分布

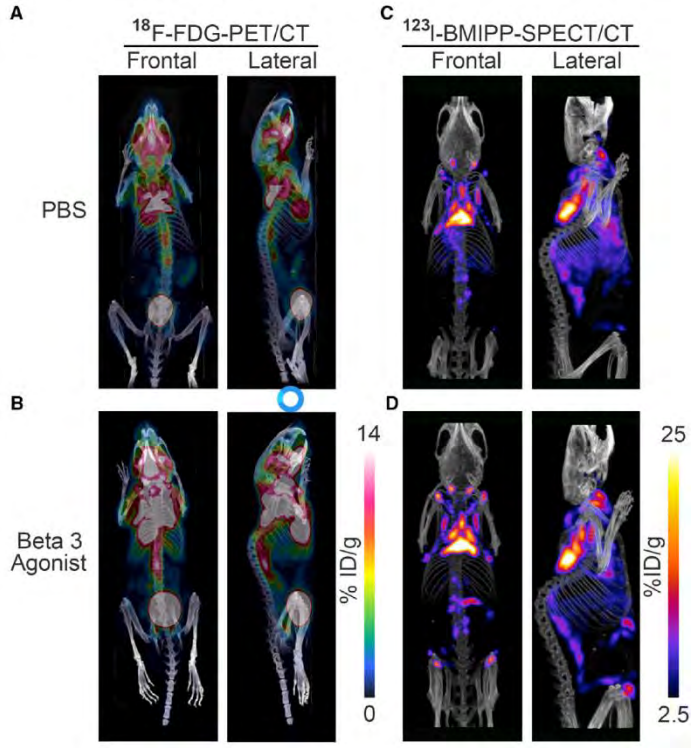

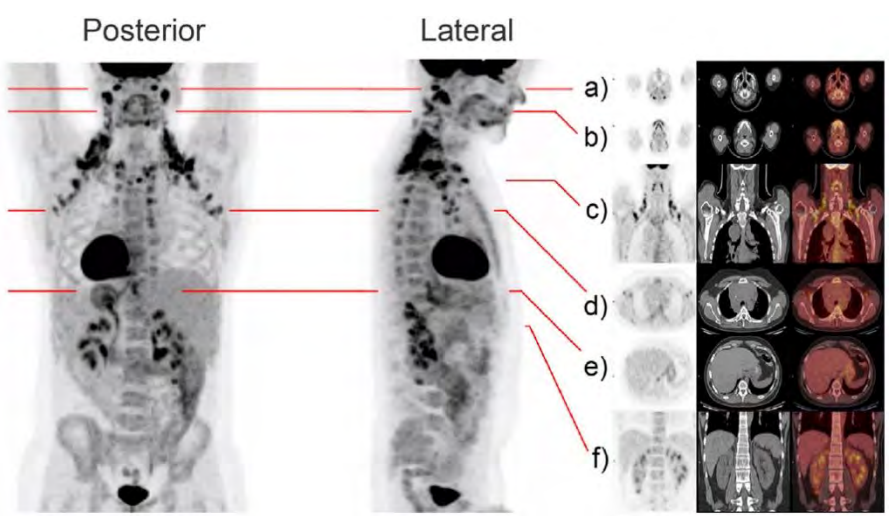

PET/CT: positron emission tomography-computed tomography. **SPECT/CT:** single-photon-emission computed tomography-computed tomography.

Cell Metab. 2018; 27:252-262.

活体代谢表型分析

- 体温检测(微型温度计直接测定、红外成像)

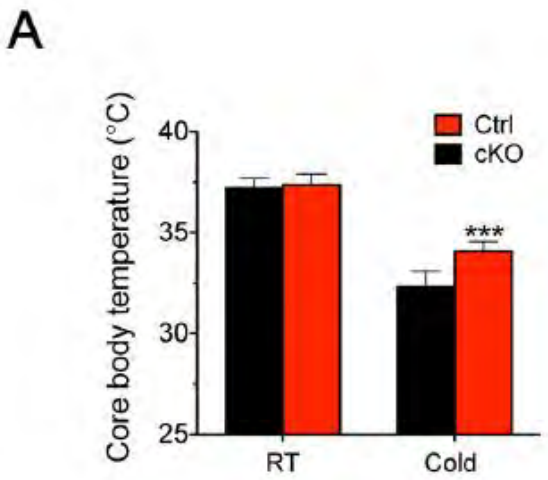

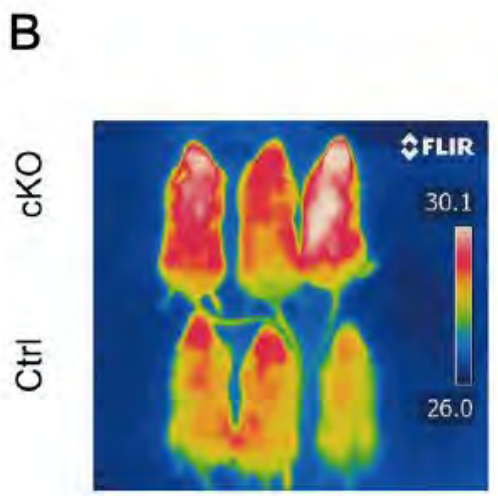

PLOS Biology | https://doi.org/10.1371/journal.pbio.2006571

活体代谢表型分析

- 血糖、血液胰岛素水平
- 胰岛素耐受性测试(Insulin tolerance test)
- 糖耐量测试(Glucose tolerance test)、丙酮酸耐量测试

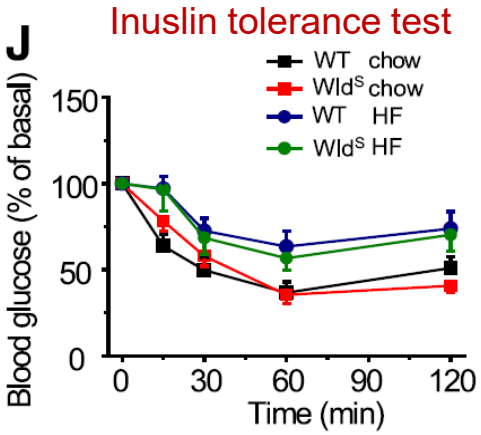

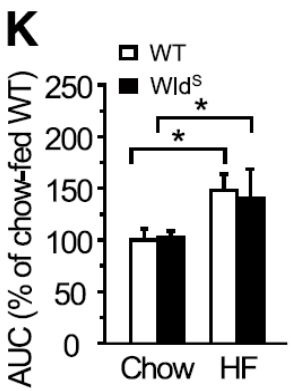

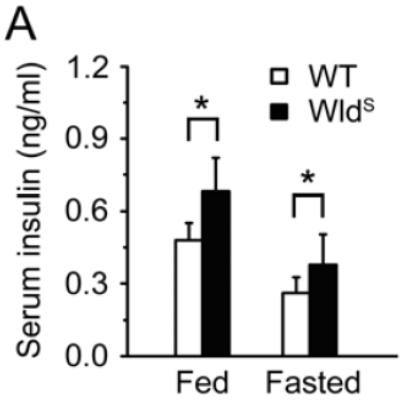

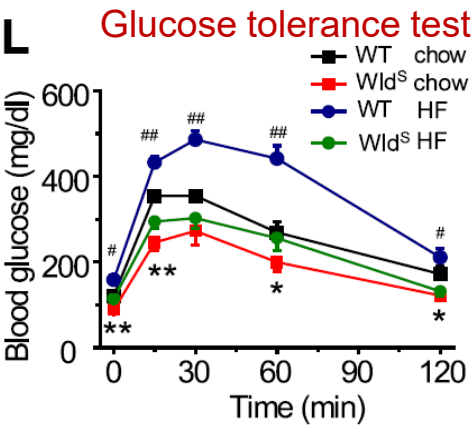

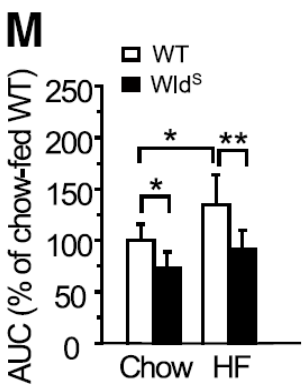

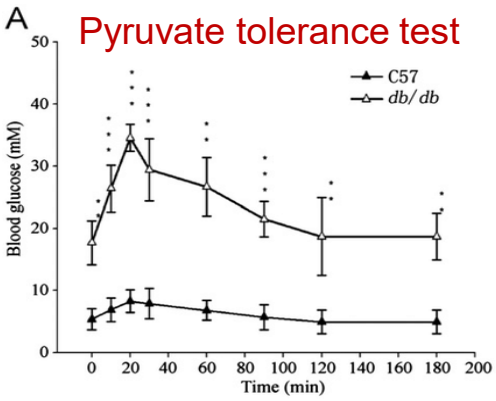

Diabetes. 2011; **60**:3197-207.

活体代谢表型分析

➢ 血糖钳夹术检测胰岛素敏感性

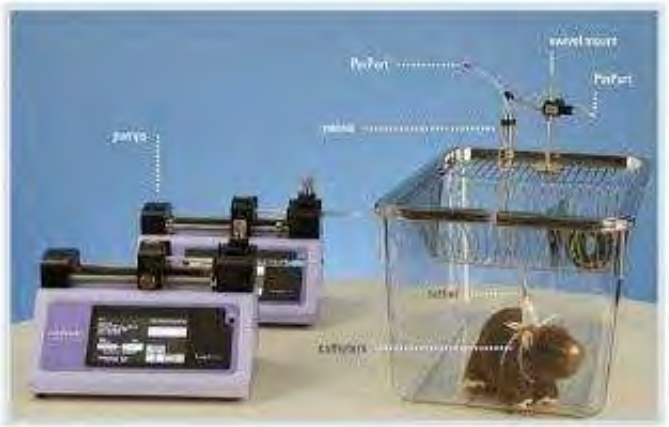

血糖钳夹术：即输注胰岛素使之达到一种特定的循环浓度，通常为100μU/ml。在血浆胰岛素浓度接近100μU/ml，维持正常血糖所需的外源葡萄糖不足150mg/(m2·min) 时，则为胰岛素抵抗。

被很多人认为是检测胰岛素敏感性的“金指标”

活体代谢表型分析

- 血糖钳夹术检测胰岛素敏感性

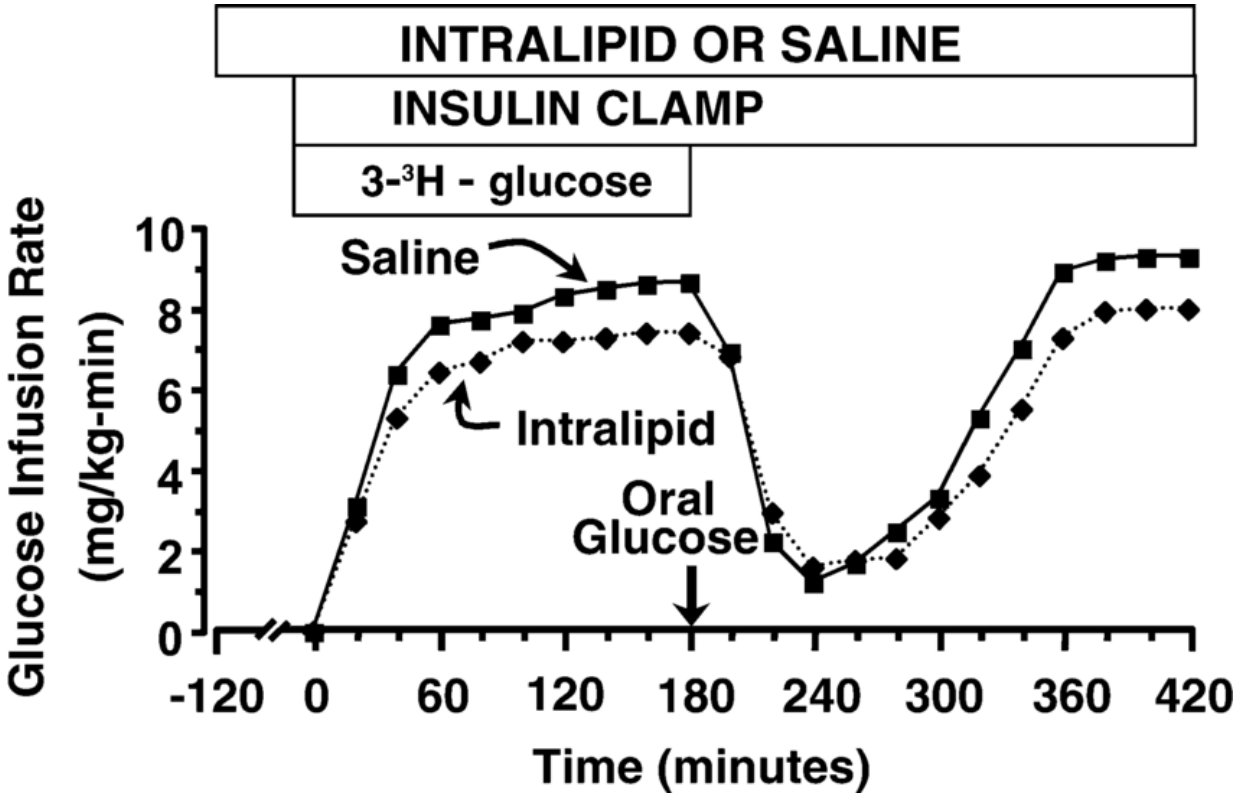

Am J Physiol Endocrinol Metab. 2002 Aug;283(2):E346-52.

活体代谢表型分析

➢ HOMA-IR

The HOMA-IR is being used extensively for estimates of β cell function and insulin resistance, both in clinical practice and studies, with the caveat that it cannot be used on patients on insulin.

HOMA-IR = (Fasting insulin in mIU/L x Fasting glucose in mg/dL) / 405

Normal reference levels for HOMA-IR range between 0.7 and 2.0.

活体代谢表型分析

- **橄榄油灌胃实验**
  检测肠道消化吸收和脂肪等的脂肪储存能力

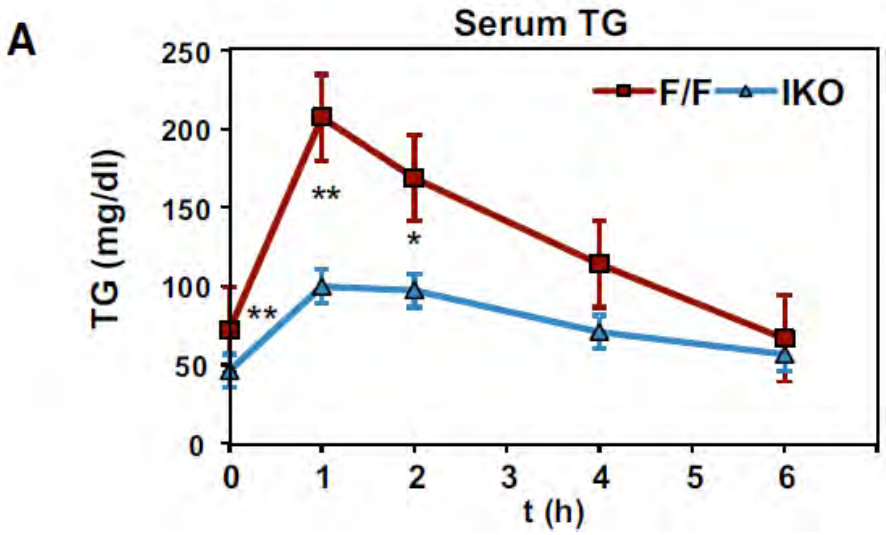

Impaired TG Absorption in Lpcat3 IKO Mice. (**A**) Postprandial TG response in male *Lpcat3*$^{fl/fl}$ (F/F) and *Lpcat3*$^{fl/fl}$ *Villin-Cre* (IKO) mice after oral gavage with olive oil (10 μg/g BW).

Cell Metab. 2016 Mar 8;23(3):492-504.

- **荧光标记脂肪酸灌胃实验 (BODYPI-Palmitate)**
  检测肠道脂肪酸吸收和脂肪等的脂肪酸摄入能力

活体代谢表型分析

- **血液代谢指标检测**
  - ✓ 血液TG、TC、HDLC、LDLC、AST、ALT、FFA等

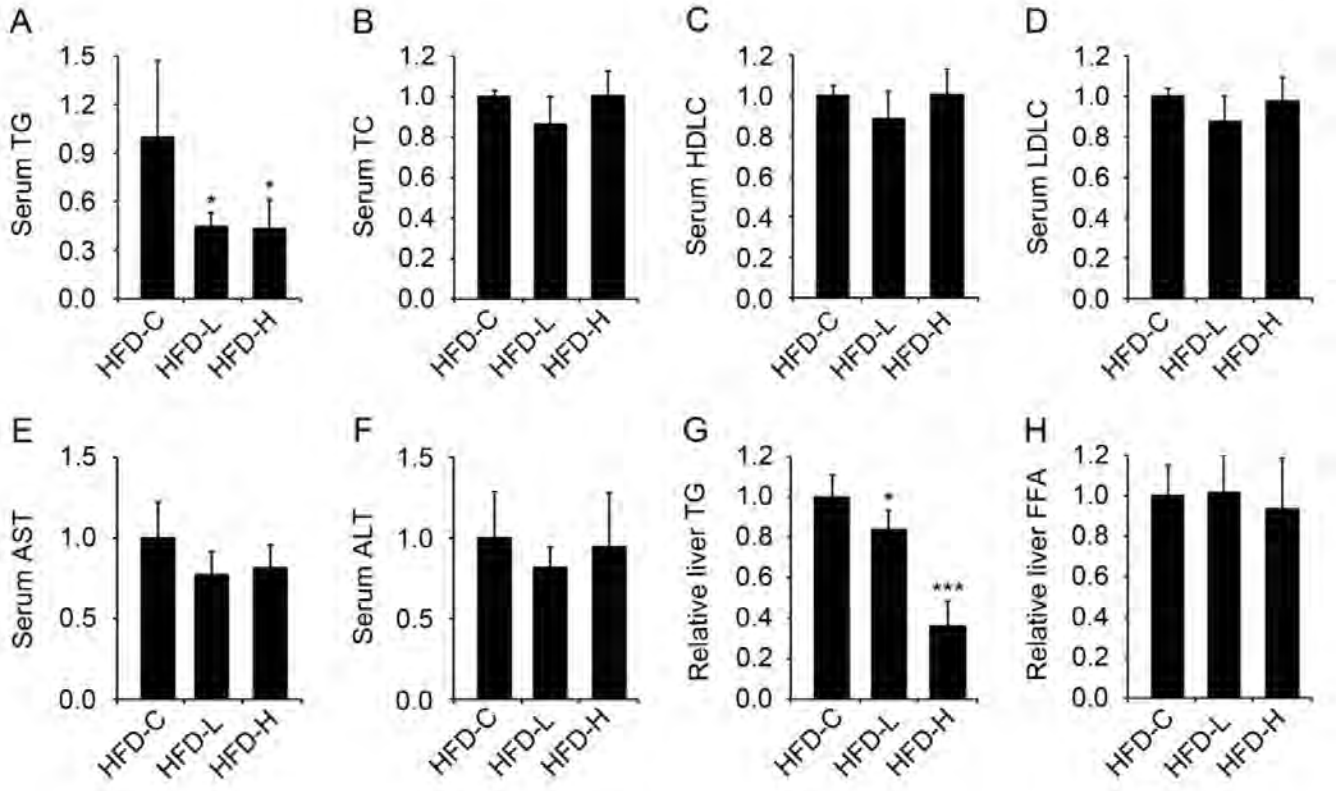

Nutrients **2017**, *9*, 805; doi:10.3390/nu9080805

活体代谢表型分析

- **肝脏功能指标检测(AST、ALT、LDH)**

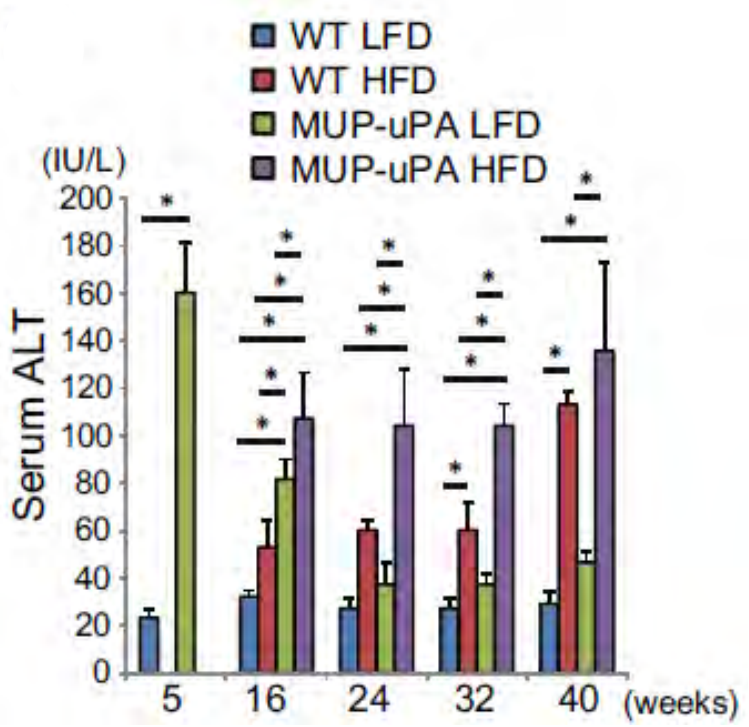

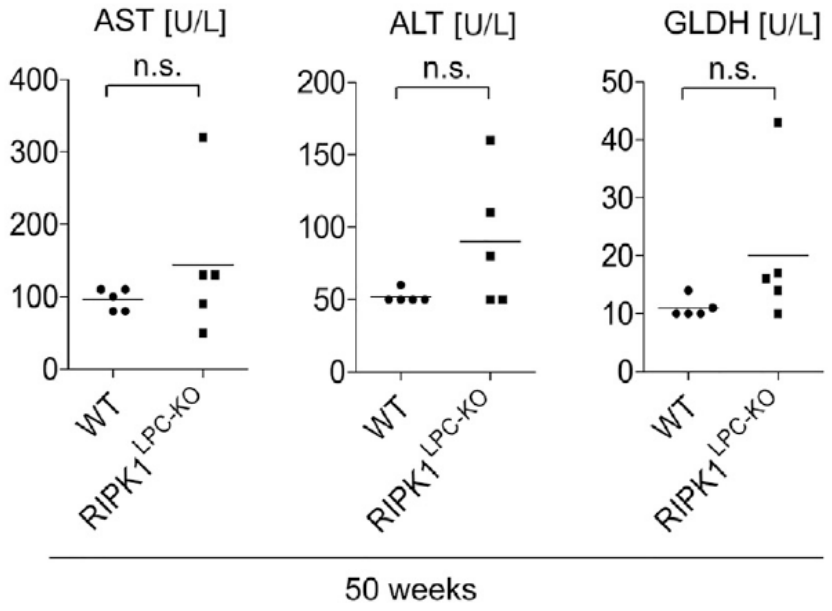

Cancer Cell. 2014; 26:331–343.

Cancer Cell 2017; 31:1-16.

活体代谢表型分析

➢ 代谢笼(Metabolic cage)检测

主要检测耗氧、产热、CO2、呼吸商(RER)、运动等

测量参数/特征：

- 活动
  X，Y，Z 轴监测
- 喂食
  消耗量监测
- 饮水
  体积监测
- 体重
  精度为 0.1g
- 跑轮
  转数监测
- 热量评估
  通过 Oxymax

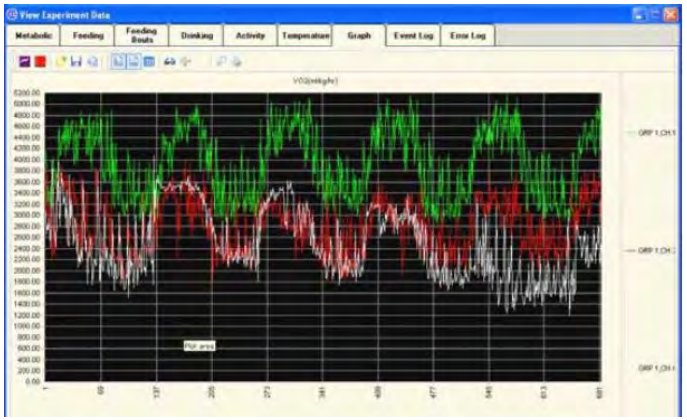

1-16通道实验动物代谢监测系统(Columbus)
营养健康所新动物房11楼代谢笼装置照片

Vi =单位时间输入代谢笼的空气量
Vo =单位时间输出代谢笼的空气量
O_2i = Vi 中的氧气含量百分比
CO_2i = Vi 中的二氧化碳含量百分比
O_2o = Vo 中氧气含量的百分比
CO_2o = Vo 中二氧化碳含量的百分比

1] $VO_2 = ViO_2i\text{-}VoO_2o$
2] $VCO_2 = VoCO_2o\text{-}ViCO_2i$
3] RER = VCO2/VO2
4] EE = 3.815 × VO2 + 1.232 × VCO2
RER, respiratory exchange ratio; EE, Energy expenditure

活体代谢表型分析

➢ 代谢笼检测示例

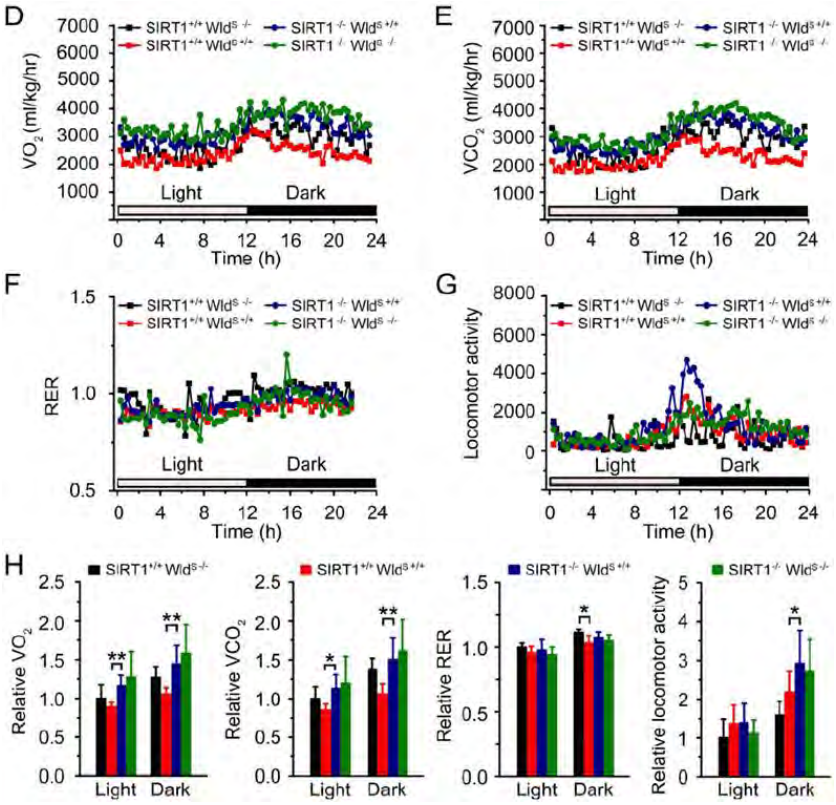

RER高，代表机体以消耗碳水化合物为主；
RER低，代表机体以消耗脂肪为主。
RER数值高于1，表示机体进行无氧呼吸。

Energy expenditure of SIRT1$^{+/+}$ WldS-/-, SIRT1$^{+/+}$ WldS$^{+/+}$, SIRT1$^{-/-}$ WldS$^{+/+}$ and SIRT1$^{-/-}$ WldS$^{-/-}$ mice. D: Oxygen consumption of 18-week-old male mice of the indicated genotypes. n = 6-8 for each group in (D-G). **E**: Carbon dioxide release of 18-week-old male mice of the indicated genotypes. **F**: Respiratory exchange ratio (RER) of 18-week-old male mice of the indicated genotypes. **G**: Locomotor activity of 18-week-old week male mice of the indicated genotypes. **H**: Statistical analysis of the results in (D-G).

Diabetes. 2011 Dec;60(12):3197-207.

活体代谢表型分析

➢ 代谢笼检测耗氧和能力消耗

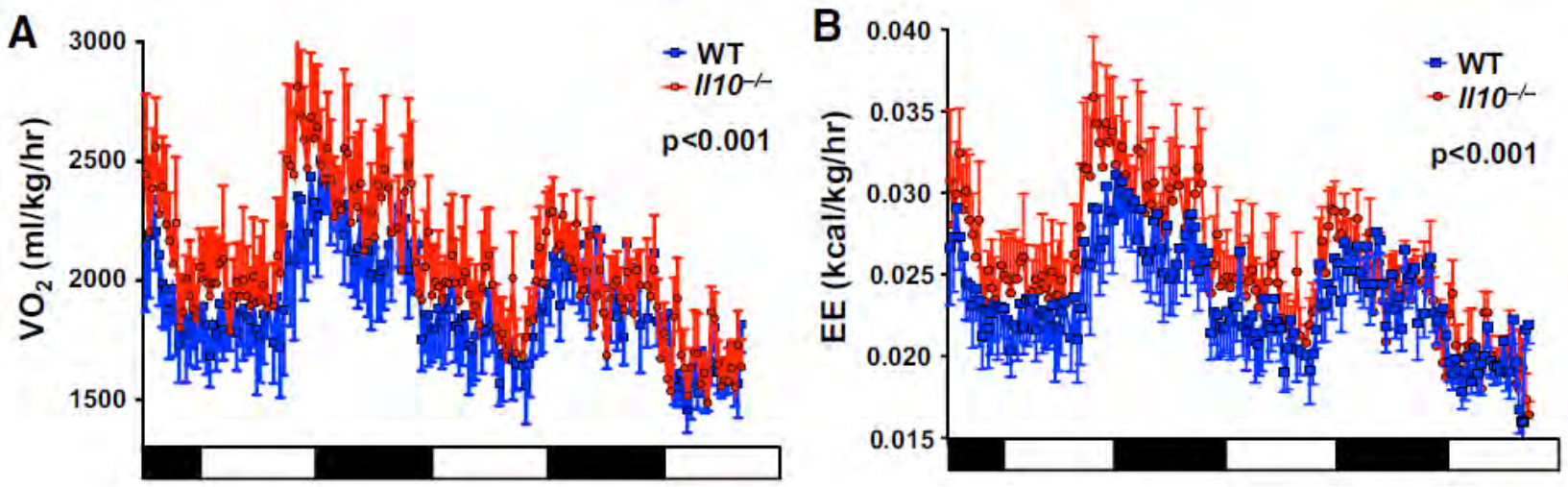

IL-10 Deficiency Promotes Energy Expenditure. (**A and B**) , VO2 (mL/kg/hr) (A) and Energy expenditure (EE) (kCal/kg/hr) (B) of chow-fed 10-week-oldWT and *Il10*$^{-/-}$ mice was analyzed by Columbus Oxymax metabolic chambers. 12-hr light/dark cycles; 72-hr total duration; and each light/dark bar represents 12 hr duration.

Cell. 2018 Jan 11;172(1-2):218-233.e17.

目 录

解剖代谢表型分析

➢ eWAT/iWAT/BAT 位置及解剖形态

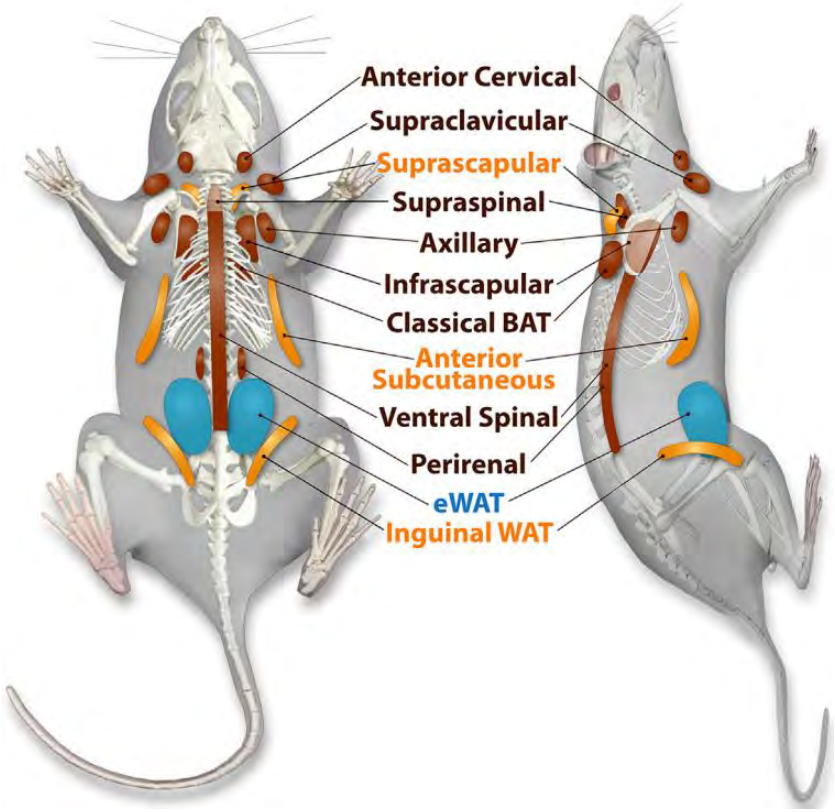

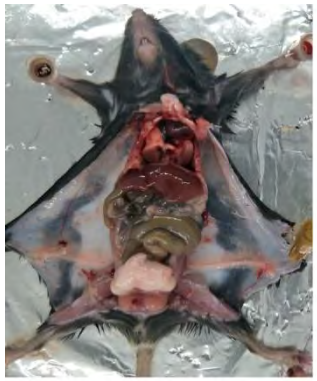

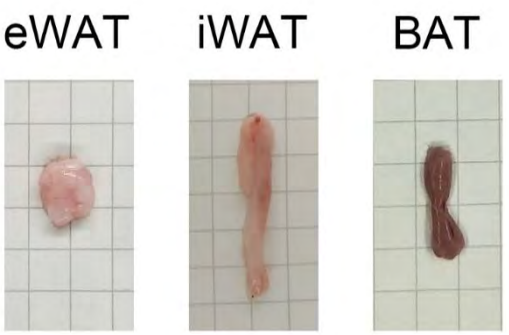

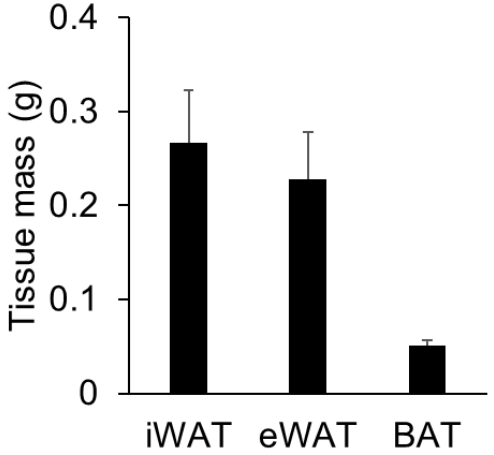

Cell Metab. 2018 Jan 9;27(1):252-262

解剖代谢表型分析

- 小鼠代谢组织解剖

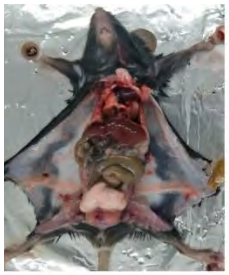

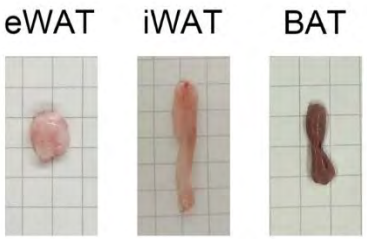

脂肪组织切片染色

➢ eWAT、iWAT、iBAT切片HE染色

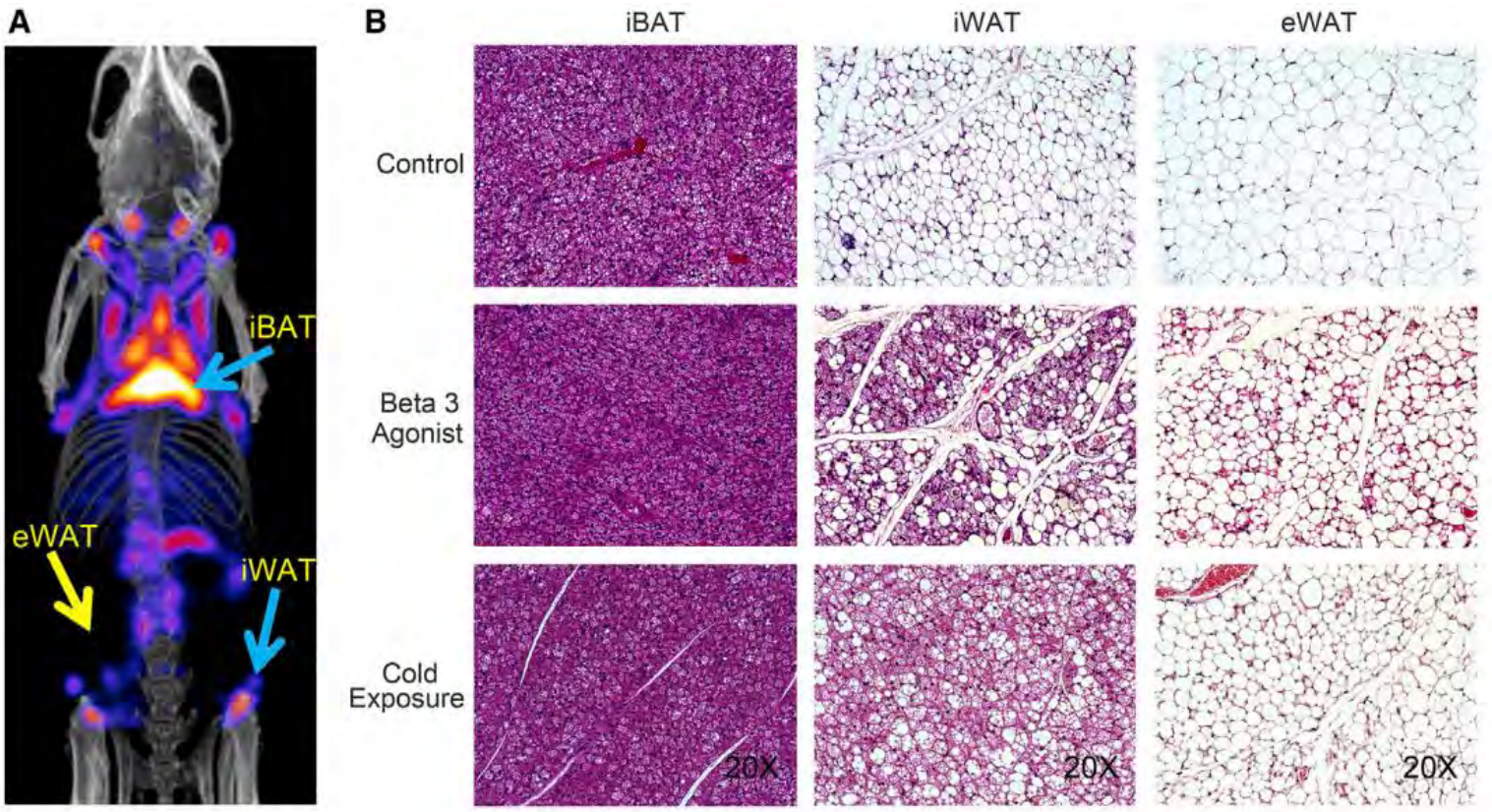

Interscapular BAT (iBAT), inguinal WAT (iWAT), and epididymal WAT (eWAT) depots.

Cell Metab. 2018; 27:252-262.

解剖代谢表型分析

- **脂肪的遗传示踪(Laz标记成熟脂肪细胞，检测脂肪细胞新生)**

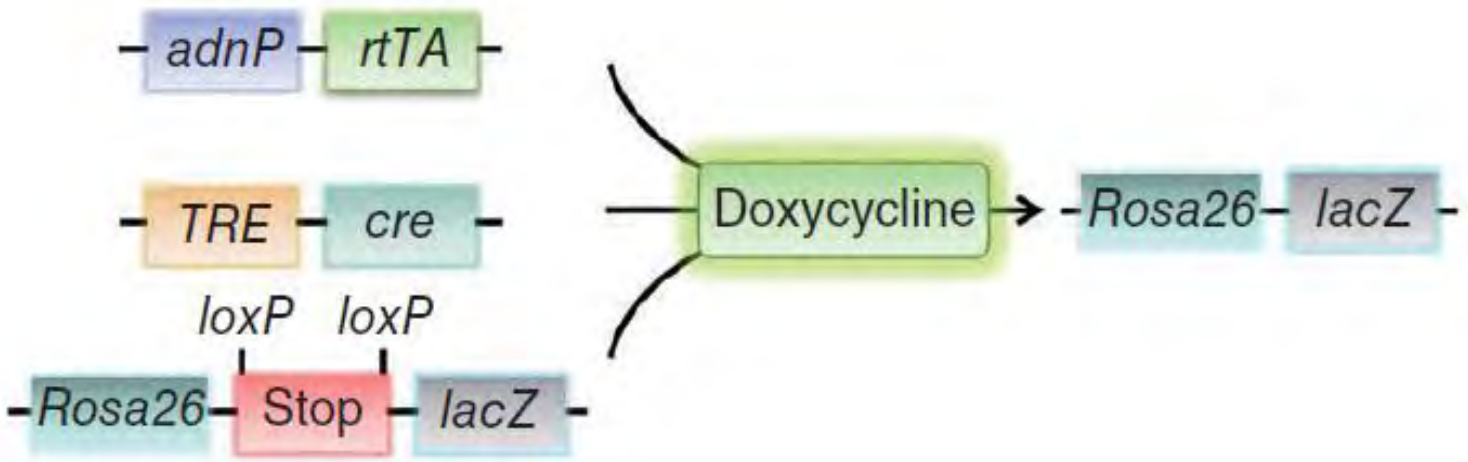

Inducible labeling of mature adipocytes. The inducible labeling system of mature adipocytes, produced by crossing *adiponectinP-rtTA* (*adnP-rtTA*) transgenic mice with *TRE-cre and Rosa26-loxP-stop-loxP-lacZ* transgenic mice. The triple transgenic mouse, called the AdipoChaser mouse, expresses rtTA in mature adipocytes but does not express LacZ in any cell type while maintained on food not containing doxycycline (dox). When doxycycline is included in the food, adipocytes that express rtTA will have the TRE promoter activated so that cre expression is induced. The Cre protein will specifically cut out the floxed transcriptional stop cassette and then turn on LacZ expression. Even after withdrawal of doxycycline from the food, these adipocytes will permanently express LacZ, whereas any new adipocytes that develop after doxycycline exposure will not express LacZ.

Nat Med. 2013 Oct;19(10):1338-44.

解剖代谢表型分析

➢ 脂肪的遗传示踪，以检测新生脂肪细胞

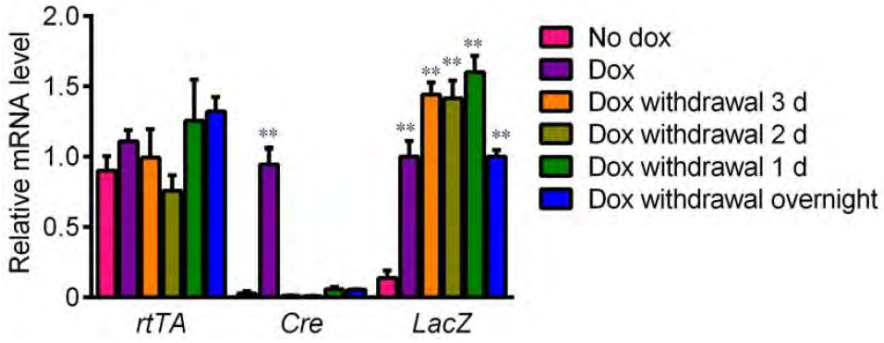

Systemic washout of doxycycline. 10 week-old male AdipoChaser mice were maintained on chow diet only (no dox) or on doxycycline diet for 7 days and then switched to chow diet prior to sacrifice for 3, 2, 1 days, or overnight. Relative mRNA expression levels of *rtTA*, *Cre* and *LacZ* in sWAT of AdipoChaser mice were measured by qPCR assay.

连续7天给小鼠喂食含有四环素的饮食可使成熟的脂肪细胞产生永久性的LacZ。3天正常饮食后，即可清除四环素。无四环素后，就不能和rtTA结合，也就不能进一步结合TRE引起Cre的表达，但之前已经翻译产生的Cre蛋白依然存在，因而会一直促进下游的表达。

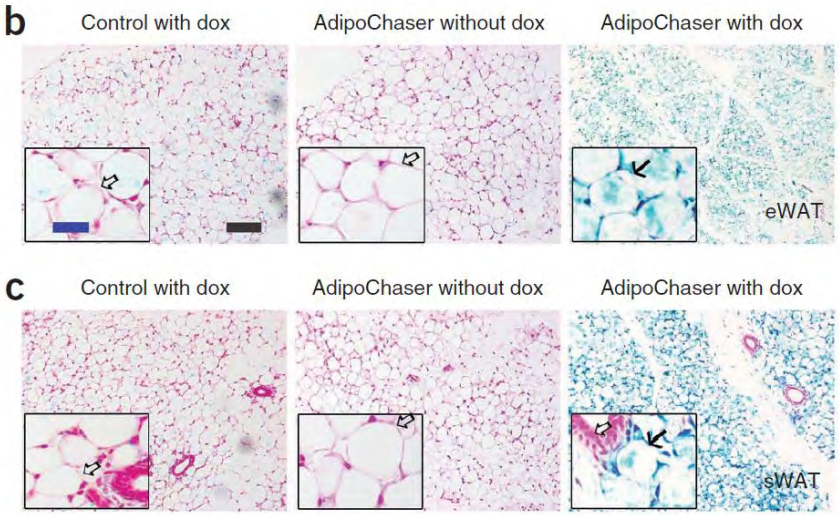

Inducible labeling of mature adipocytes. (**b,c**) Representative β-gal (blue) staining of eWAT (b) and sWAT (c) in male control (mice with only *TRE-cre* and *Rosa26-loxP-stop-loxP-lacZ*) or AdipoChaser mice. Solid arrows (b,c), LacZ-positive cells; open arrows (b,c), LacZ-negative cells. Scale bar (black, shown in b, applies to b and c), 200 μm; (blue, shownin b, applies to the insets in b and c), 50 μm.

Nat Med. 2013 Oct;19(10):1338-44.

解剖代谢表型分析

➢ 脂肪的遗传示踪，以检测新生脂肪细胞

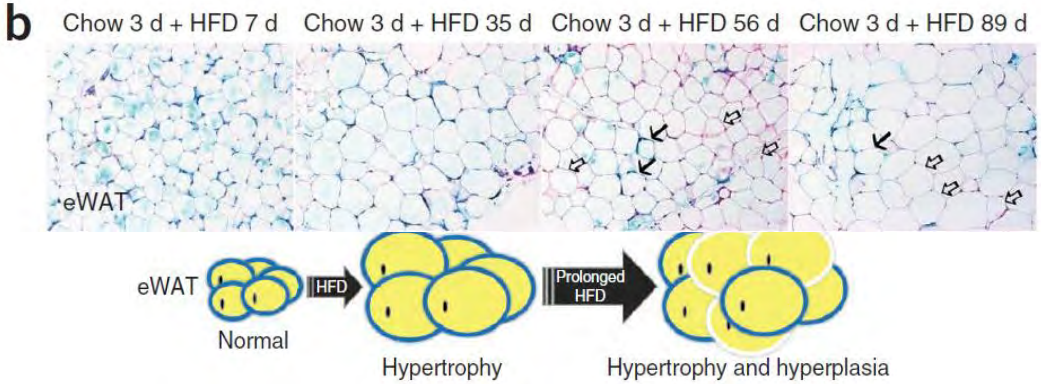

HFD-induced adipose tissue hypertrophy and hyperplasia. Representative β-gal staining of eWAT from 9- to 10-week-old male AdipoChaser mice that were kept on doxycycline diet for 7 d followed by chow diet for 3 d and HFD for 7, 35, 56 or 89 d. Solid arrows, LacZ-positive cells; open arrows, LacZ-negative cells.

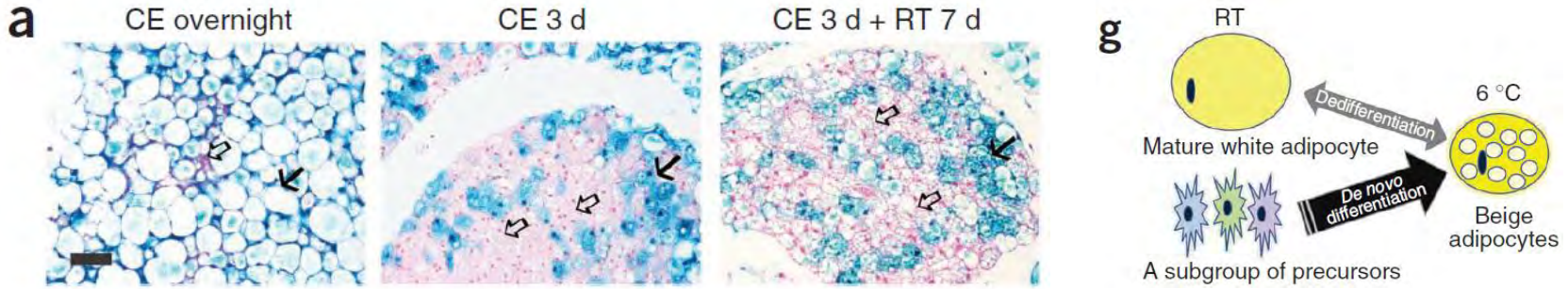

Lineage of the brown-like adipocytes in subcutaneous adipose tissue after cold exposure. (**a**) Representative β-gal staining of sWAT from 10-week-old male AdipoChaser mice that were kept on doxycycline diet for 7 d followed by chow diet for 3 d and then exposed to cold (CE) overnight (left) or for 3 d (middle) or exposed to cold for 3 d followed by 7 d in room temperature (RT; right). (**g**) Schematic model showing that the beige cell population arises predominantly from *de novo* adipogenesis rather than transdifferentiation. After cold exposure or β3 agonist treatment, most beige adipocytes are induced by differentiating from cell populations other than existing mature adipocytes (beige precursors) rather than through dedifferentiation of mature white adipocytes.

Nat Med. 2013 Oct;19(10):1338-44.

解剖代谢表型分析

➢ 脂肪肝发展进程

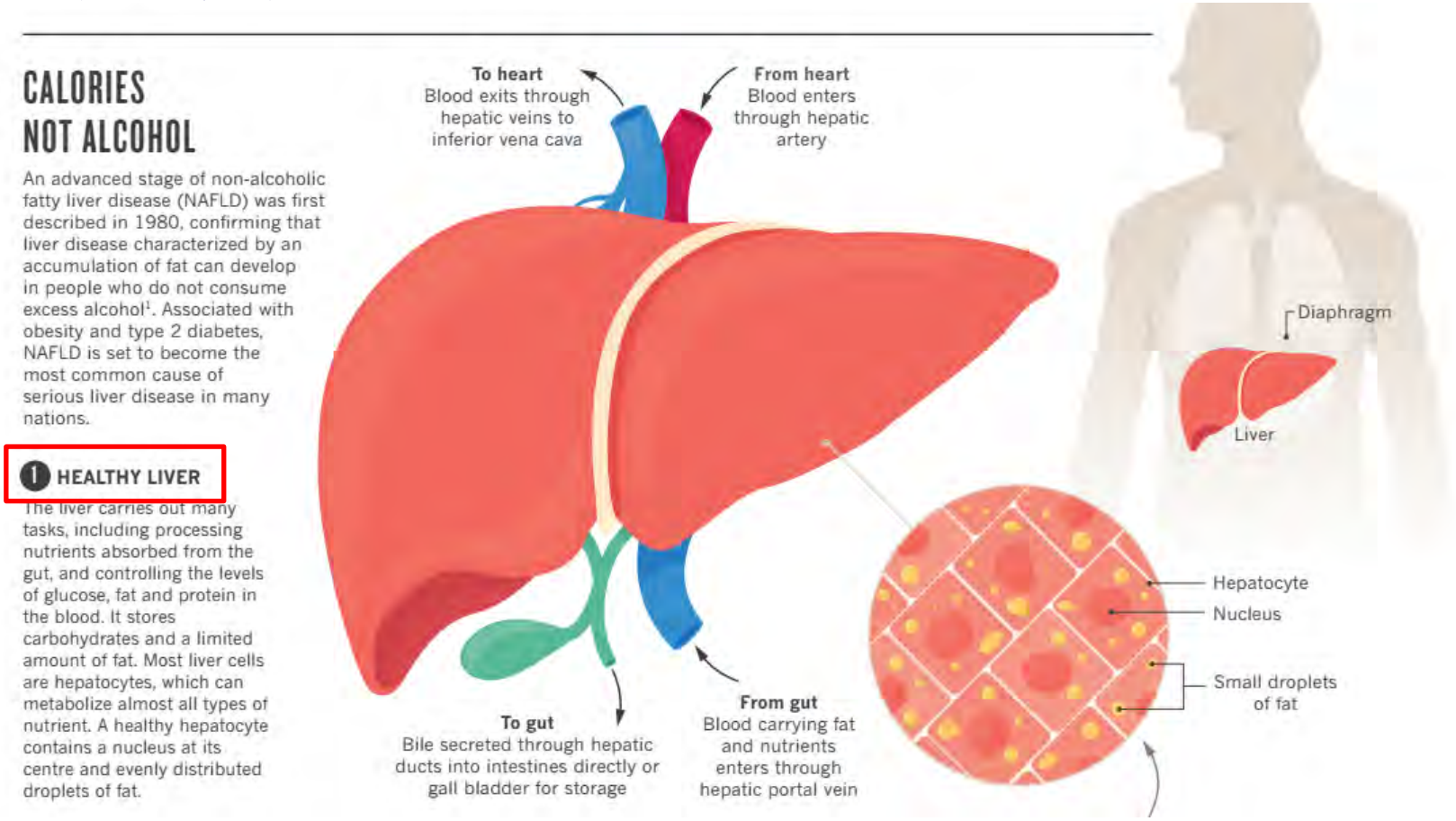

Nature. 2017 Oct 11;550(7675):S102-S103.

解剖代谢表型分析

➢ 脂肪肝发展进程

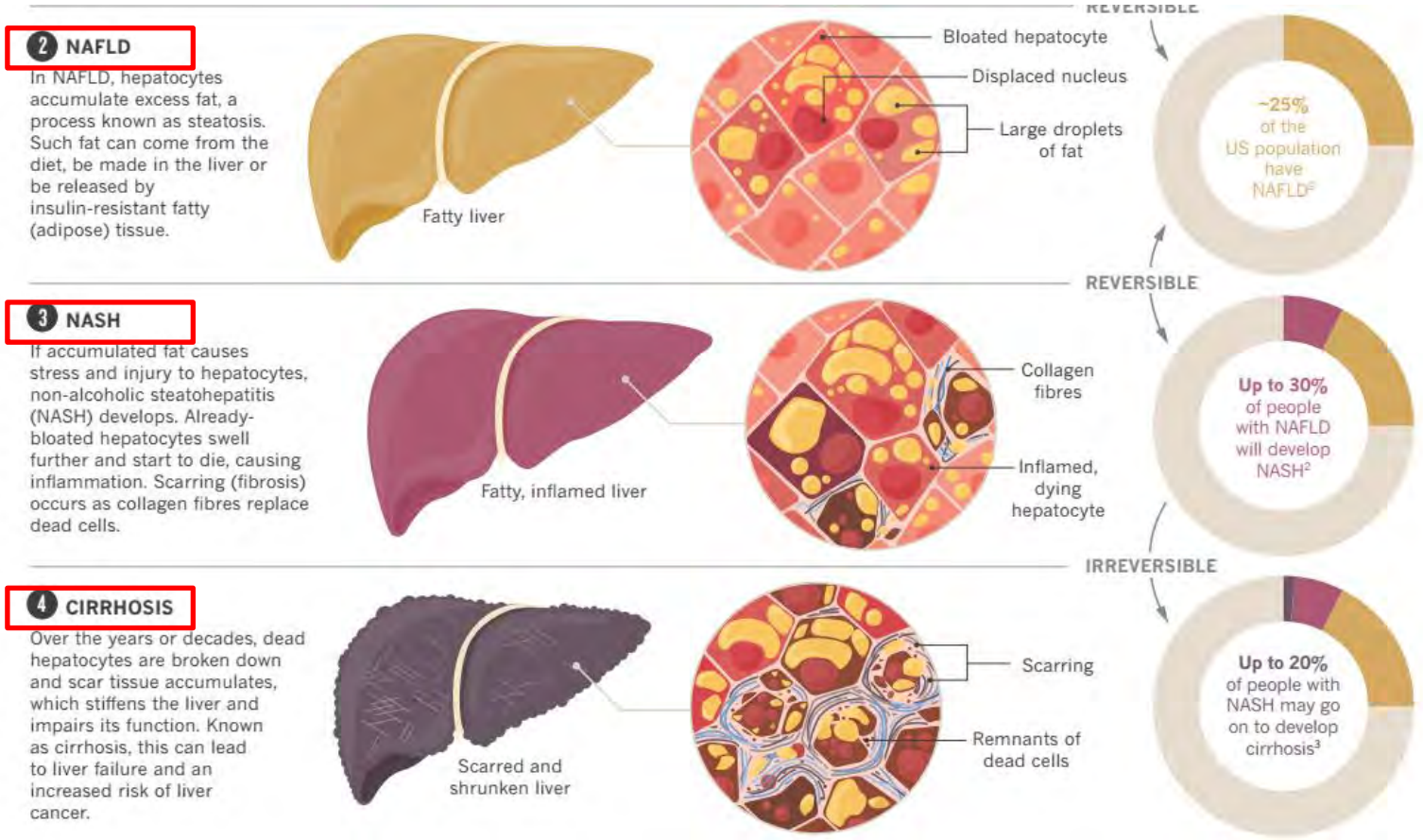

Nature. 2017 Oct 11;550(7675):S102-S103.

脂肪肝切片染色

➢ 脂肪肝发展进程

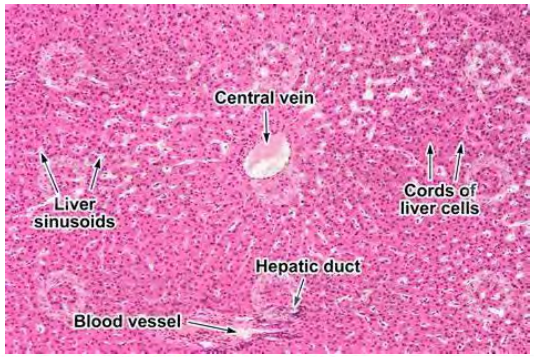

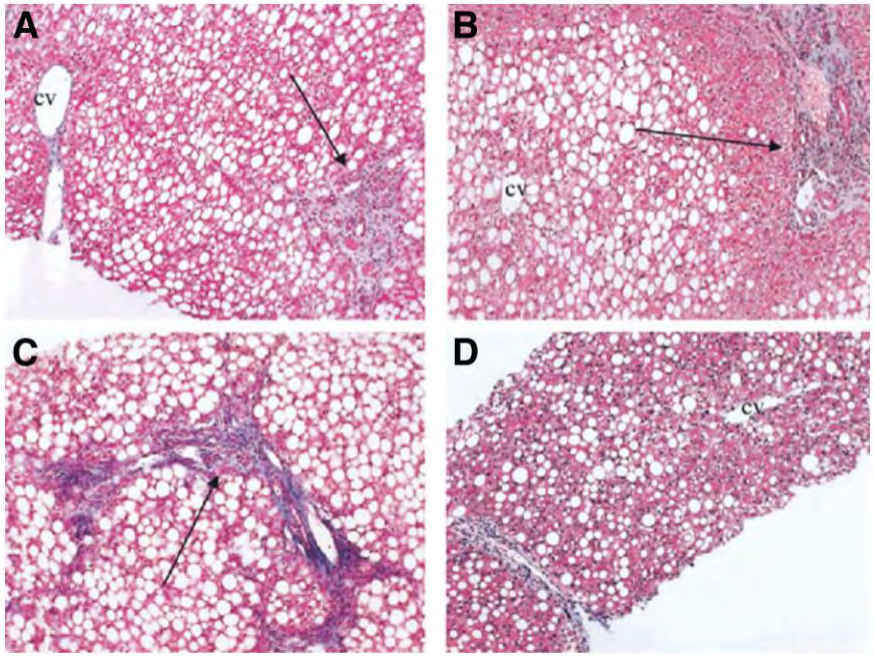

Typical histologic pattern seen in children with type 2 NASH.

(A,B) Shows absence of ballooning degeneration and perisinusoidal fibrosis in the presence of steatosis and portal inflammation.

(C) Portal fibrotic expansion and marked steatosis.

(D) Periportal inflammation without steatosis in zone 1 (around portal tract) and mild portal fibrosis in the absence of any fibrosis in zone 3 (around central vein).

Nature. 2017 Oct 11;550(7675):S102-S103.

电镜检测

➢ 电镜检测细胞核、线粒体、脂滴、溶酶体等的形态变化

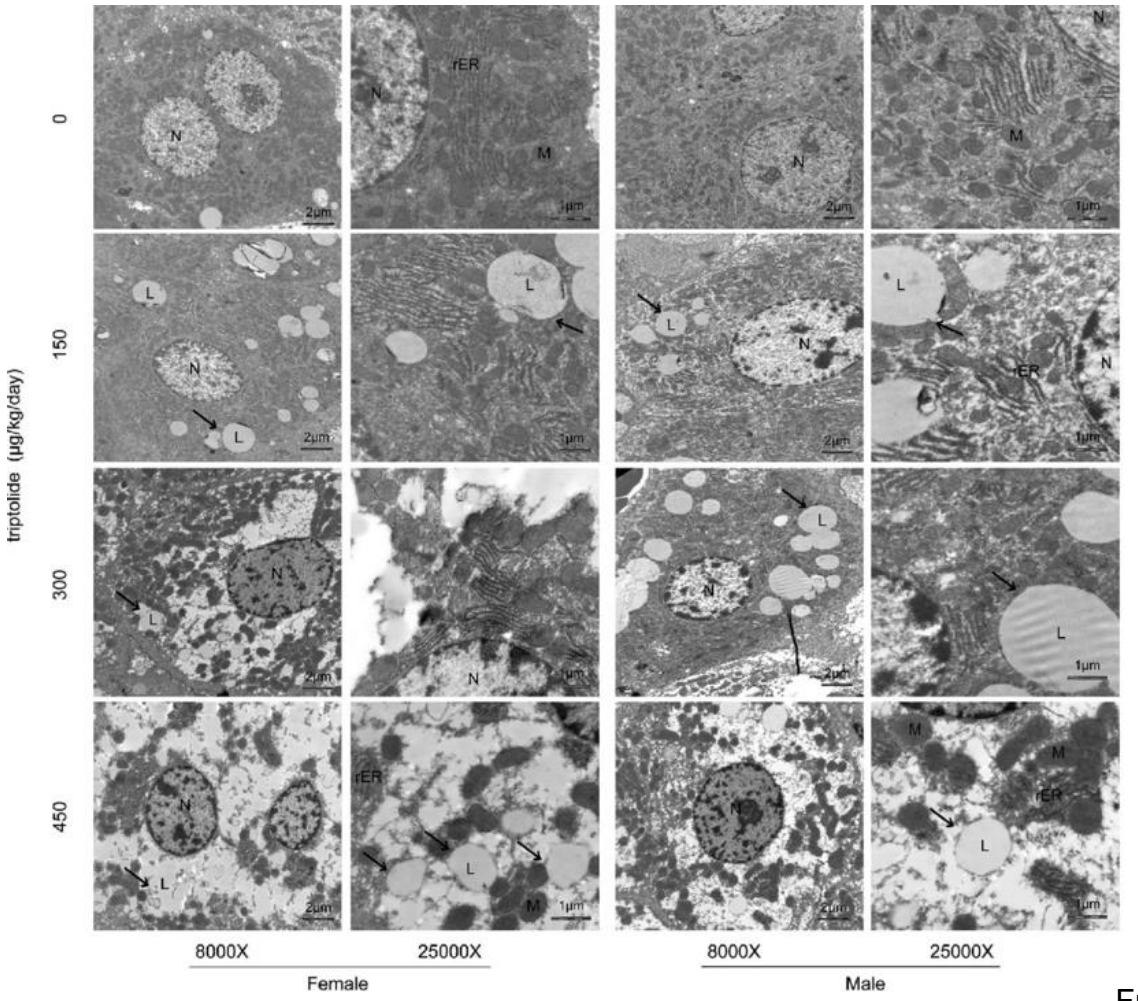

The results of electron microscopy examination of the liver following triptolide treatment (8000X and 25000X). Rats were administered 0, 150, 300, or 450 μg triptolide/kg/day by gavage for 28 days. Lipid droplets (L); mitochondria (M); rough endoplasmic reticulum (rER) and nuclei (N) are shown. More lipid droplets (arrow) were observed in the triptolide-treated female rats compared with the male rats.

Frontiers in Pharmacology 2016； 7(e100685)

解剖代谢表型分析

- 血清及肝脏中TG、TC、LDL-C、HDLC、FFA等

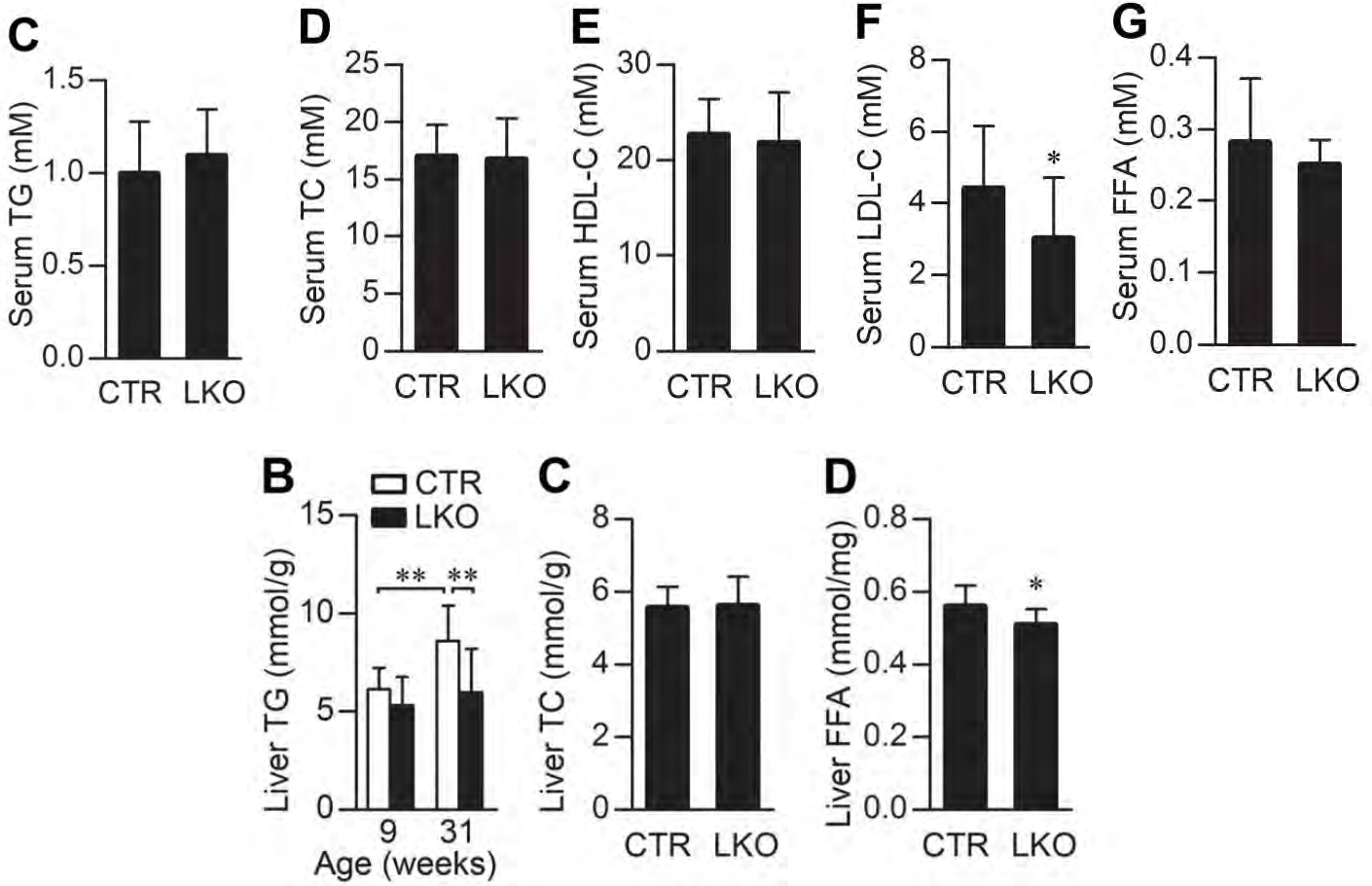

J Lipid Res. 2012 Mar;53(3):358-67.

解剖代谢表型分析

➢ 胰岛HE染色和Insulin染色

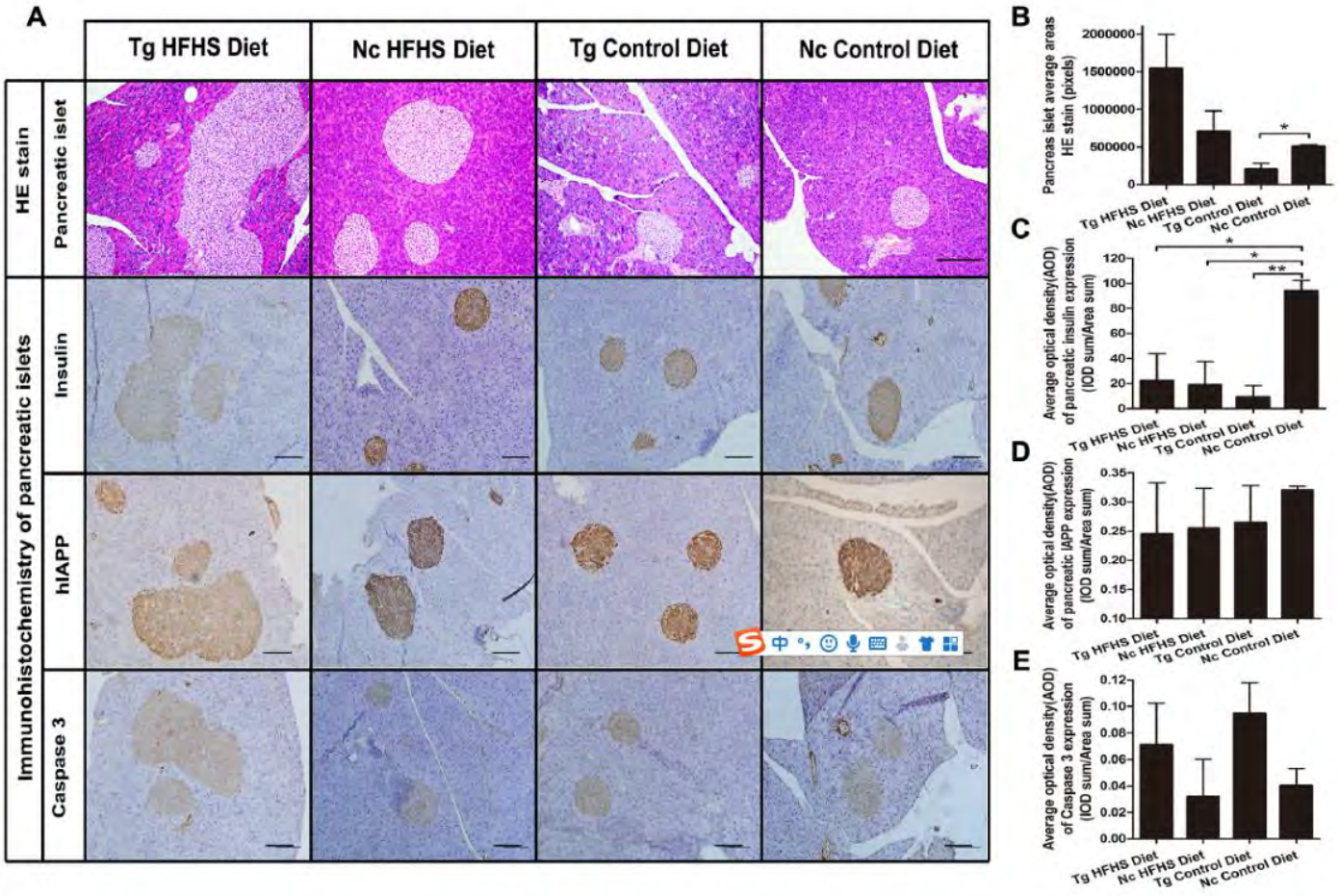

Kong et al. (2018), Kill two birds with one stone: making multi-transgenic pre-diabetes mouse models through insulin resistance and pancreatic apoptosis pathogenesis.

解剖代谢表型分析

- **Insulin染色和胰岛大小的计算**

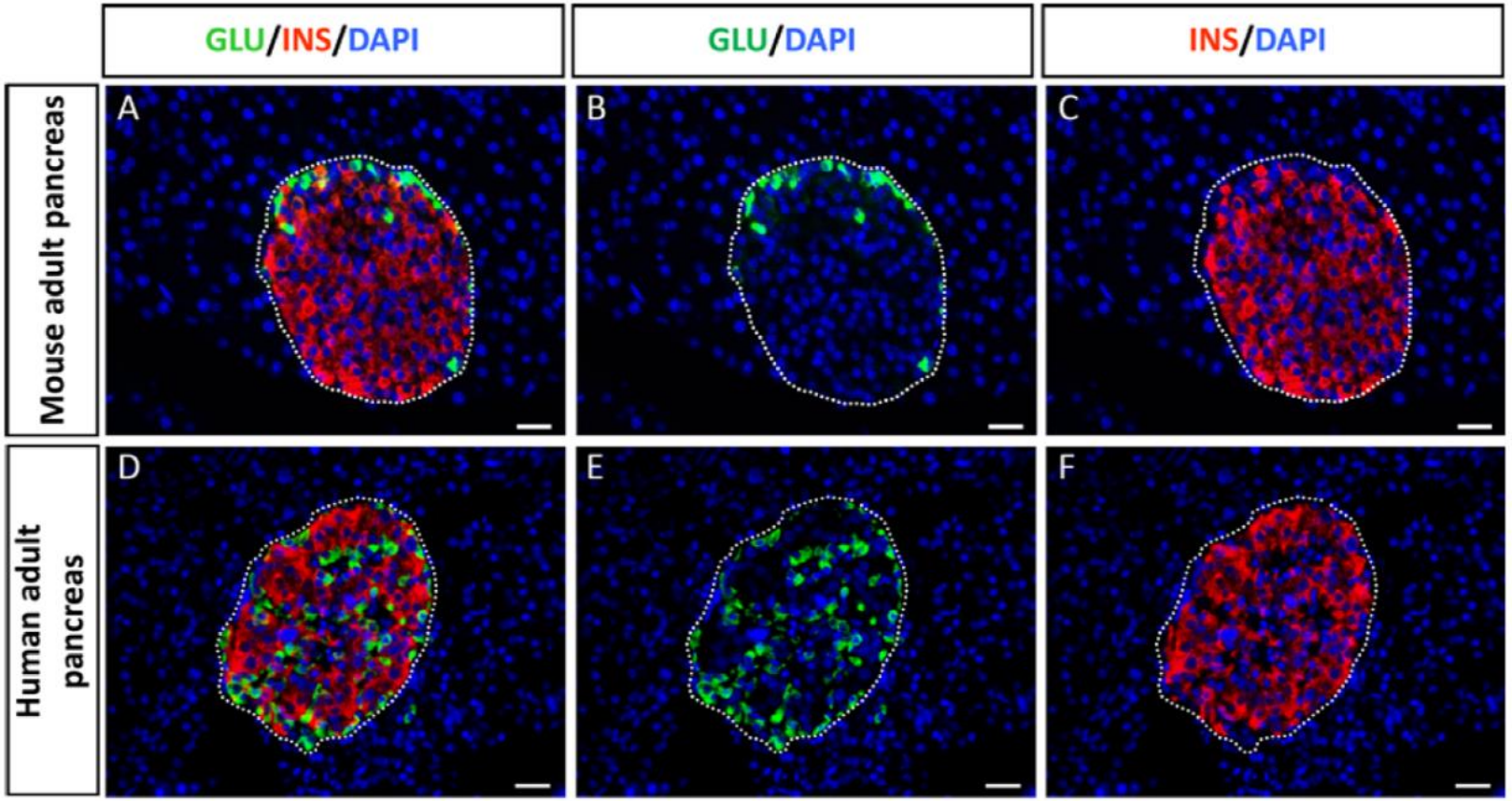

Beta Cells within Single Human Islets Originate from Multiple Progenitors

解剖代谢表型分析

➢ Insulin染色和胰岛及β细胞大小的计算

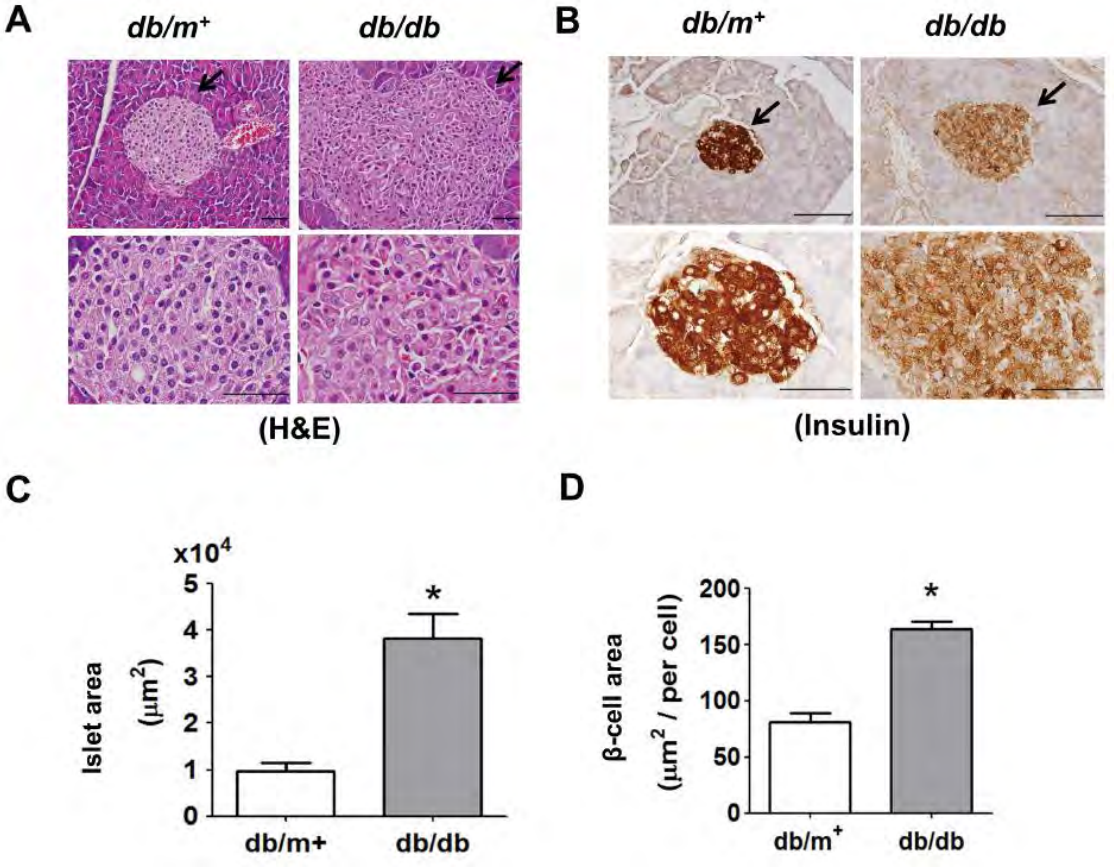

Histology and immunohistochemical staining for insulin in pancreatic islets of db/db diabetic mice.

The pathological role of advanced glycation end products-downregulated heat shock protein 60 in islet β-cell hypertrophy and dysfunction

解剖代谢表型分析

➢ 脂肪炎症

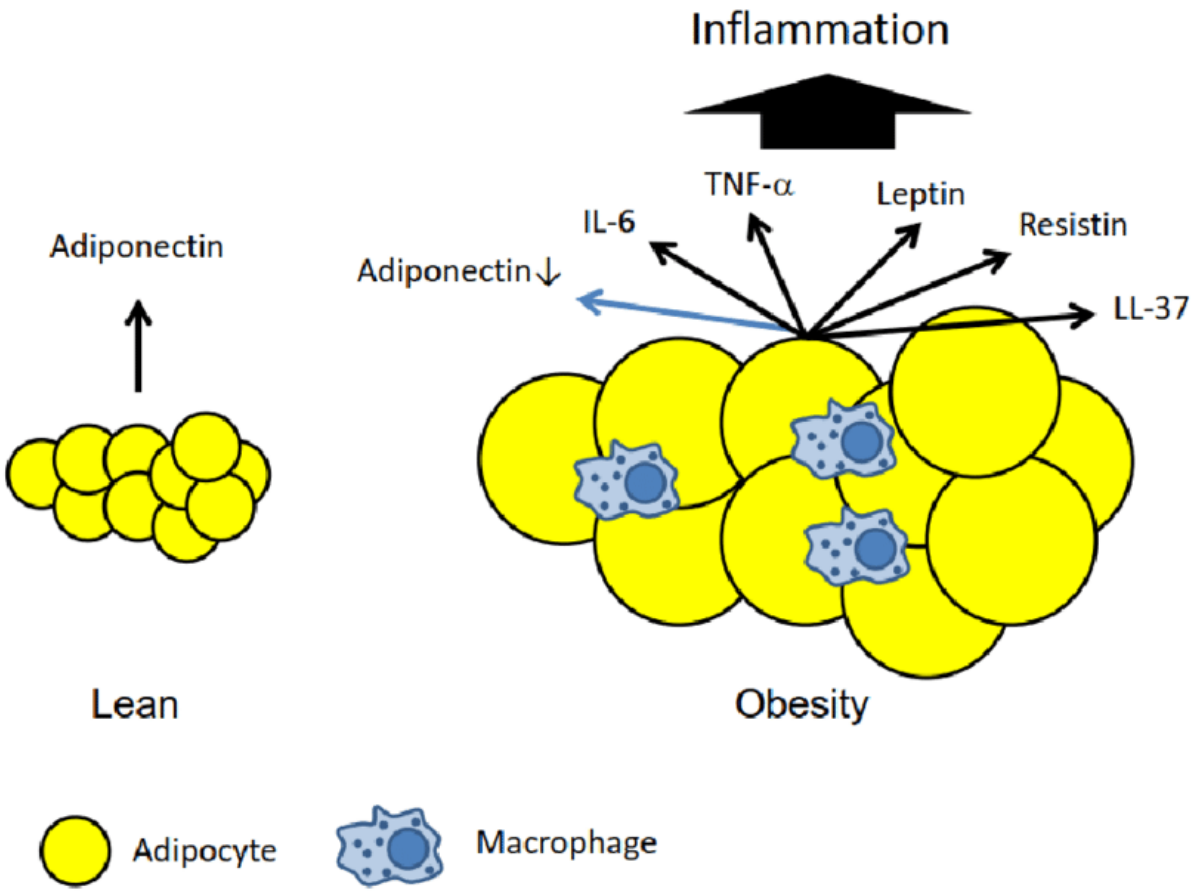

Trends in Immunotherapy, 2017: *1*:67-74.

解剖代谢表型分析

➢ 脂肪炎症

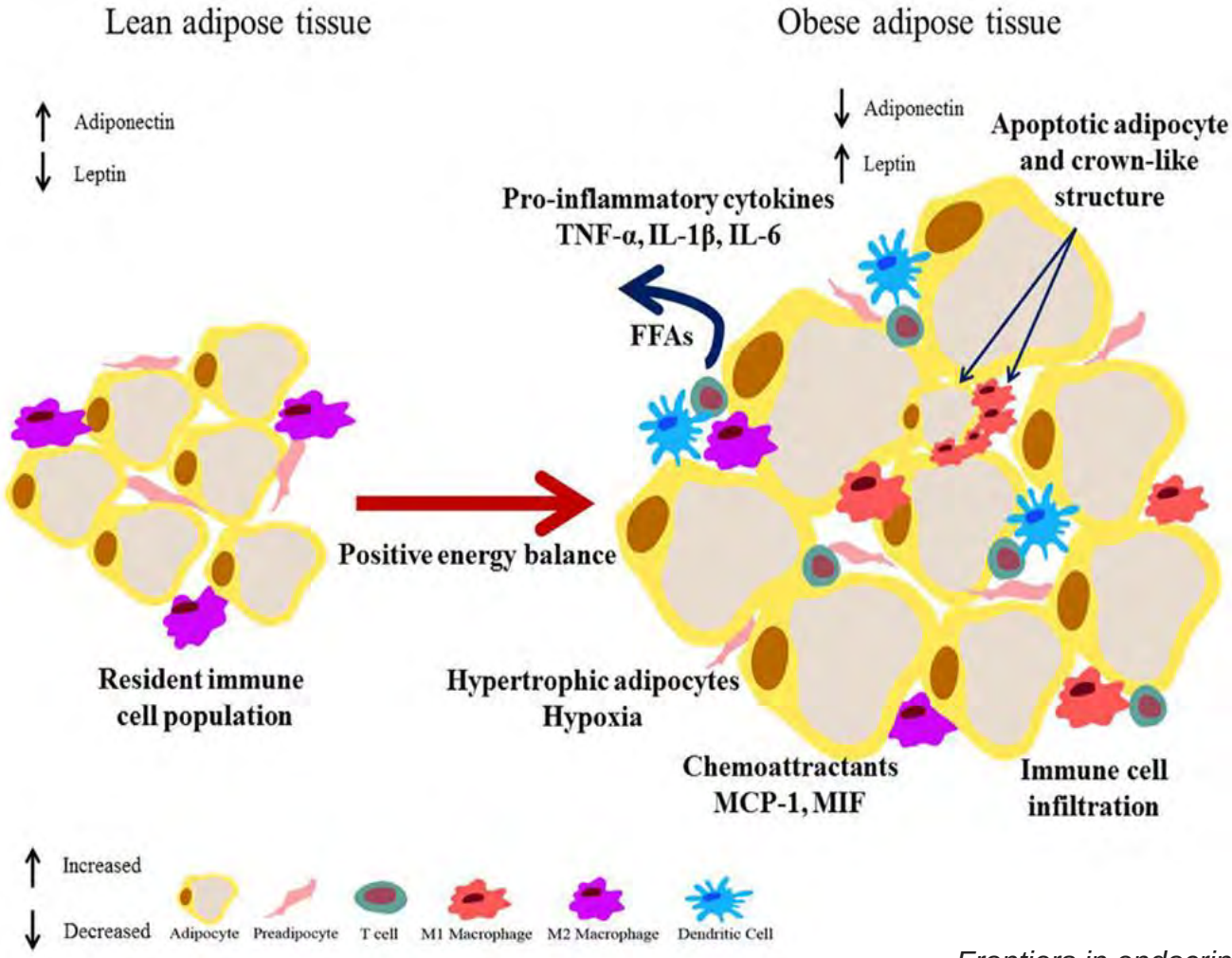

Frontiers in endocrinology, 2013; *4*: 52.

解剖代谢表型分析

- **脂肪和肝脏的炎症染色**

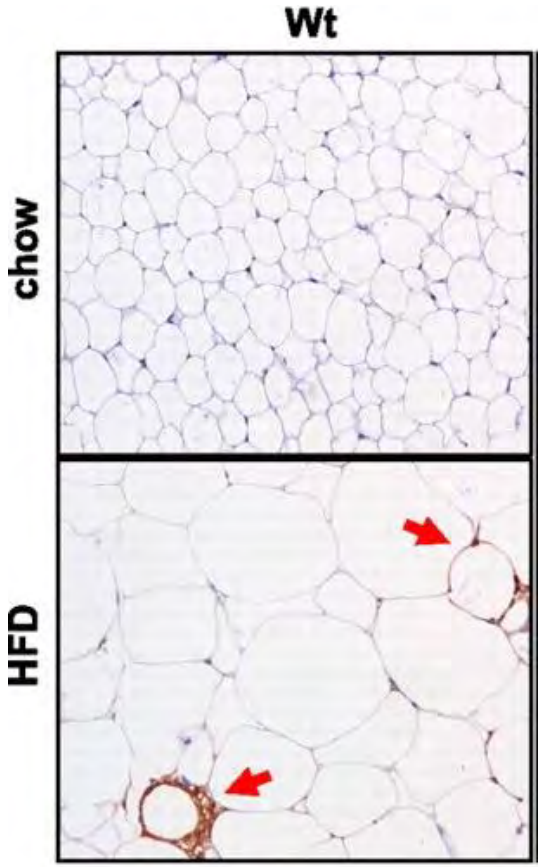

Diabetes. 2012; *61*(7):1801-1813.

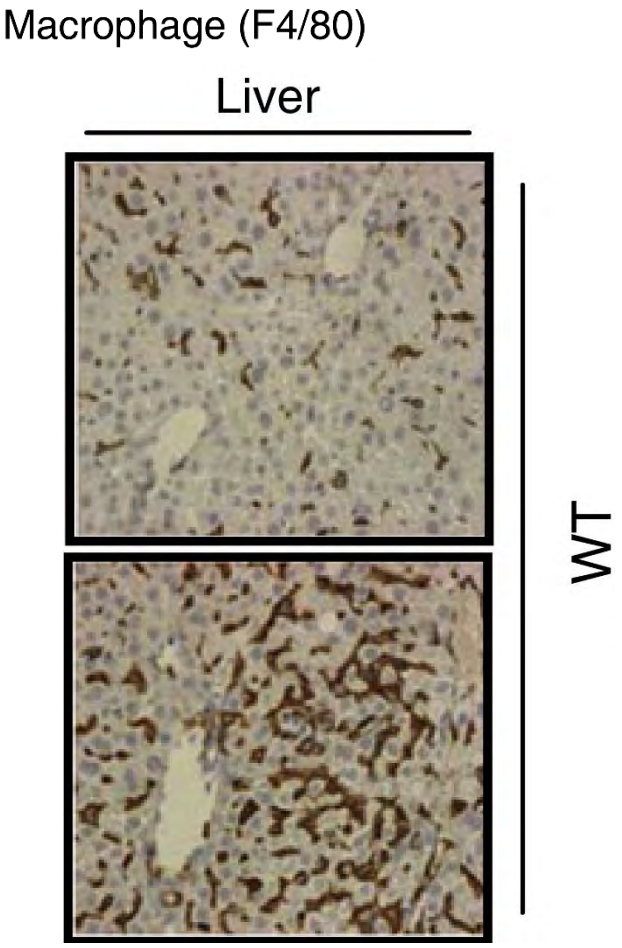

Cell. 2010; *140*(2):197-208.

解剖代谢表型分析

➢ 肠道切片的电镜检测和油红染色

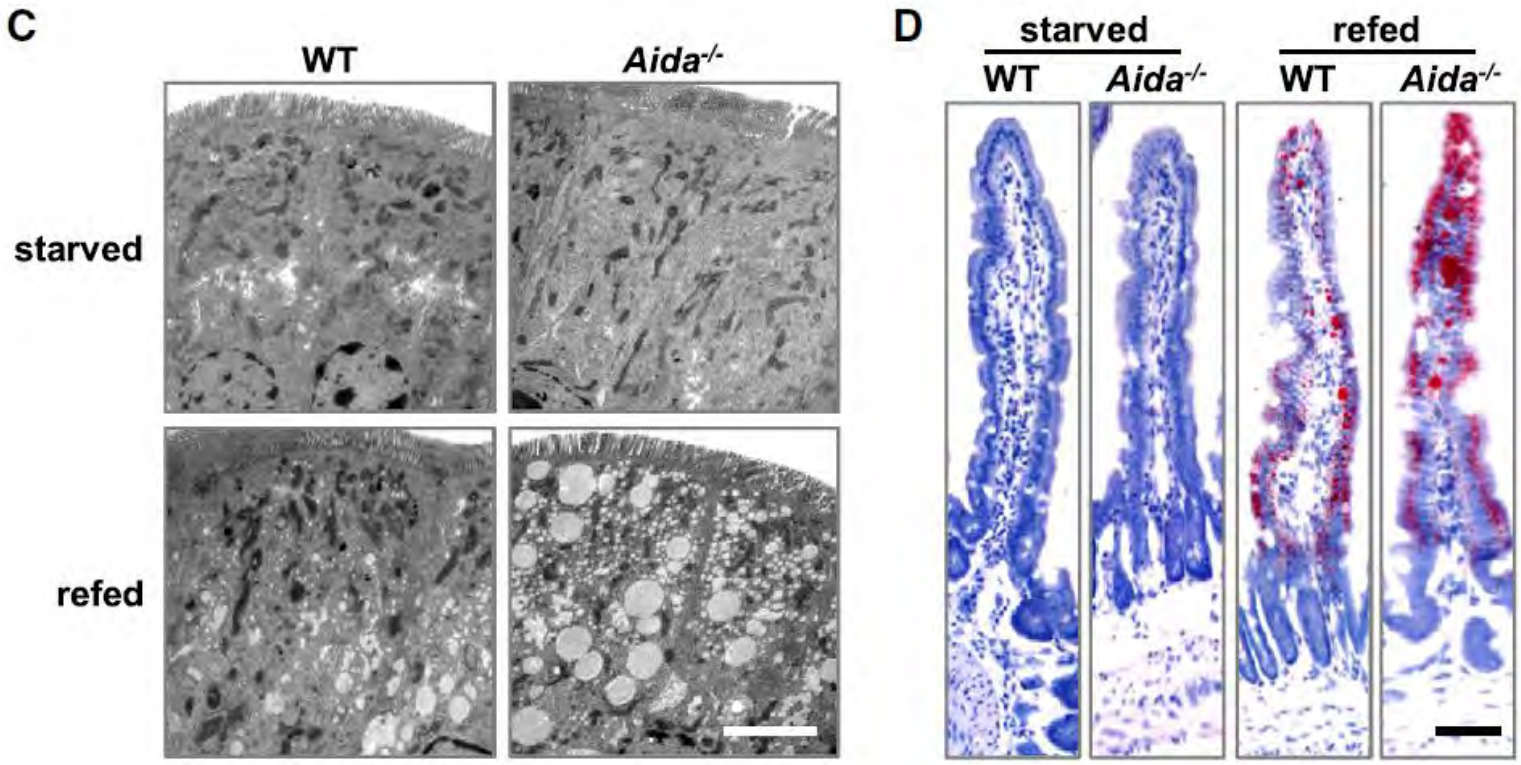

Aida Deficiency Upregulates Lipid Absorption in the Small Intestine. (**C**) Lipid droplets in enterocytes of the proximal small intestine from 3-day HFD fed male *Aida*$^{-/-}$ / or WT mice visualized by electron microscopy. Mice were fasted for 8 hr followed by high-fat refeeding or left unfed for another 1 hr. Scale bar, 5 mm. (**D**) Oil-Red-O staining of villus of proximal small intestine from 3-day HFD-fed male *Aida*$^{-/-}$ or WT mice. Mice were treated as in (C).

Cell Metab. 2018 Apr 3;27(4):843-853.

解剖代谢表型分析

➢ 荧光标记脂肪酸示踪实验 (BODIPY-Palmitate)

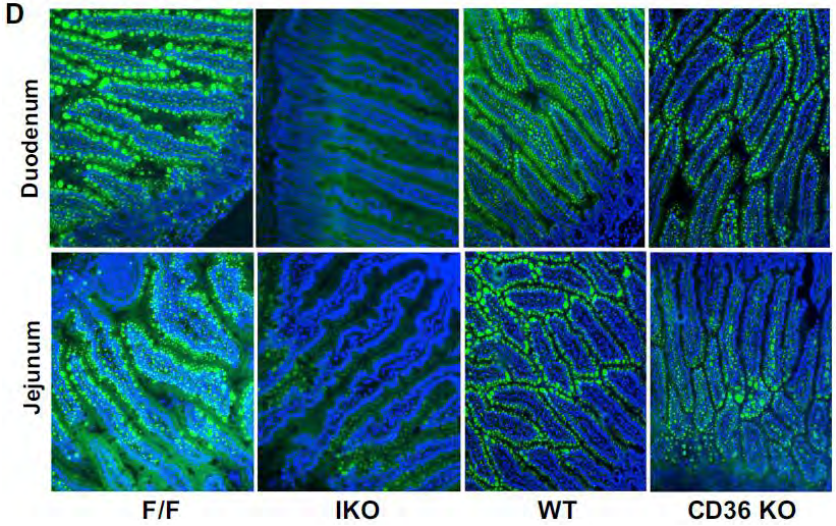

Impaired TG Absorption in Lpcat3 IKO Mice. Fluorescence images of small intestines of *Lpcat3*$^{fl/fl}$ (F/F) and *Lpcat3*$^{fl/fl}$ *Villin-Cre* (IKO) mice, and wild-type C57BL/6 and *Cd36*$^{-/-}$ mice after oral gavage with olive oil containing BODIPY-labeled FA for 2 hr.

Cell Metab. 2016 Mar 8;23(3):492-504.

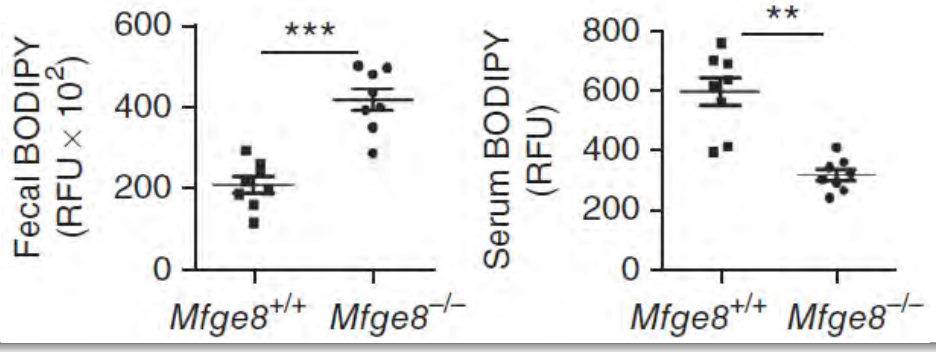

Mfge8 mediates absorption of dietary fats. Fecal and serum BODIPY concentrations in Mfge8$^{+/+}$ and Mfge8$^{-/-}$ mice after gavage with a mixture of BODIPY fatty acid analog and a nonabsorbable rhodamine-PEG.

Nat Med. 2014 Feb;20(2):175-83.

解剖代谢表型分析

➢ 肠道菌群

Intermittent Fasting Promotes White Adipose Browning and Decreases Obesity by Shaping the Gut Microbiota

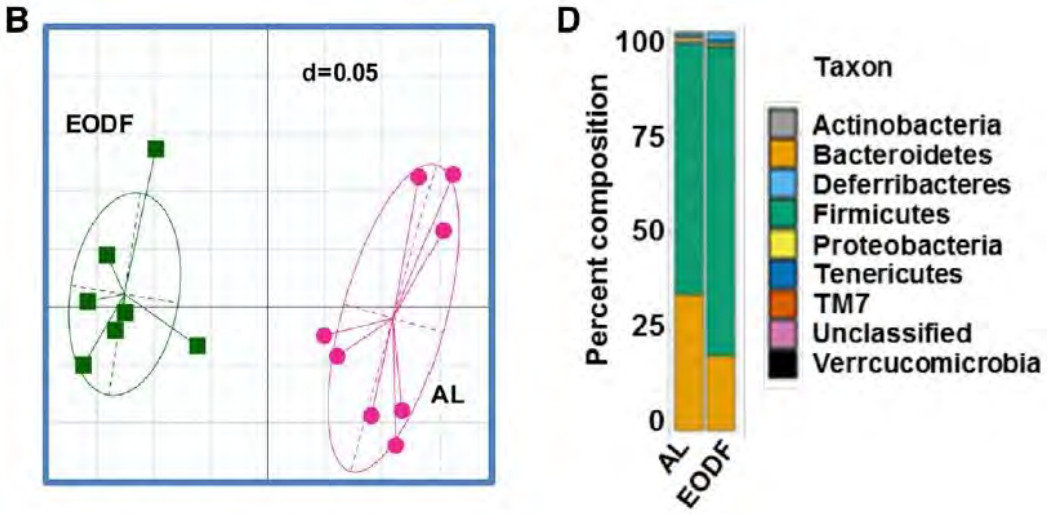

Gut Microbiota Mediates EODF-Induced WAT Beiging.

(**B**) UniFrac distances of AL and EODF mice; (**D**) Hierarchical clustering diagram comparing ceca of AL and EODF mice.

UniFrac distances：是用于比较生物群落的距离度量，利用各样品序列间的进化信息来比较样品在特定的进化谱系中是否有显著的微生物群落差异。

Cell Metab. 2017 Oct 3;26(4):672-685.

解剖代谢表型分析

➢ 脂肪组织内交感神经免疫荧光

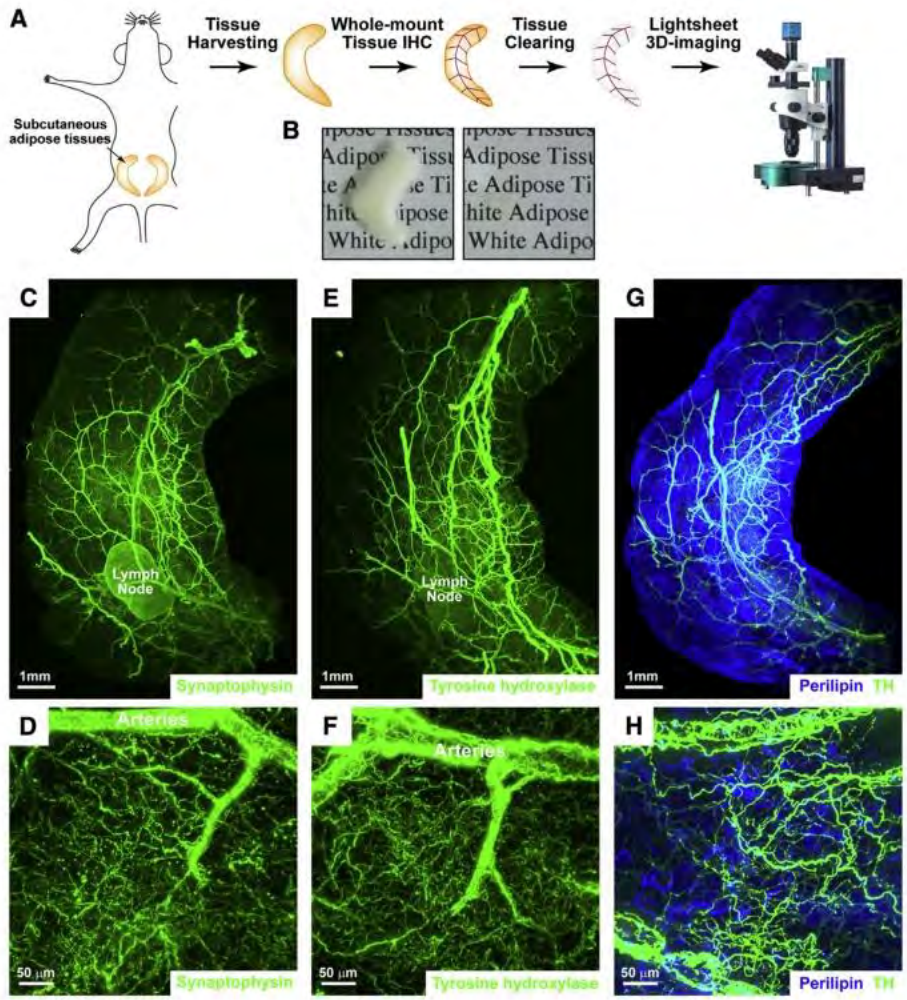

Figure 1. Dense Intra-adipose Sympathetic Arborizations Are Visualized by Volume Fluorescence-Imaging Technique

(A) Flowchart of the whole-mount immunolabeling and volume fluorescence imaging of iWAT.

(B) iWAT of the wild-type mice before (left) and after (right) whole-mount immunolabeling and tissue optical clearing.

(C and D) Representative 3D projections of iWAT immunolabeled by the neuronal marker synaptophysin and imaged at either 1.26× (C) or 10× (D) magnification on the lightsheet microscope.

(E and F) Representative 3D projections of iWAT immunolabeled by the sympathetic marker tyrosine hydroxylase and imaged at either 1.26× (E) or 10× (F) magnification.

(G and H) Representative 3D projections of iWAT co-immunolabeled by tyrosine hydroxylase (green) and the adipocyte marker perilipin (blue) and imaged at either 1.26× (G) or 10× (H) magnification. See also Figure S1 and Movies S1 and S2.

Cell Metab. 2017 Oct 3;26(4):686-692.

解剖代谢表型分析

- ob/ob和db/db小鼠脂肪组织内交感神经纤维显著减少

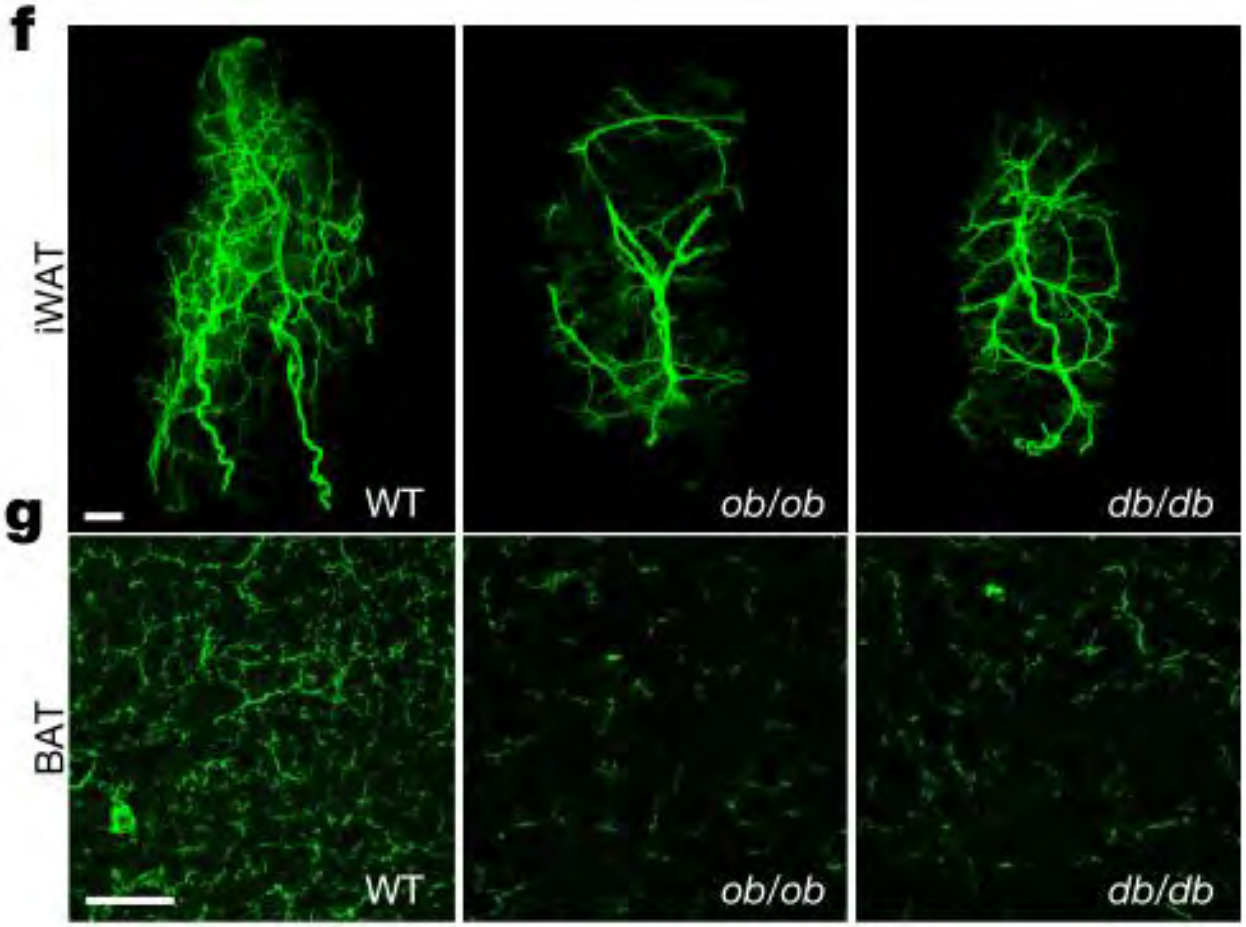

Nature. 2020 Jul;583(7818):839-844.

目 录

分子代谢表型分析

➢ 脂肪和胆固醇代谢通路

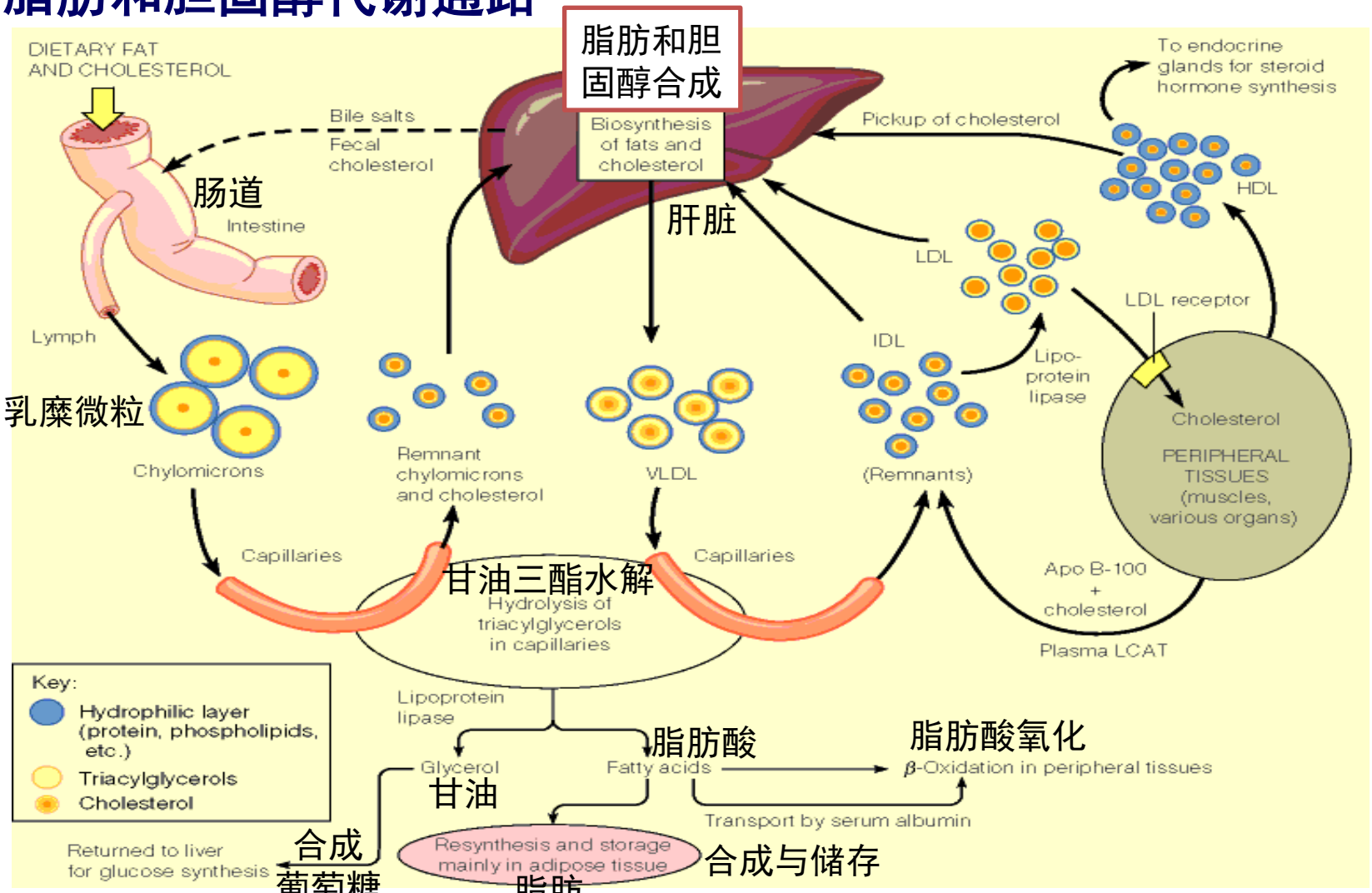

分子代谢表型分析

➢ 脂肪细胞中脂肪酸从头合成

葡萄糖

脂肪酸

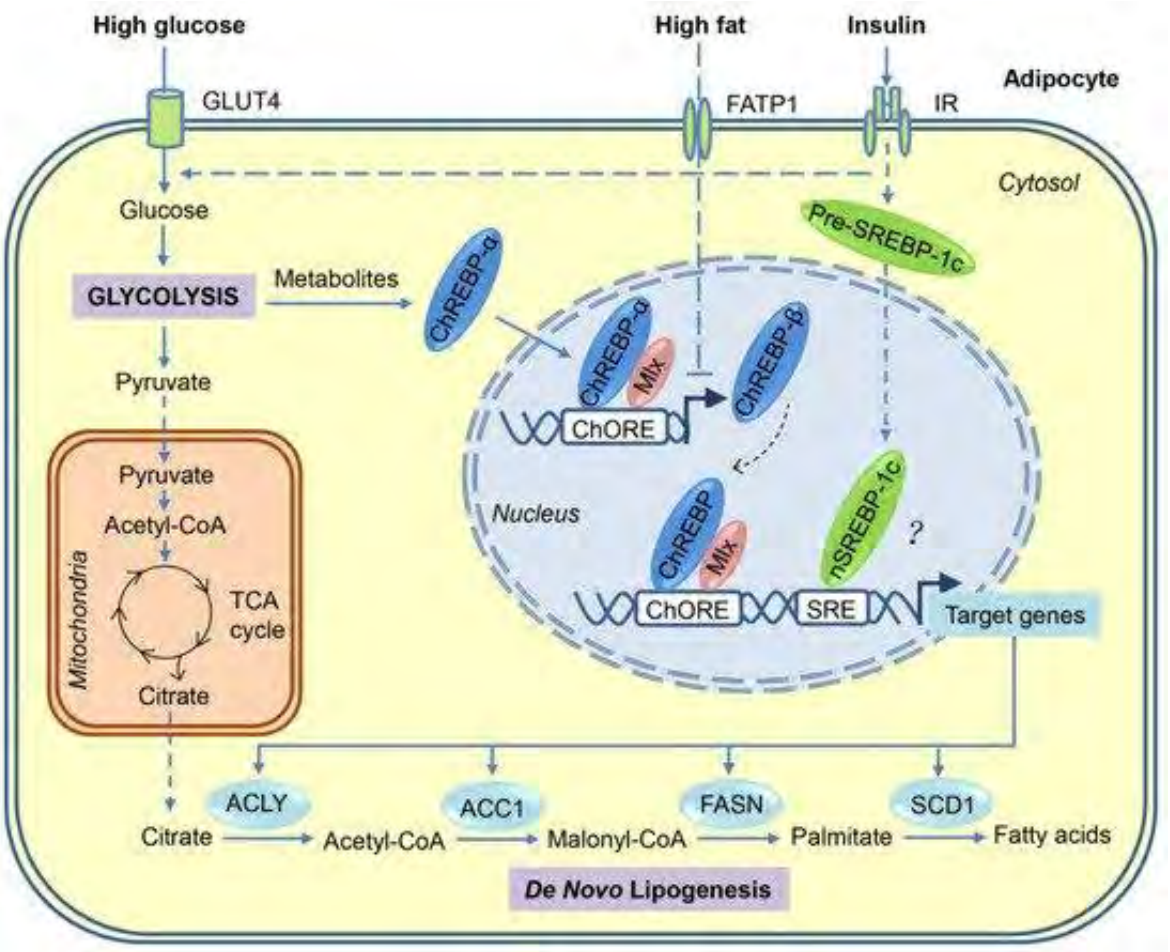

Nutrients. 2018; 10:1383.

分子代谢表型分析

➢ 脂解(Lipolysis)

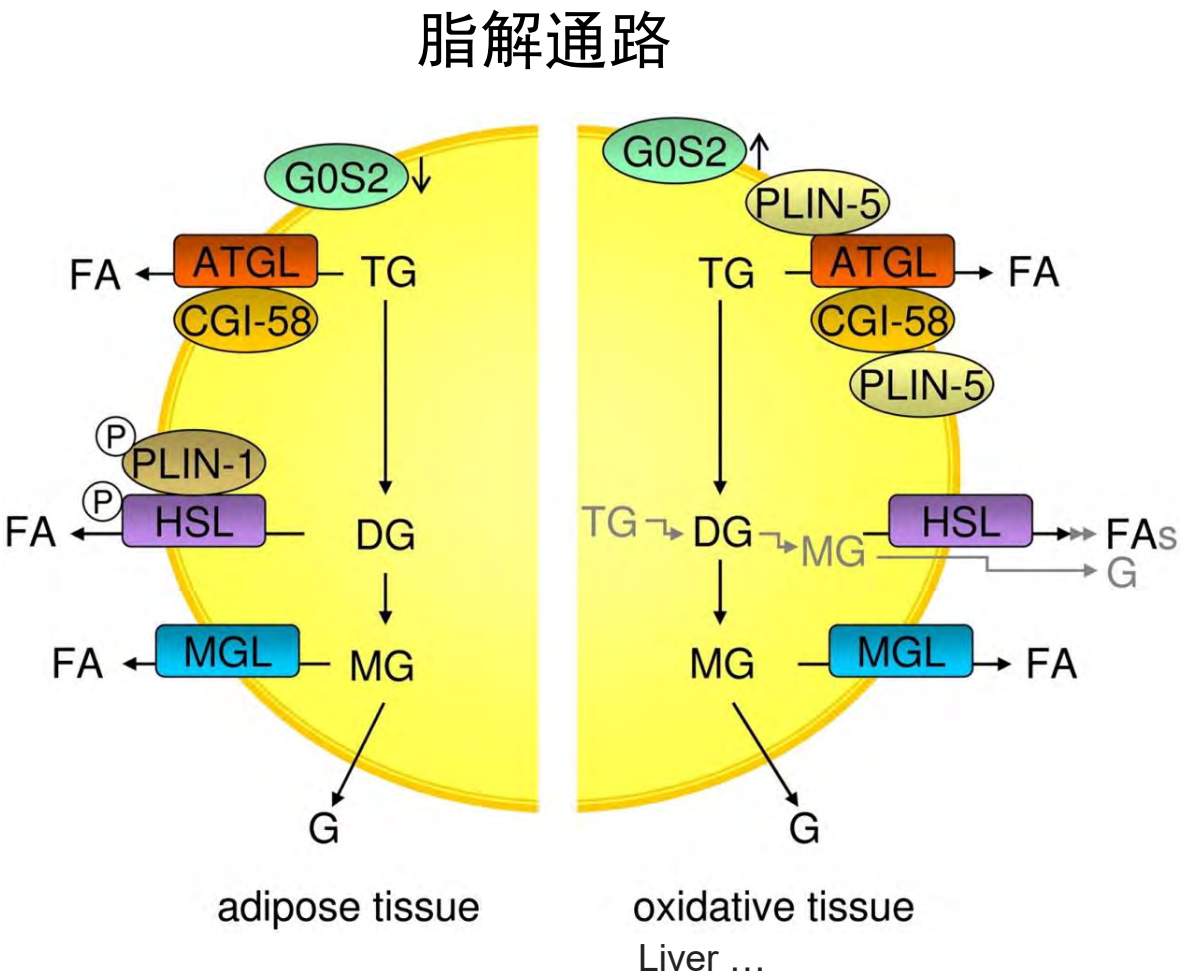

Cell metabolism. 2012; *15*(3):279-291.

分子代谢表型分析

➢ 脂肪酸氧化(fatty acid oxidation)

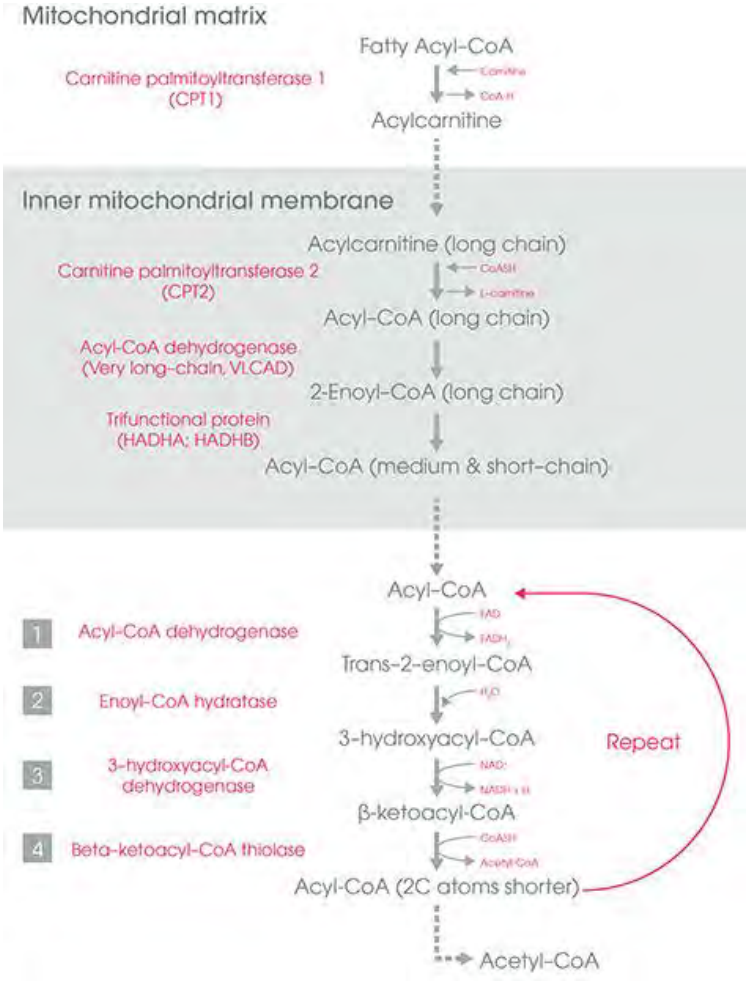

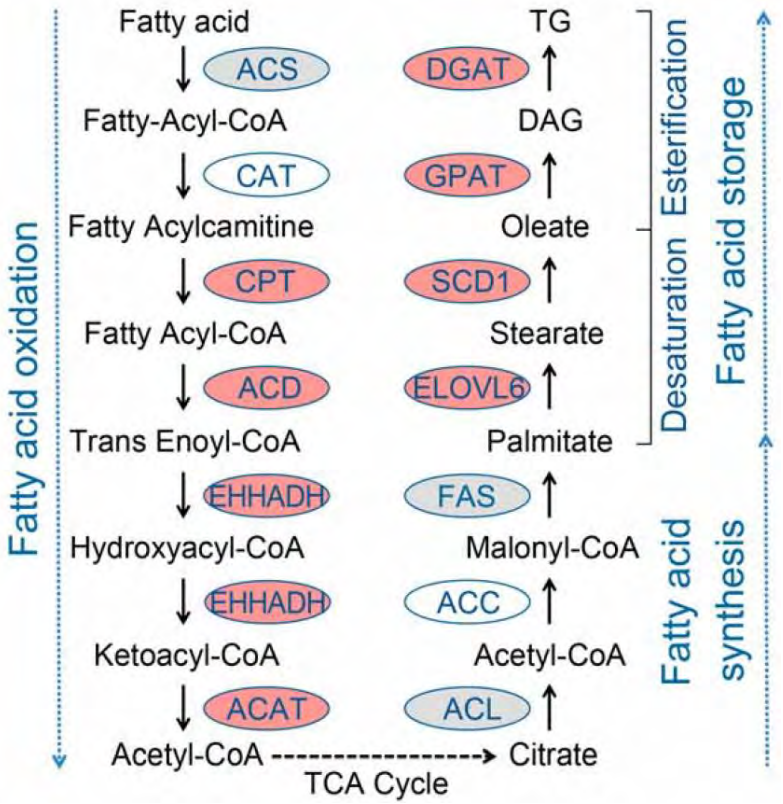

Schematic of fatty acid metabolism and the expression of enzymes directly participated in fatty acid oxidation, synthesis and storage in diabetic mouse liver. Red color represents the enzyme genes upregulated in diabetic mouse liver.

分子代谢表型分析

➢ qPCR/RNA-seq检测关键基因的变化

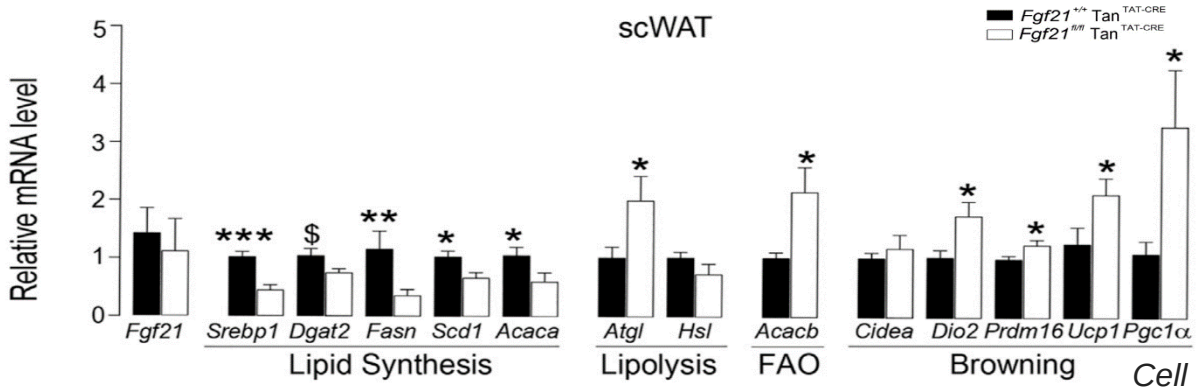

Cell metabolism. 2019; *30*(4), 833-844.

✓ RNA-seq结果的GO、KEGG、网络分析(Ingenuity)等

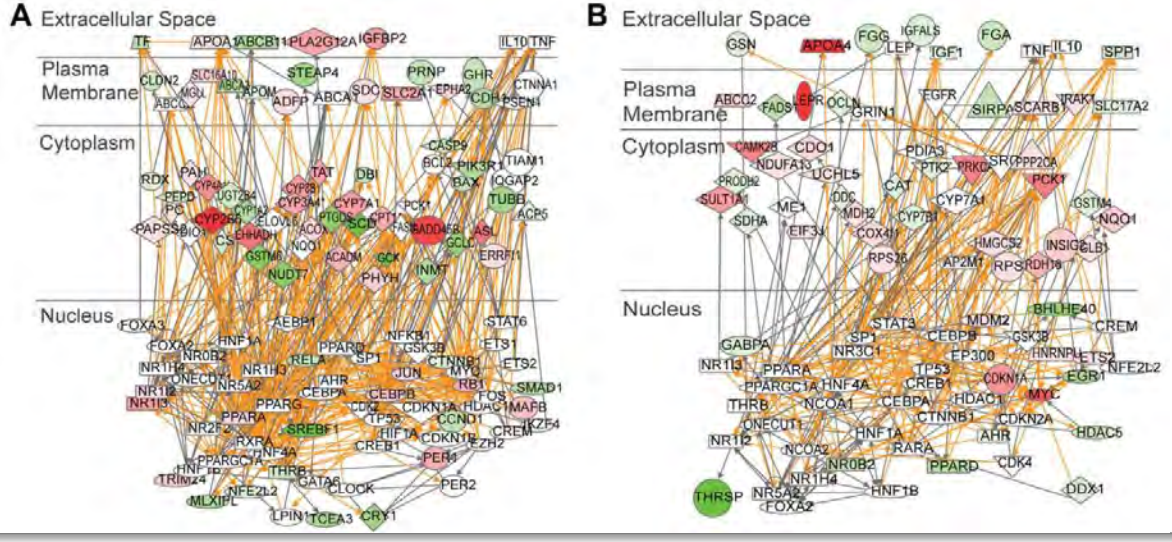

PLoS ONE. 2011; 6(11): e27553

分子代谢表型分析

- **Western、蛋白组学等检测关键蛋白变化**

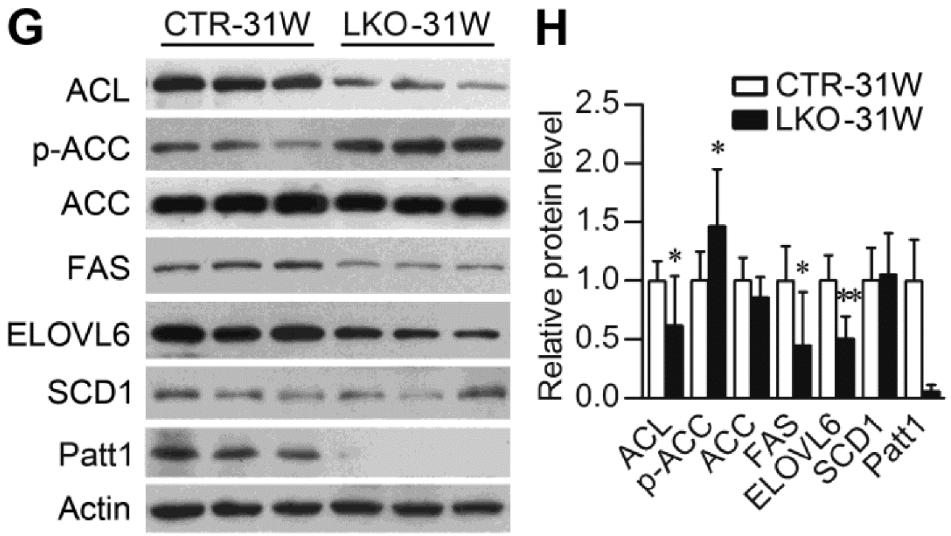

J Lipid Res. 2012; 53(3):358-67.

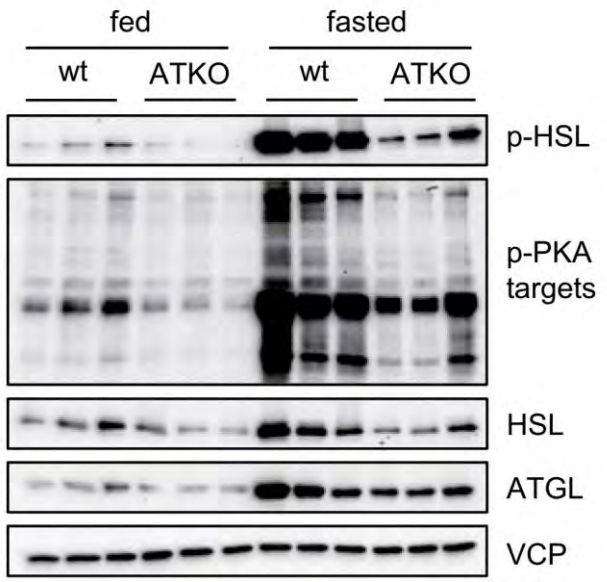

Cell metabolism. 2013; *17*(4):575-585.

分子代谢表型分析

➢ 关键酶活性检测

乙酰辅酶 A 羧化酶(Acetyl-coenzyme A carboxylase, ACC)的酶活力和长链酰基辅酶A合成酶(long chain acyl-CoA synthetase, ACS) 可以通过将ACC的酶活力检测耦合丙酮酸激酶、乳酸脱氢酶，并通过监测NAD水平进行定量分析。
肉碱脂酰转移酶 1 (Carnitine palmitoyltransferase-1, CPT-1) 酶活力的检测可以通过将 CPT-1 的酶活力耦合辅酶A的释放及其与 4, 4'-二硫代联吡啶的反应而进行定量分析。

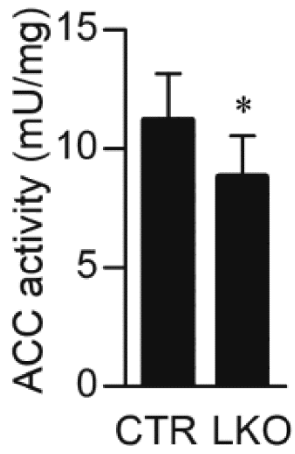

The activity of ACC, the rate-limiting enzyme in lipid synthesis, was attenuated in the liver of male Patt1.

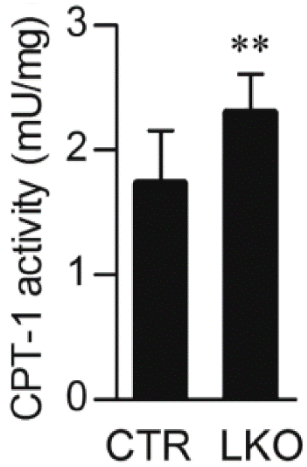

CPT-1 activity in the liver of male Patt1 LKO mice was upregulated.

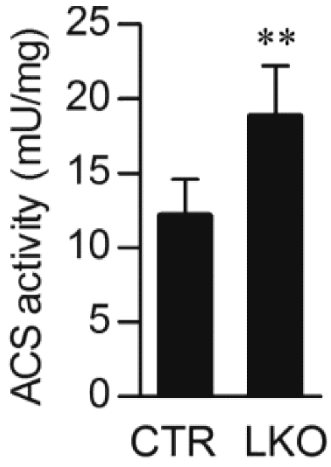

The enzyme activity of ACS, a crucial enzyme catalyzing the pre-step reaction for β-oxidation of fatty acids, was upregulated in the liver of Patt1 LKO mice.

分子代谢表型分析

➢ 脂肪酸摄入、合成、氧化功能实验检测脂代谢变化

在原代培养细胞中加入^{3}H标记的葡萄糖或棕榈酸，培养一段时间(通常为1个小时)。然后收集细胞，加入闪烁液检测^{3}H的放射性。

^{3}H-palmitate

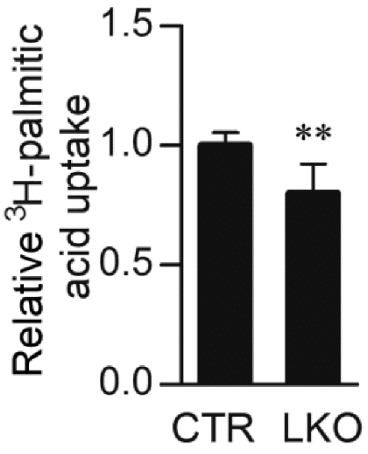

Fatty acid uptake in hepatocytes of Patt1 LKO mice was attenuated as measured by ^{3}H-palmitate incorporation.

^{3}H-Glucose >>> Lipid

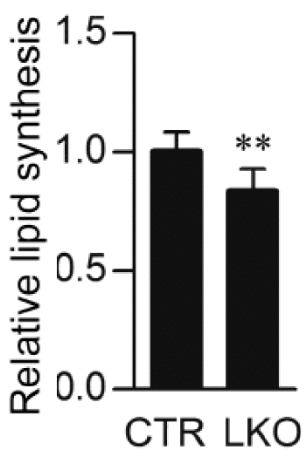

Lipid synthesis in hepatocytes of Patt1 LKO mice was decreased as measured by the incorporation of ^{3}H-glucose into lipid.

^{3}H-palmitate >>> $^{3}H_2O$

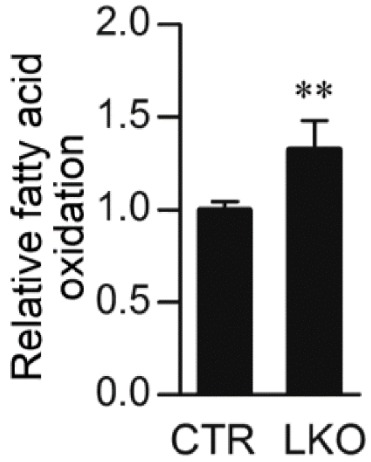

Fatty acid oxidation in hepatocytes of Patt1 LKO mice was increased as determined by the liberation of $^{3}H_2O$ from ^{3}H-palmitic acid oxidation.

分子代谢表型分析

➢ 脂肪酸摄入、合成、氧化功能实验检测脂代谢变化

在原代培养细胞中加入^{3}H标记的葡萄糖或棕榈酸，培养一段时间(通常为1个小时)。然后收集细胞，加入闪烁液检测^{3}H的放射性。

^{3}H-palmitate

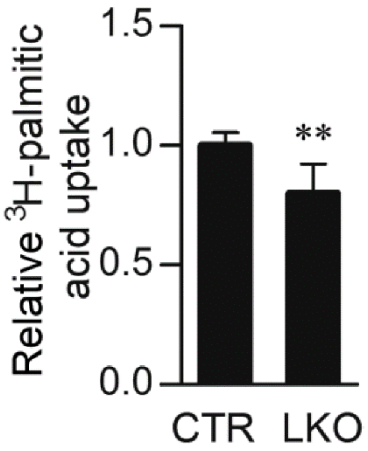

Fatty acid uptake in hepatocytes of Patt1 LKO mice was attenuated as measured by ^{3}H-palmitate incorporation.

^{3}H-Glucose >>> Lipid

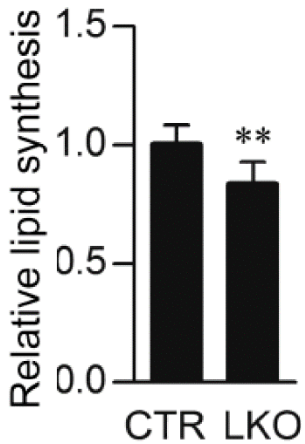

Lipid synthesis in hepatocytes of Patt1 LKO mice was decreased as measured by the incorporation of ^{3}H-glucose into lipid.

^{3}H-palmitate >>> $^{3}H_2O$

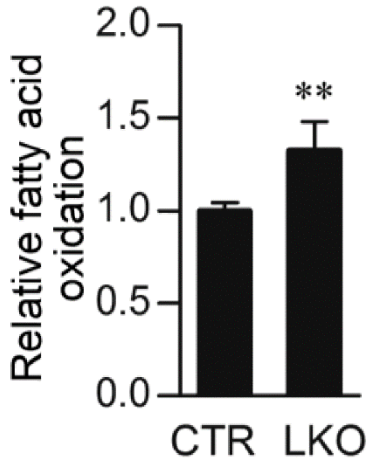

Fatty acid oxidation in hepatocytes of Patt1 LKO mice was increased as determined by the liberation of $^{3}H_2O$ from ^{3}H-palmitic acid oxidation.

荧光标记脂肪酸
^{13}C标记葡萄糖

^{13}C标记葡萄糖

分子代谢表型分析

➢ 白脂米色化和褐脂的白化

两种脂肪组织:白色脂肪组织(white adipose tissue, WAT)和棕色脂肪组织(brown adipose tissue,BAT)。前者为贮存能量,后者在维持体温和能量平衡方面发挥重要作用.

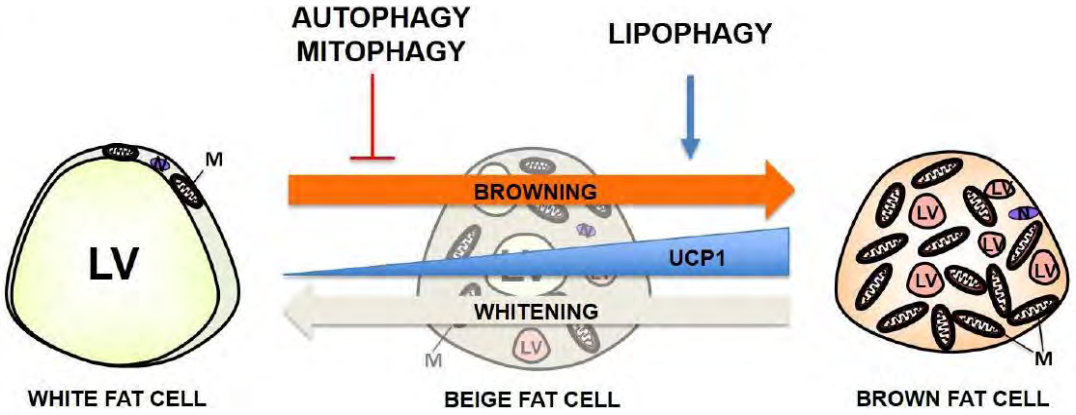

WAT	ANTI - OBESITY	BAT
Single large lipid vacuole	AUTOPHAGY TARGETING DRUGS	Multiple small lipid vacuoles
Small number of mitochondria		Enriched amount of mitochondria
Adipocytokine and FFA release		High level of UCP1
Stores excess energy as fat		Dissipating heat through thermogenesis
Main cause of adiposity, hyperlipidemia and insulin resistance		Low in human patients with obesity or diabetes

分子代谢表型分析

- 白脂米色化过程中UCP1升高。
- 褐色脂肪白色化过程中UCP1水平下降。

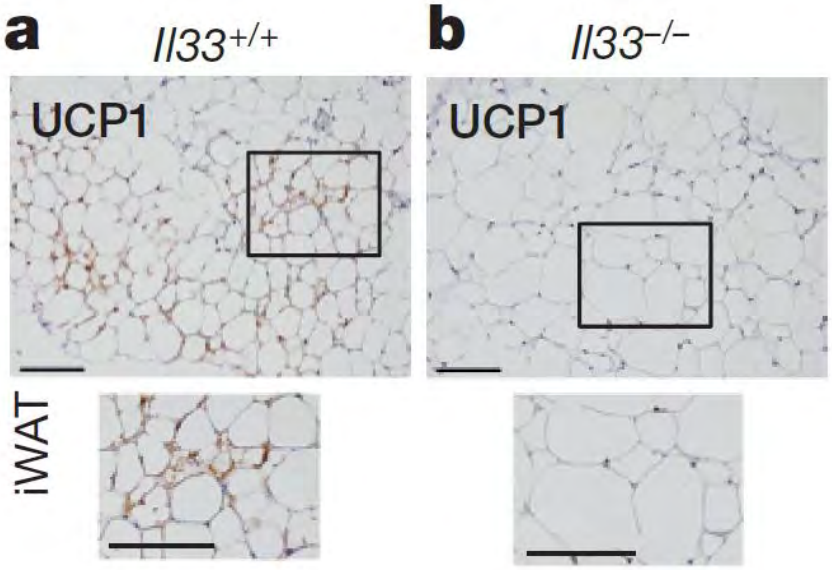

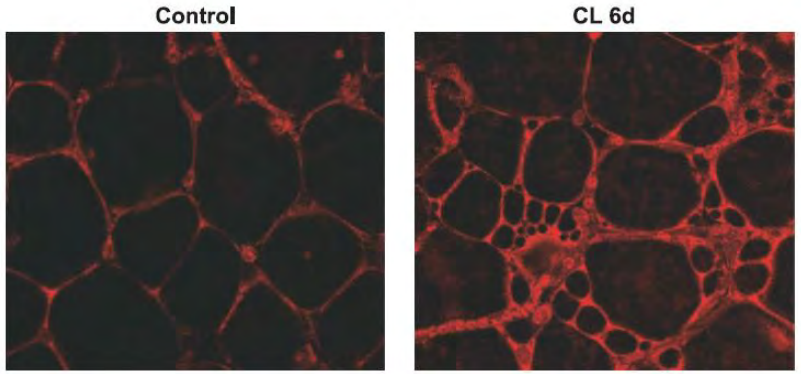

Nature. 519, 242–246,2015

Am J Physiol Endocrinol Metab 2003; 285: E1230–E1236.

分子代谢表型分析

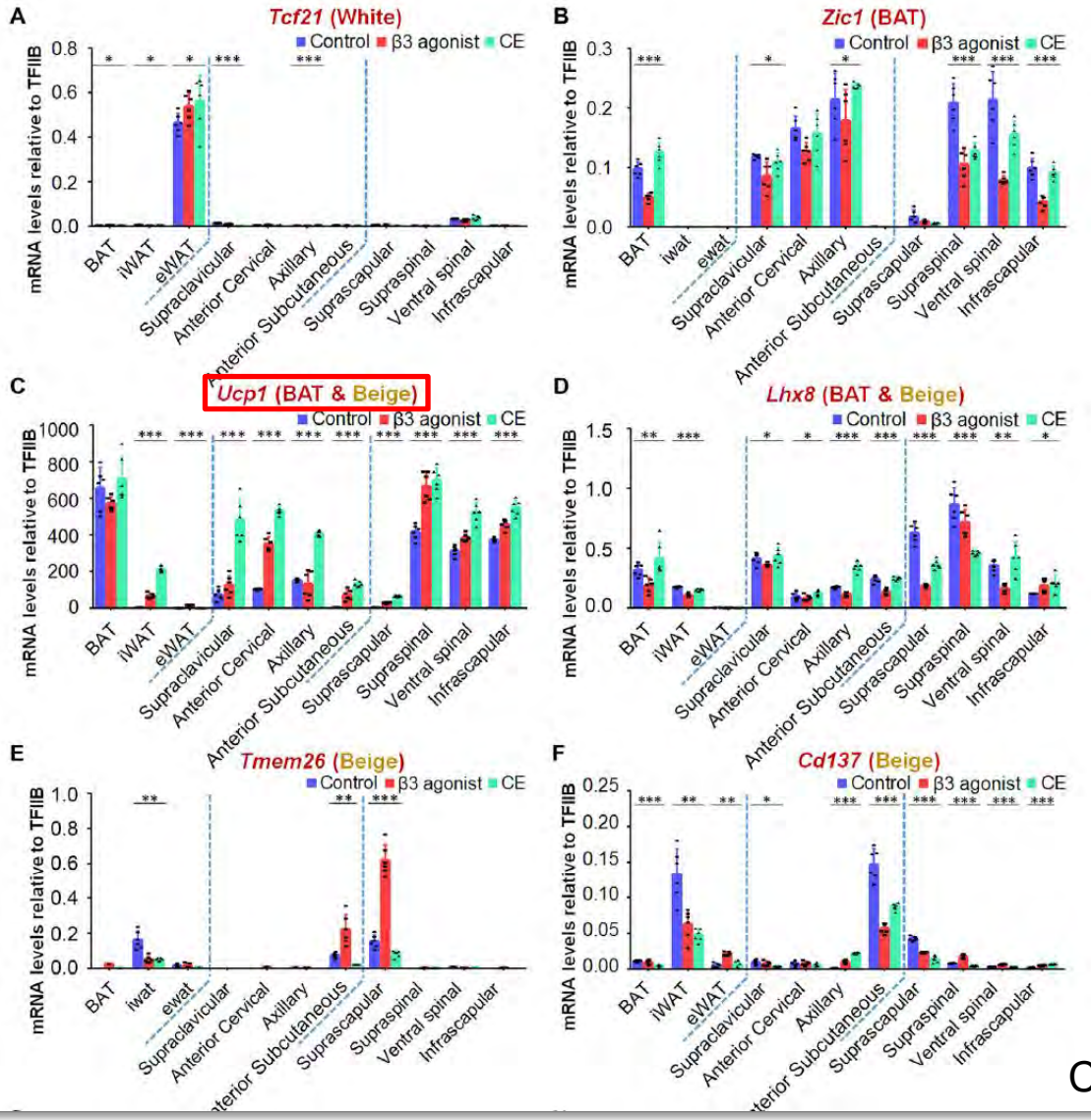

- 不同脂肪组织的分子标记

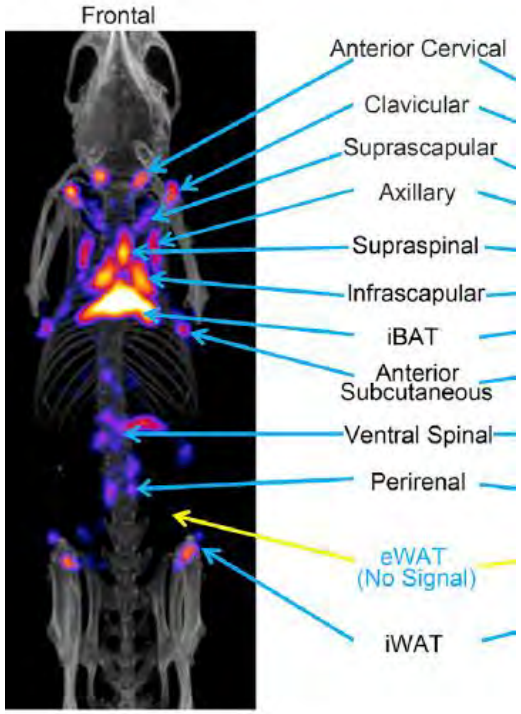

Cell Metabolism. 2018; 27:252–262.

分子代谢表型分析

➢ 糖代谢主要通路(糖酵解、糖异生、糖原合成和分解)

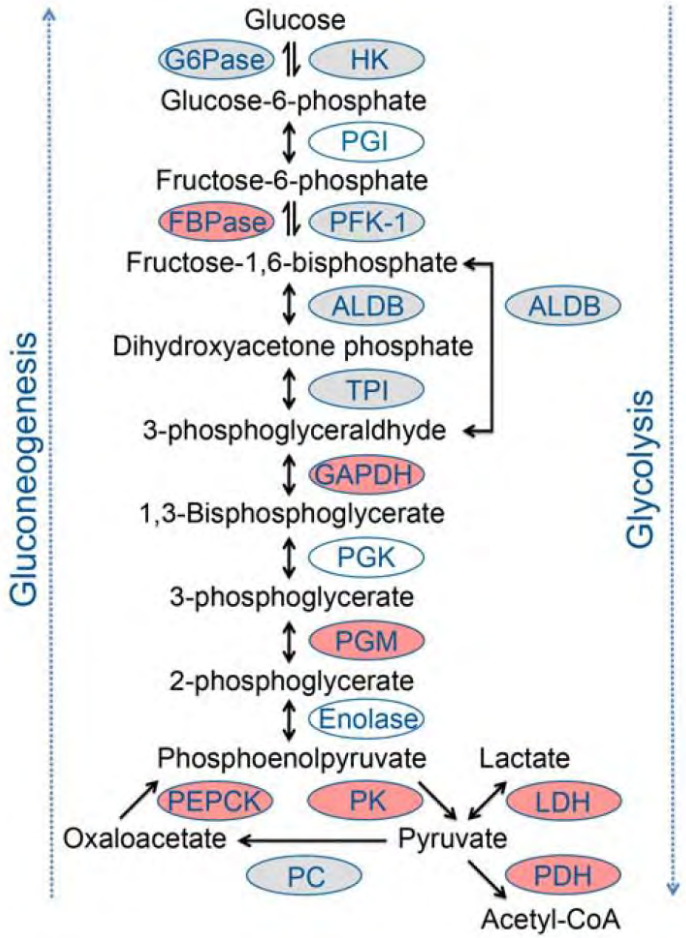

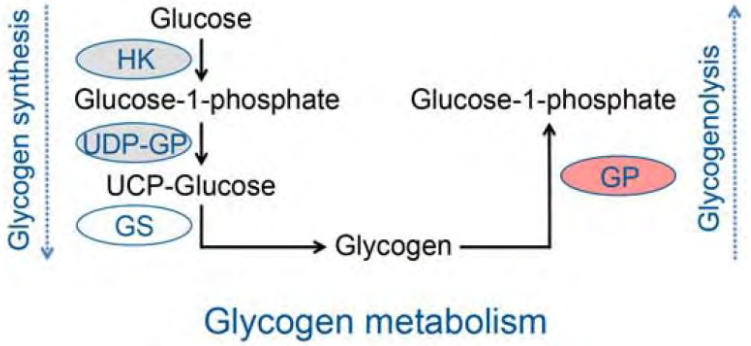

Glycogen metabolism

Schematic of gluconeogenesis, glycolysis and glycogen metabolism, and the expression of enzymes directly participated in these processes of diabetic mouse liver. The key enzymes include HK, PFK-1 and PK for glycolysis, G6Pase, FBPase and PEPCK for gluconeogenesis, HK, UDP-GP and GS for glycogen synthesis, and GP for glycogenolysis.

分子代谢表型分析

➢ 肝脏糖酵解限速酶HK、PFK等的活性检测

通过一系列酶促偶联反应（coupling reaction）,将底物果糖-6-磷酸的消耗转化为NAD的生成，通过检测OD_{340nm}降低即可检测PFK活力。

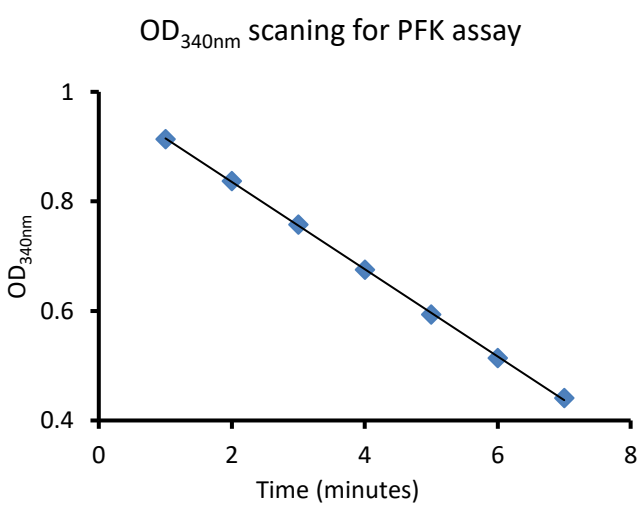

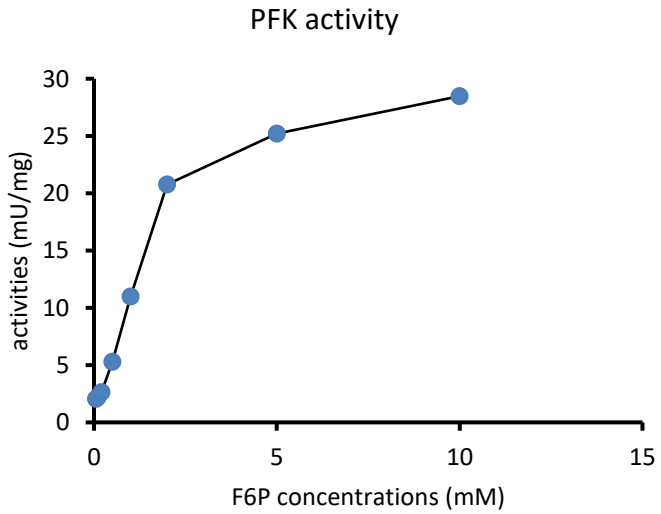

左图：检测到PFK反应的光吸收线性下降
右图：随着底物浓度提高PFK活力逐渐饱和

分子代谢表型分析

- **Seahorse检测细胞糖酵解**

  Seahorse是一种利用光学传感器检测细胞耗氧量(Oxygen comsumption rate, OCR)和胞外酸化率(Extracelluar acidification rate, ECAR)来反应酵解和氧化磷酸化的代谢状况。通常加入葡萄糖、寡霉素、2-脱氧葡萄糖等试剂监测OCR和ECAR变化。

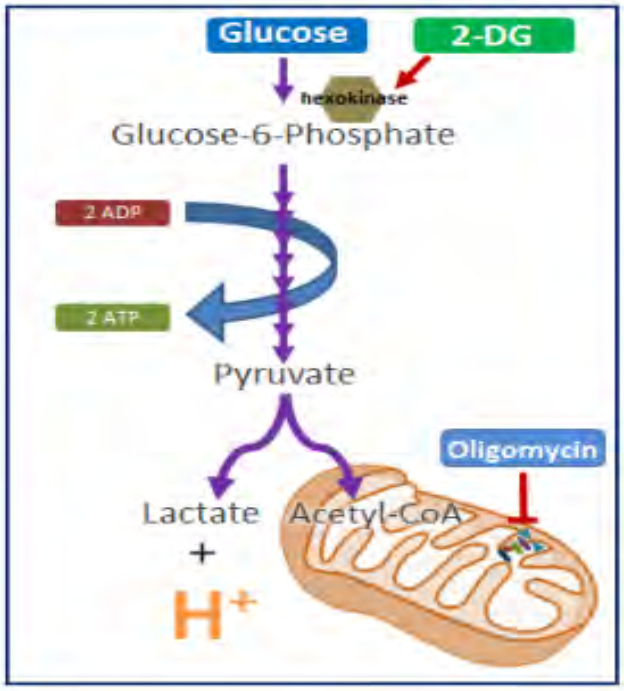

Compound	Description	Effect on ECAR
Glucose	substrate for hexokinase; required for glycolysis	Increase
Oligomycin	binds ATP synthase; inhibits mitochondrial ATP production	Increase
2-deoxyglucose	competitive inhibitor of hexokinase	Decrease

分子代谢表型分析

- **Seahorse检测效果图**

  图中加入glucose后ECAR的升高幅度代表糖酵解活力大小。

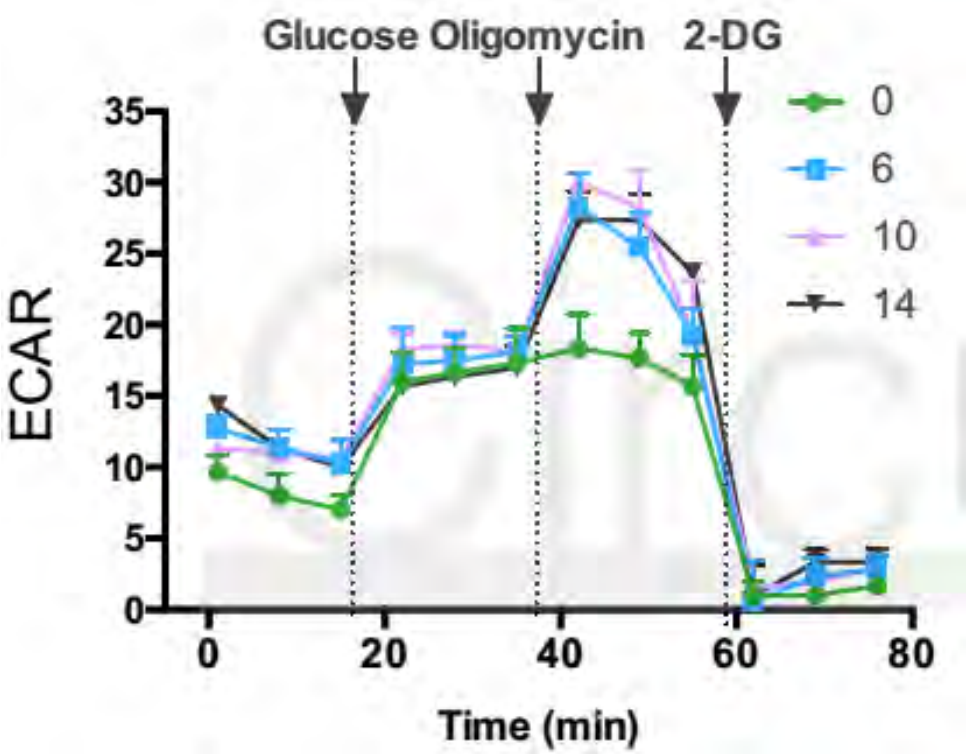

Circulation. 2019 Jan 2;139(1):119-133.

分子代谢表型分析

➢ 组织或细胞糖异生检测(限速酶检测、功能检测)

通常加入乳酸或氨基酸等作为糖异生底物，利用组织或细胞的糖异生能力将之转化为葡萄糖。可以通过比色、氧化电极、同位素质谱等分析手段检测。下图所示为稳定同位素标记的乳酸异生为葡萄糖的示意图。

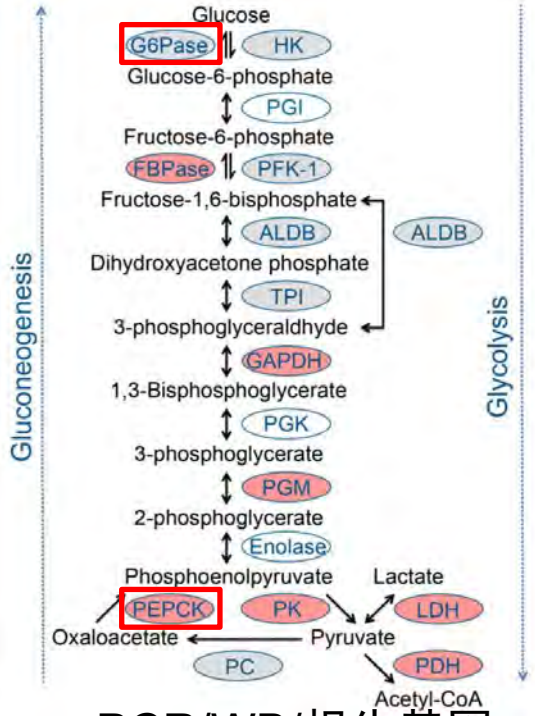

qPCR/WB/报告基因检测PEPCK和G6Pase

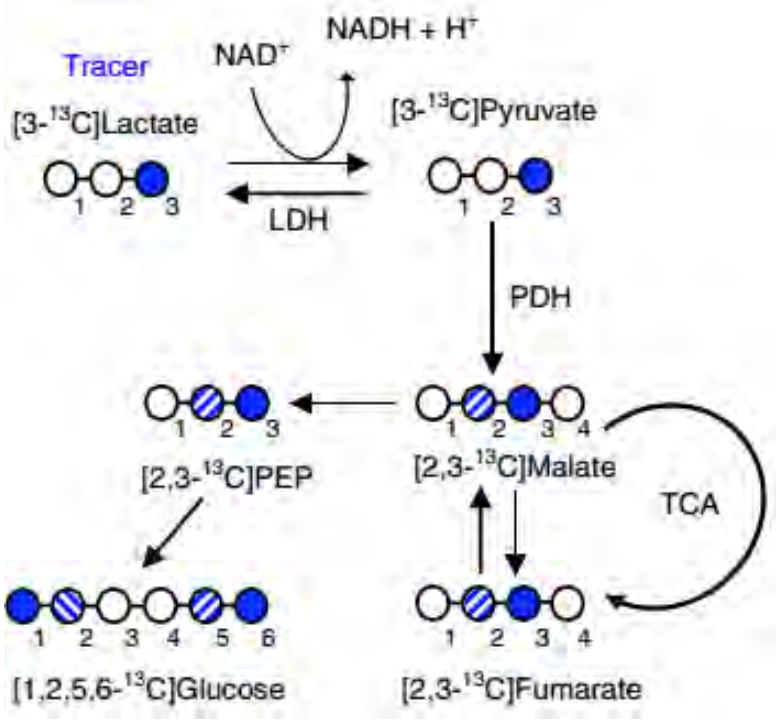

Circulation. 2019 Jan 2;139(1):119-133.

分子代谢表型分析

➢ 组织或细胞糖异生检测

下图所示为metformin处理后，用同位素质谱检测同位素标记的乳酸与氨基酸异生为同位素葡萄糖的比例存在差异，即乳酸与氨基酸的糖异生能力存在差异。

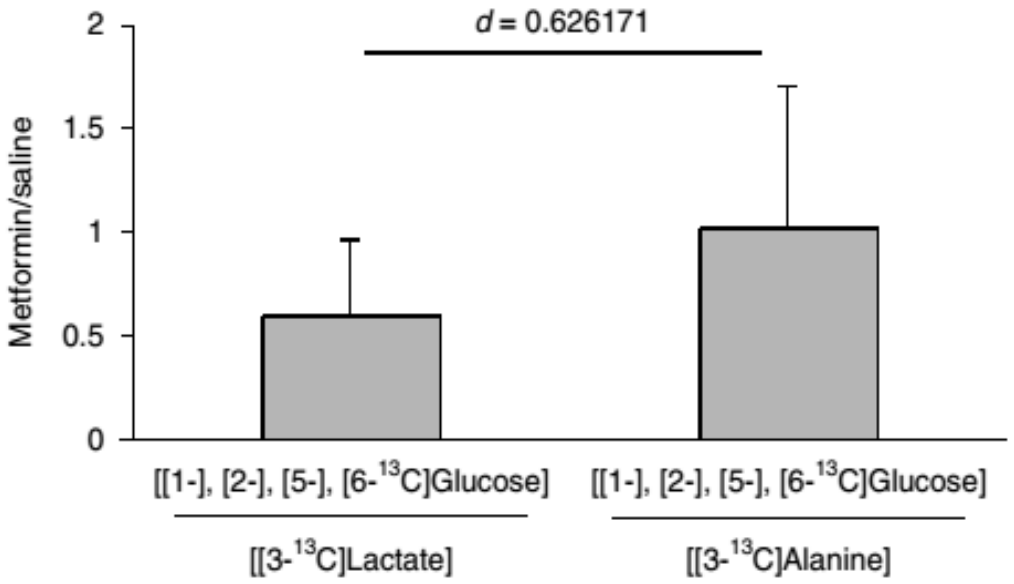

Nat Med. 2018 Sep;24(9):1384-1394.

分子代谢表型分析

➢ 糖原合成能力检测

放射性同位素标记葡萄糖，检测糖原中放射性含量。
糖原合成酶和糖原磷酸酶活性检测等。
糖原含量测定等。

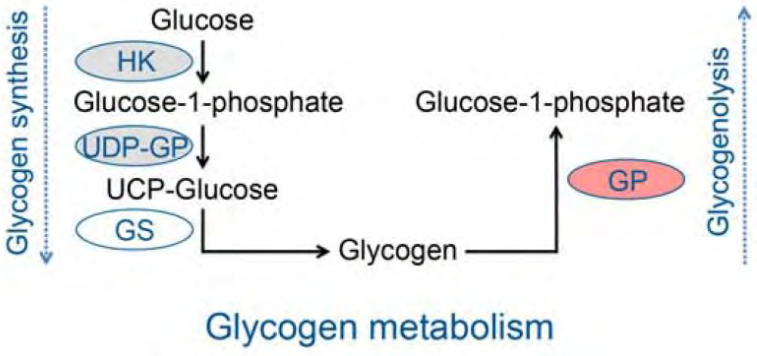

Glycogen metabolism

✓ 蒽酮法检测糖原含量

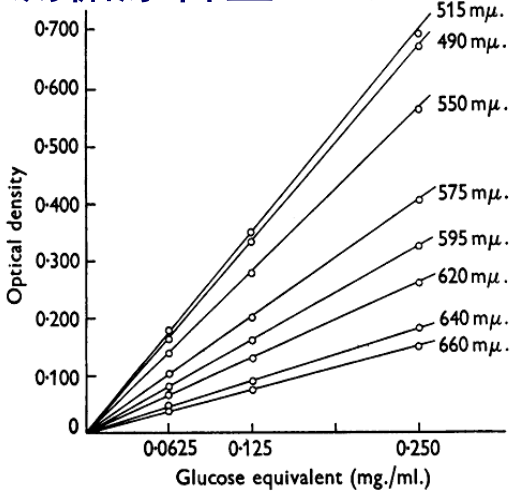

Relations between optical density of a glycogen-iodine complex and glucose equivalent of glycogen at various, mμ(nm).

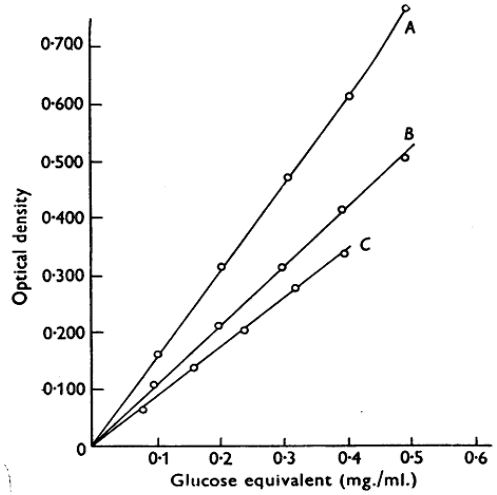

Calibration curves for glycogen from different sources. Optical densities were read at 650nm. A, mouse liver. B, rabbit liver. C. rabbit muscle.

Biochem J. 1954 Jul;57(3):410-6.

分子代谢表型分析

➢ 肠道的摄入与转运

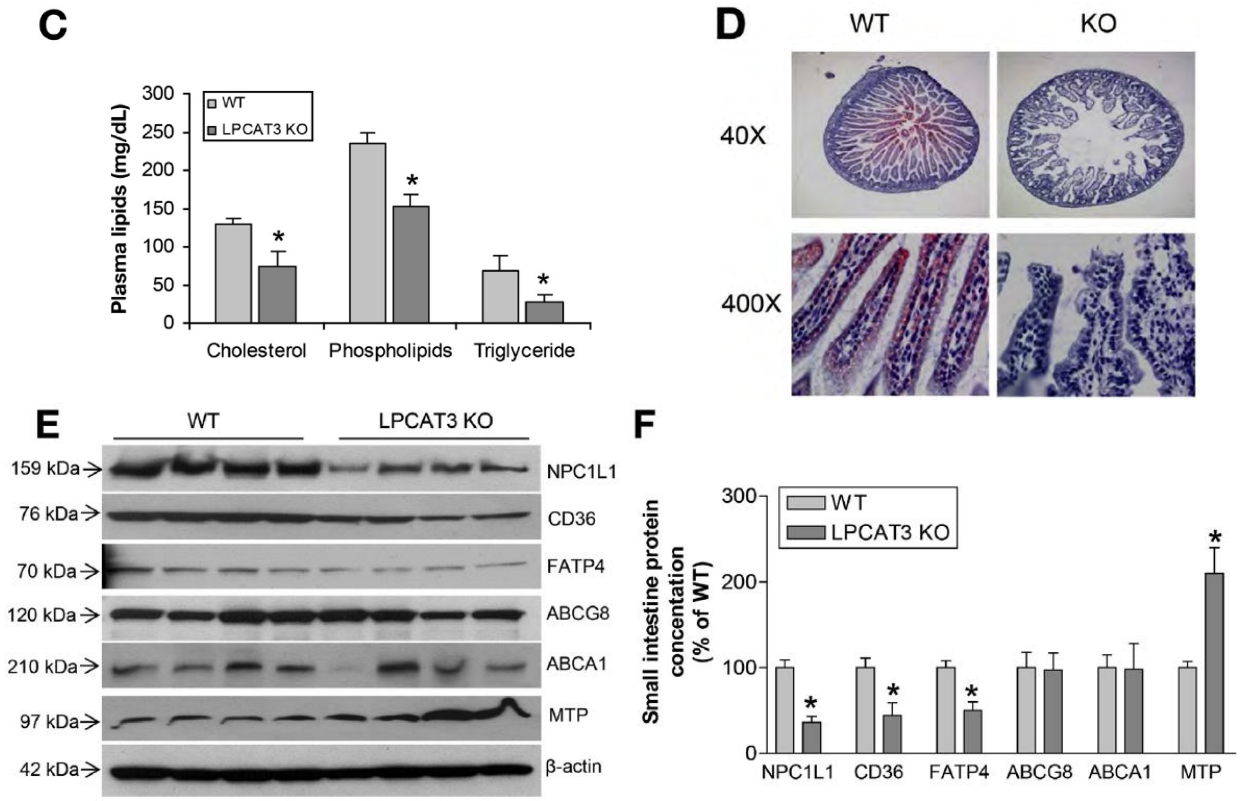

Characterization of LPCAT3 KO mouse. (**C**) Total cholesterol, phospholipid, and triglyceride levels in the plasma from 10-day-old WT and LPCAT3 KO mice. (**D**) Small intestine Oil Red O staining from 10-dayold mice. (**E**, F) Western blots fluorogram and quantitation of NPC1L1, CD36, FATP4, ABCG8, ABCA1, and MTP in enterocyte homogenates from LPCAT3 KO and WT small intestine. β-Actin was used as a loading control.

Gastroenterology. 2015 Nov;149(6):1519-29.

分子代谢表型分析

➢ 肠道菌群与代谢物

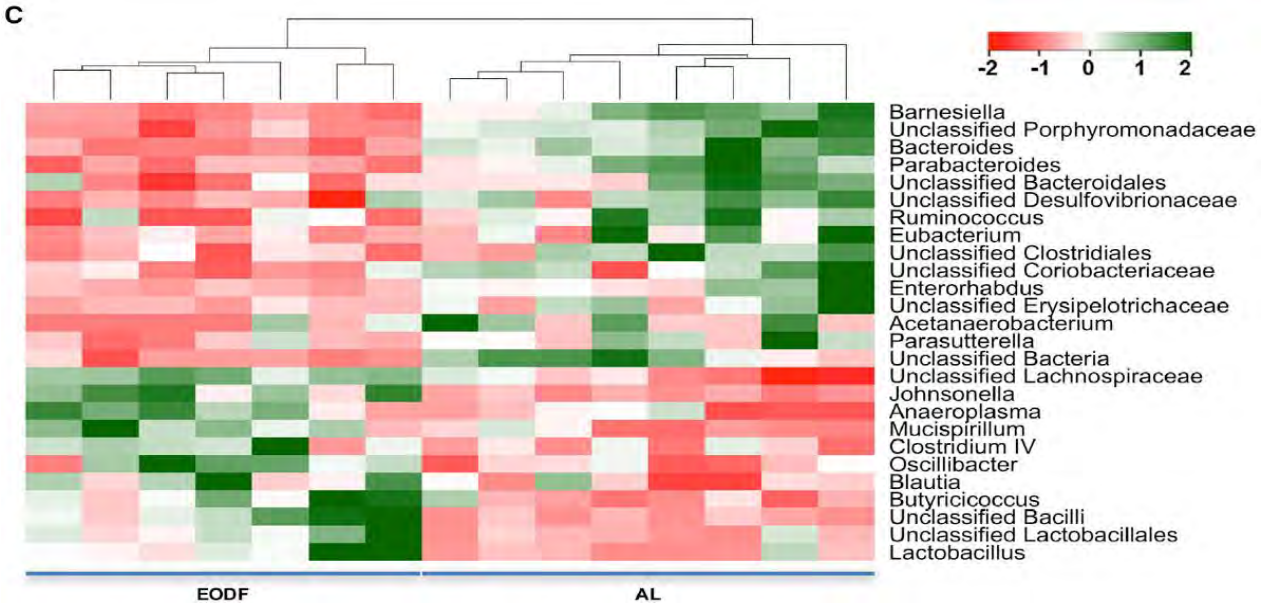

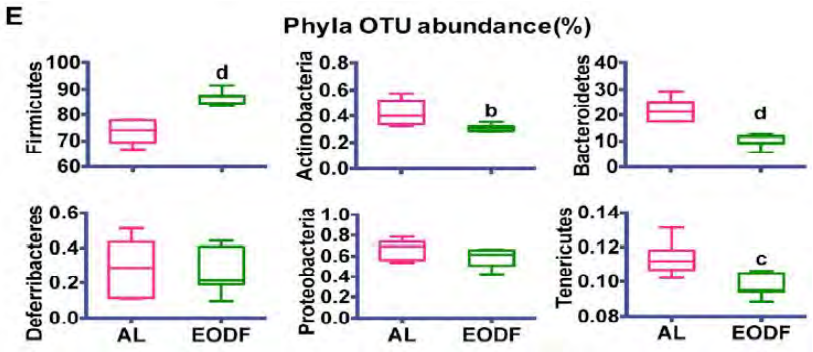

Gut Microbiota Mediates EODF-Induced WAT Beiging. (C) Z scores for genera between AL and EODF mice; (E) Representative Phyla Operational Taxonomic Unit (OTU) abundance (%) of ceca of AL and EODF mice;

Cell Metab. 2017 Oct 3;26(4):672-685.e4.

分子代谢表型分析

➢ 肠道菌群与代谢物

通过核磁共振(NMR)或质谱的方式检测肠道内容物代谢物水平

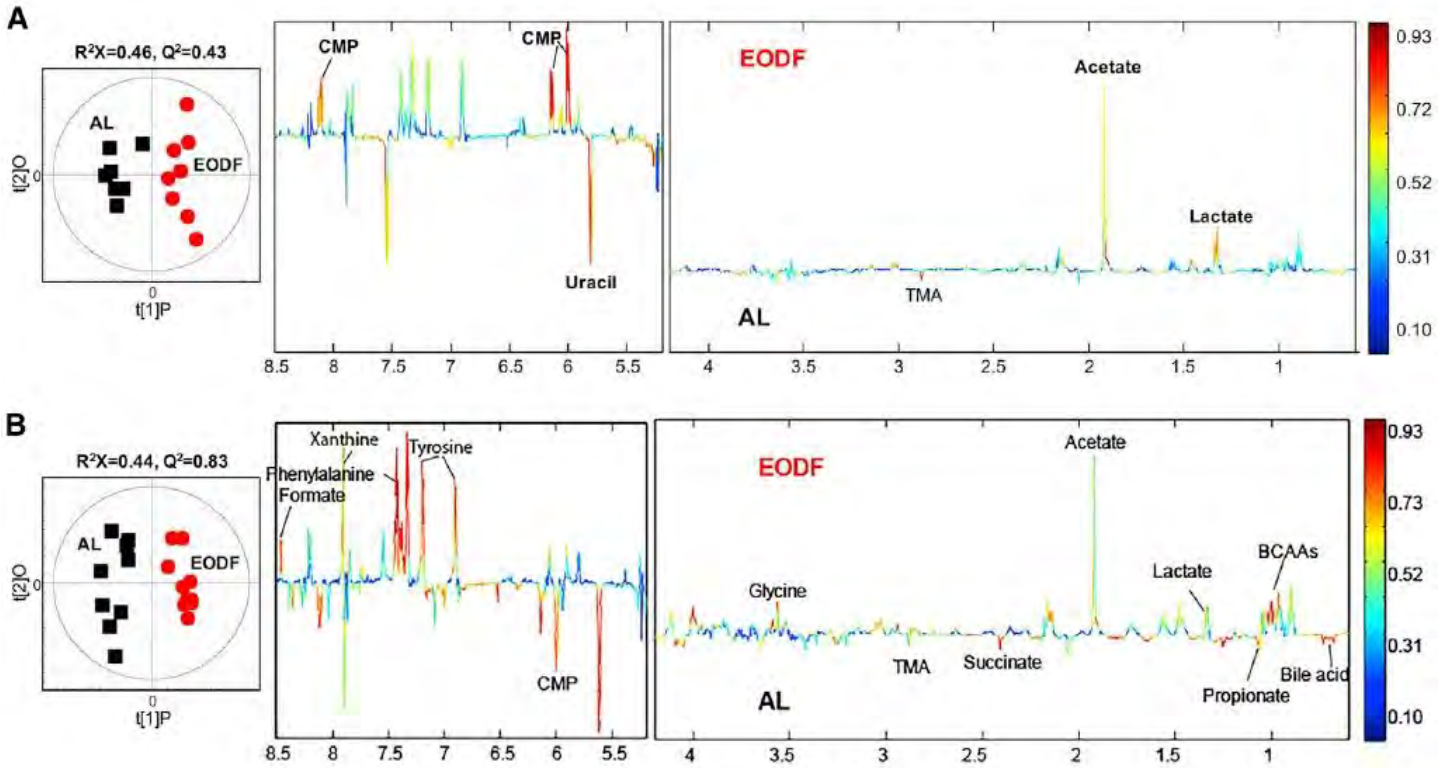

Microbiota Metabolites Underlie the Mechanism of EODF-Induced Beiging. (**A**) Orthogonal projection to latent structure-discriminant analysis (OPLS-DA) scores (left) and correlation-coefficient-coded loadings plots for the models (right) from NMR spectra of cecal content aqueous extracts from mice after long-term EODF treatment; (**B**) OPLS-DA scores (left) and correlation-coefficient-coded loadings plots for the models (right) from NMR spectra of cecal content aqueous extracts from mice after short-term EODF treatment; n = 10 mice/group.

Cell Metab. 2017 Oct 3;26(4):672-685.

分子代谢表型分析

➢ 肠道菌群与代谢物

菌群或差异菌移植，差异代谢物喂养

菌群移植实验

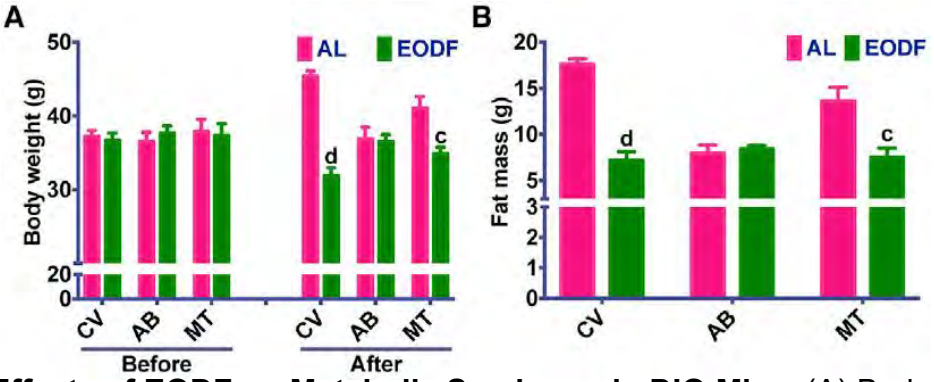

Gut Microbiota Mediates the Effects of EODF on Metabolic Syndrome in DIO Mice. (A) Body weight. Before EODF or microbiota transplantation (MT) treatment, all mice were given access to control vehicle (CV) water or water supplemented with an antibiotics cocktail (AB) for 4 weeks. n = 6–8 mice/group.

代谢物分析

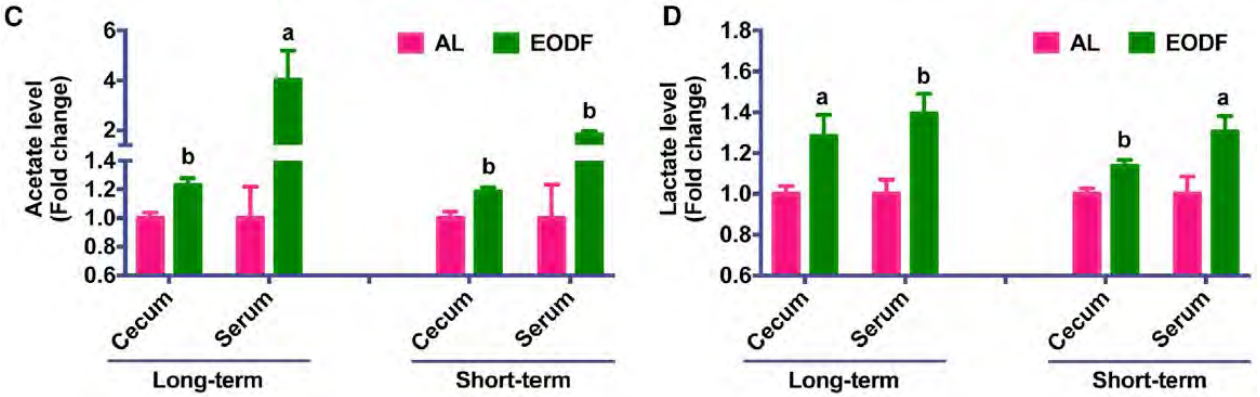

Microbiota Metabolites Underlie the Mechanism of EODF-Induced Beiging. (C and D) Cecum and serum acetate (C) and lactate (D) levels from mice after long-term and short-term EODF treatment. Cell Metab. 2017 Oct 3;26(4):672-685.

代谢的神经调控

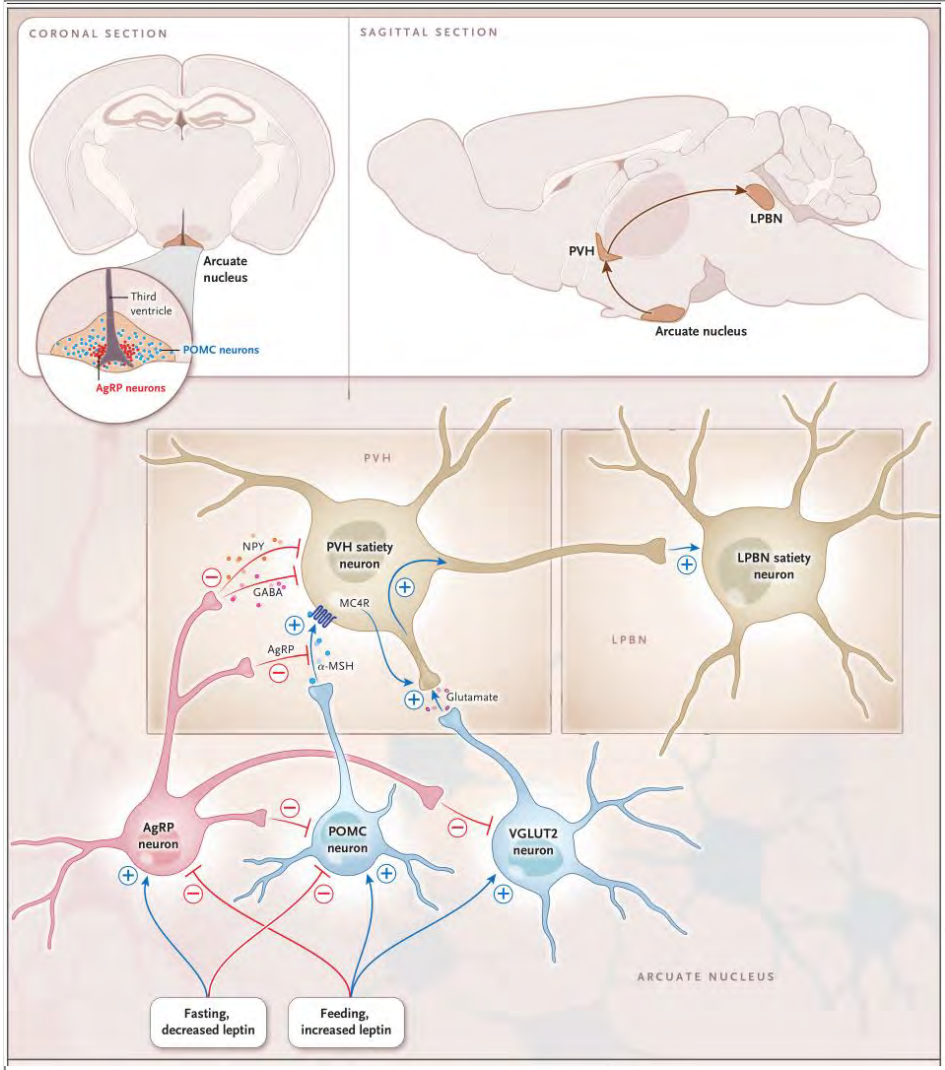

下丘脑多个区域包括弓状核(ARC)、室旁核(PVN)、背内侧核(DMH)、腹内侧核(VMH)以及中脑臂旁核(LPBN)与摄食相关

Figure . Neural Control of Energy Balance and Hunger.
The anatomical location of key structures, the neuronal wiring diagram, and the synaptic mechanisms by which the arcuate nucleus–based system regulates hunger and satiety are shown. Agouti-related peptide (AgRP), proopiomelanocortin(POMC), and vesicular glutamate transporter 2 (VGLUT2) neurons in the arcuate nucleus project to and regulate the activity of melanocortin 4 receptor (MC4R)–expressing satiety neurons in the paraventricular nucleus of the hypothalamus (PVH). These PVH satiety neurons then project to and regulate the activity of satiety neurons in the lateral parabrachial nucleus (LPBN). α-MSH denotes alpha melanocyte-stimulating hormone, GABA γ-aminobutyric acid, and NPY neuropeptide Y.

N Engl J Med. 2019; 380:459-471

代谢的神经调控

- 下丘脑弓状核(ARC)、室旁核(PVN) 、背内侧核(DMH)、腹内侧核(VMH)以及中脑臂旁核(LPBN)等与摄食相关

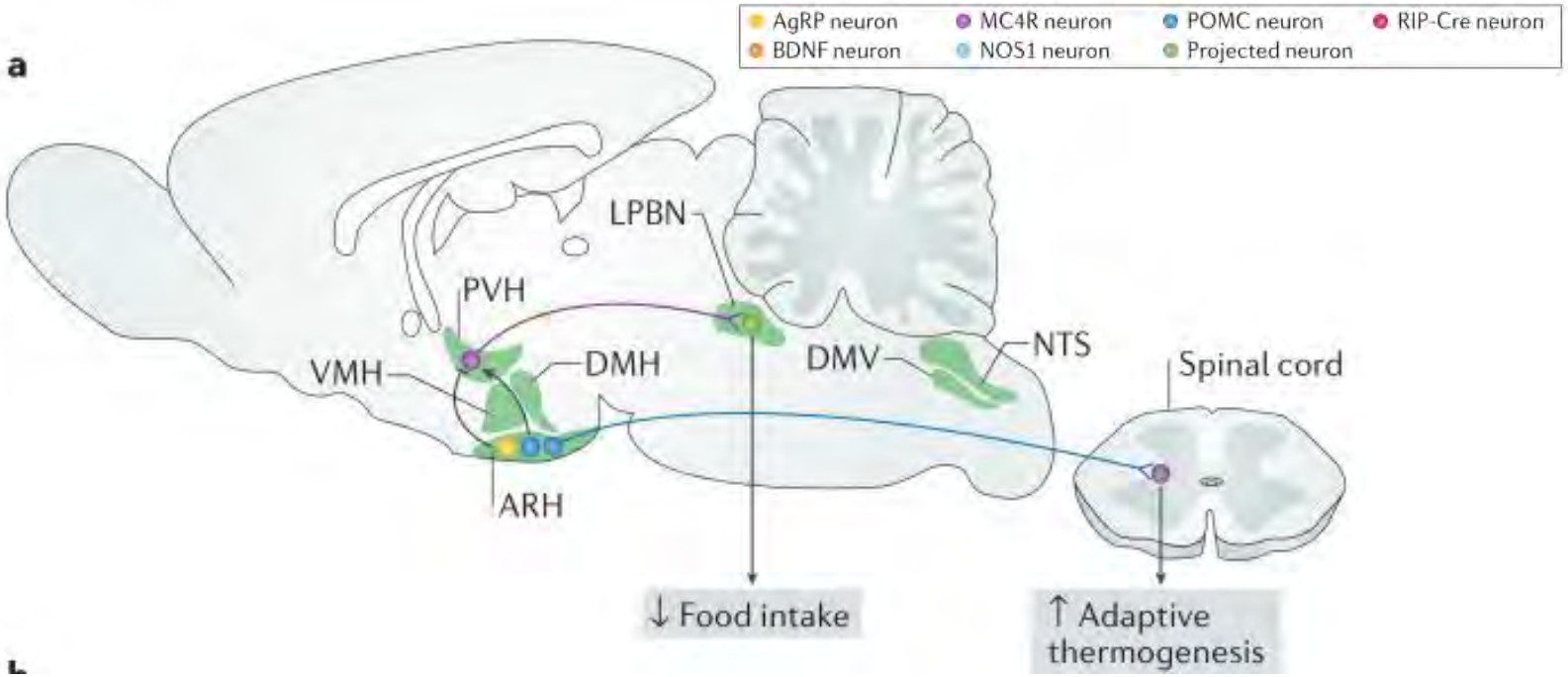

Neural circuits that mediate the effect of melanocortin on food intake and energy expenditure are shown. Proopiomelanocortin (POMC) neurons and agouti-related peptide (AgRP) neurons in the arcuate nucleus of the hypothalamus (ARH) regulate food intake through stimulating or inhibiting lateral parabrachial nucleus (LPBN)-projecting melanocortin 4 receptor (MC4R)-expressing neurons in the paraventricular hypothalamus (PVH),respectively. POMC neurons that project to the spinal cord stimulate adaptive thermogenesis in brown adipose tissues through the MC4R in sympathetic preganglionic neurons that are located in the intermediolateral column (IML).

Nature Reviews Neuroscience 2016; 17:282-292.

代谢的神经调控

➢ ARC区pomc神经元敲除Lepr导致摄食量增加引起肥胖

The ARC contains orexigenic NPY/AGRP and anorexigenic CART/POMC neurons, which are direct leptin targets

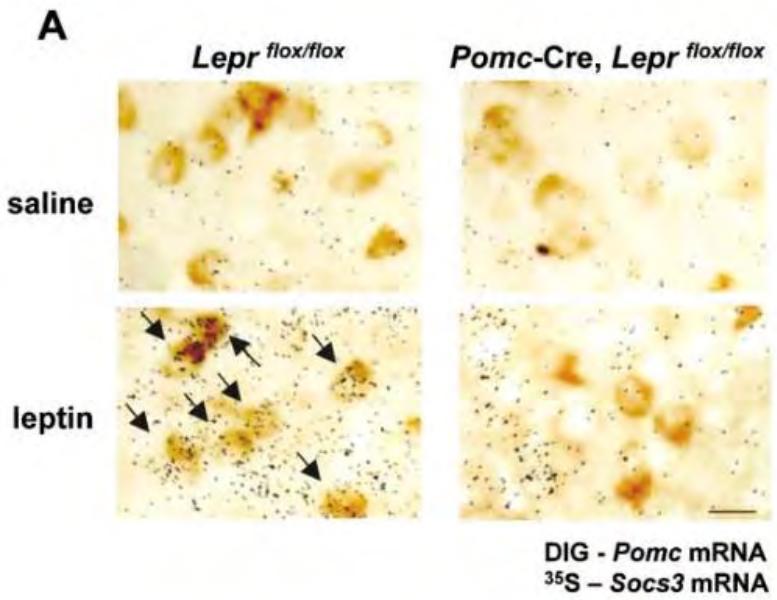

Representative in situ hybridization for Pomc (DIG, brown stain) and Socs3 (35 S, silver grains) mRNA.

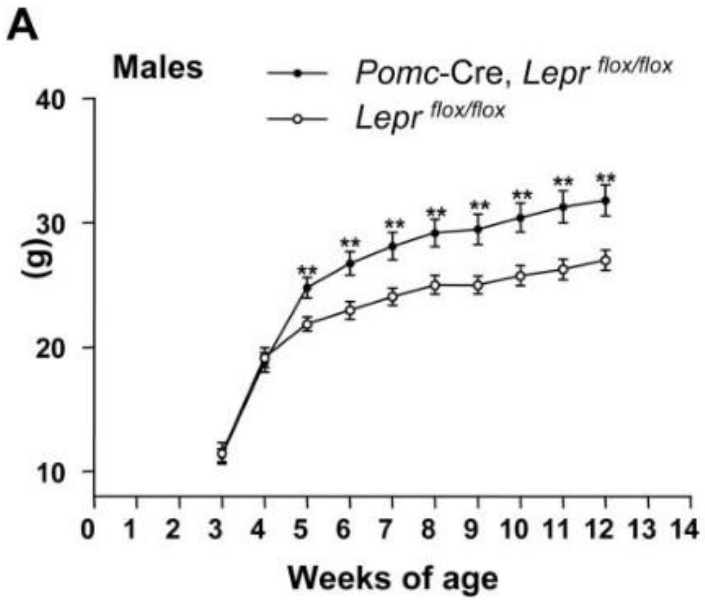

Body weight curve of male Lepr flox/flox and Pomc-Cre, Lepr flox/flox mice.

Neuron. 2004; 6:983-991.

代谢的神经调控

➢ 敲除PVN区BDNF导致摄食量增加引起肥胖

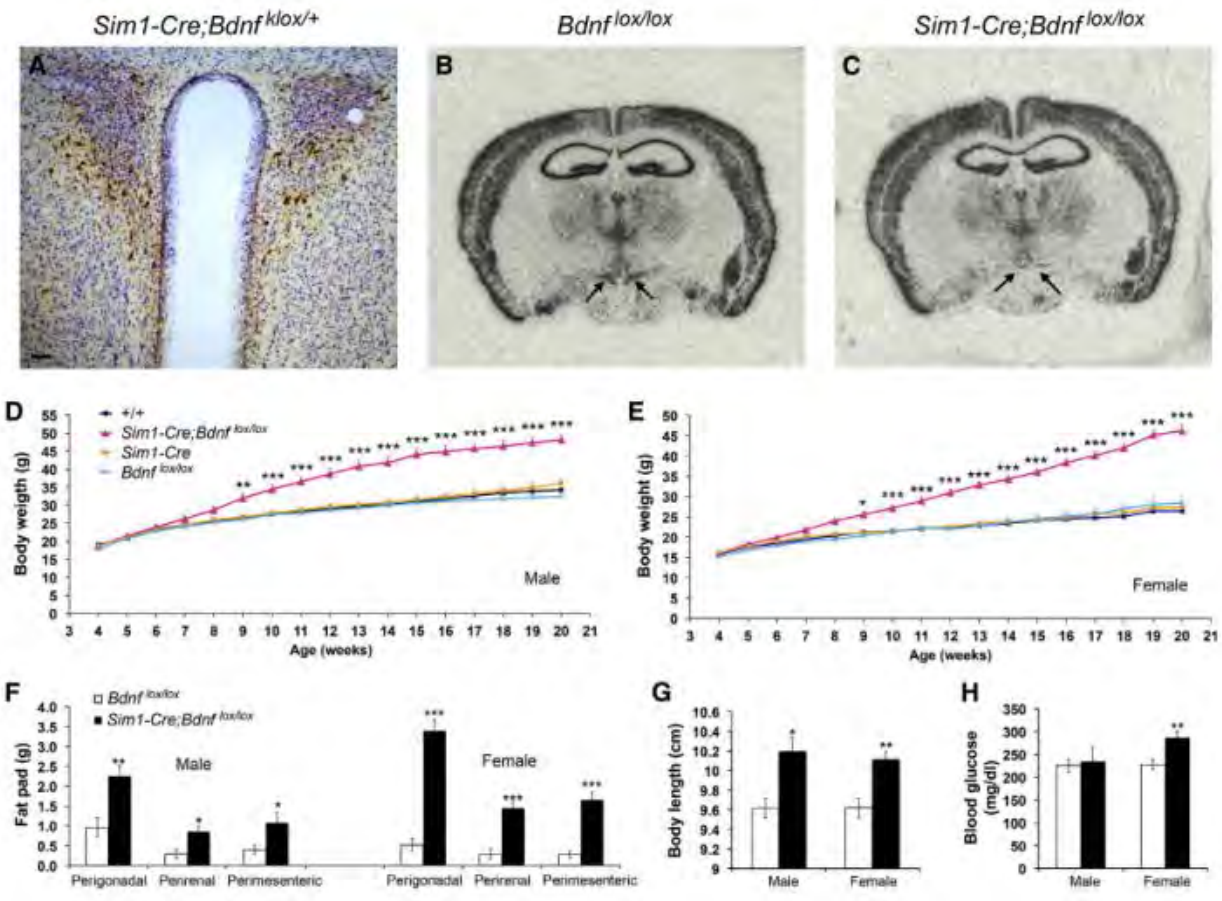

Deletion of the Bdnf Gene in the PVH Using the Sim1-Cre Transgene. (A) Immunohistochemistry image showing b-galactosidase-expressing neurons in the PVH of Sim1-Cre;Bdnf klox/+ mice. The brain section was counterstained with Nissl.
(B and C) In situ hybridization of Bdnf mRNA revealing abolishment of Bdnf gene expression in the PVH of Sim1-Cre;Bdnf lox/lox mice at 4 months of age.Arrows denote the PVH.

(D) Body weight of male Sim1-Cre;Bdnf lox/lox mice and littermate controls. Two-way ANOVA indicates a significant effect of genotypes on body weight:
(E) Body weight of female Sim1-Cre;Bdnf lox/lox mice and littermate controls. (F–H) Fat pad mass, body length, and blood glucose levels in Bdnf lox/lox mice and Sim1-Cre;Bdnf lox/lox mice at 20 weeks

Cell Metab. 2015 Jul 7;22(1):175-88.

代谢的神经调控

➢ 敲除VMH区AC3导致摄食量增加引起肥胖

Hypothalamic nuclei, including ventromedial hypothalamus (VMH), have been demonstrated to have specific functions in the regulation of energy balance. Evidence from human studies and transgenic mice lacking the type 3 adenylyl cyclase (AC3) indicates that AC3 plays a role in the regulation of body weight.

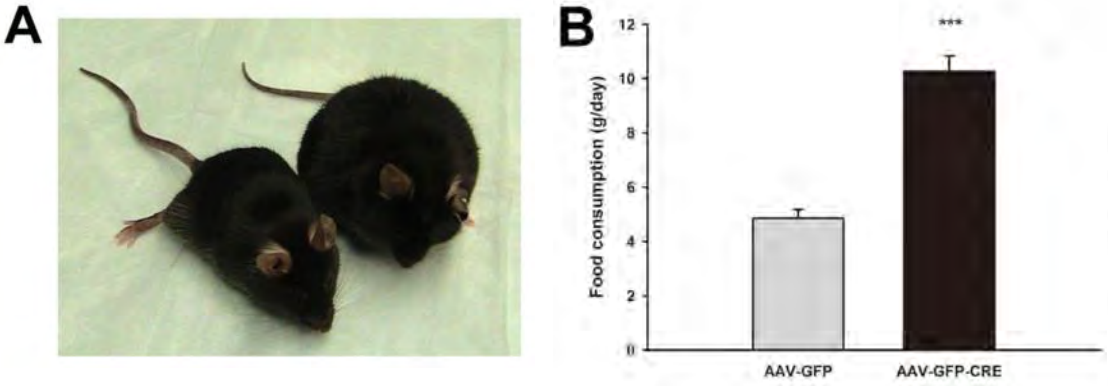

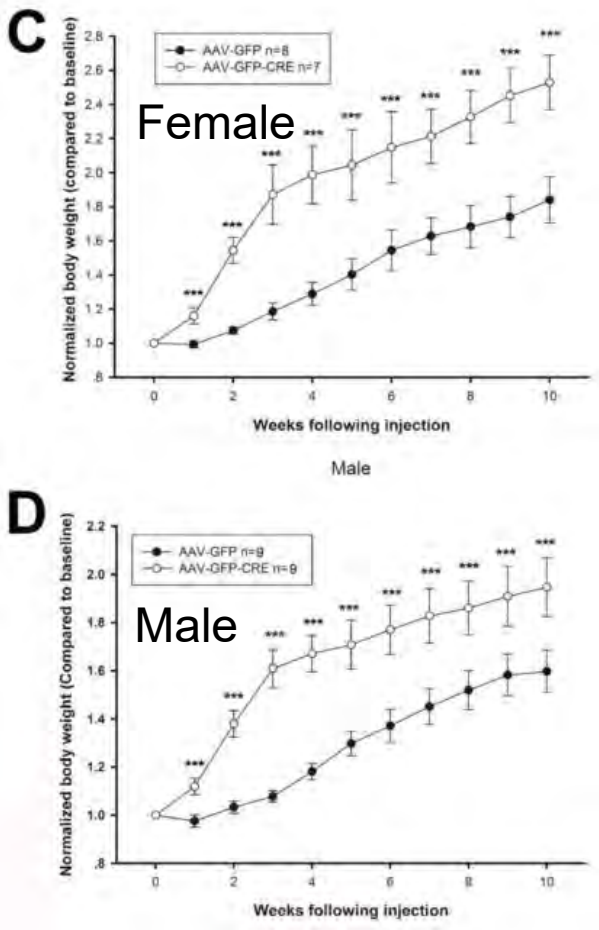

AC3 in the hypothalamus contributes to obesity.
A.Representative mice **at weeks 10 after AAV-GFP and AAV-GFP-CRE injections**. B. Daily food consumption of AC3 lox/lox mice with AAV-GFP and AAV-GFP-CRE injections. C-D. Body weight in female (C), Male (D)mice after introhypothalamus injection of AAV-GFP and AAV-GFP-CRE.

Integr Obes Diabetes. 2016;2(2):225-228.

分子代谢表型分析

- **特定神经元的激活或抑制的分子标记**
  - ✓ LiCl，LPS抑制摄食时LPBN神经元激活

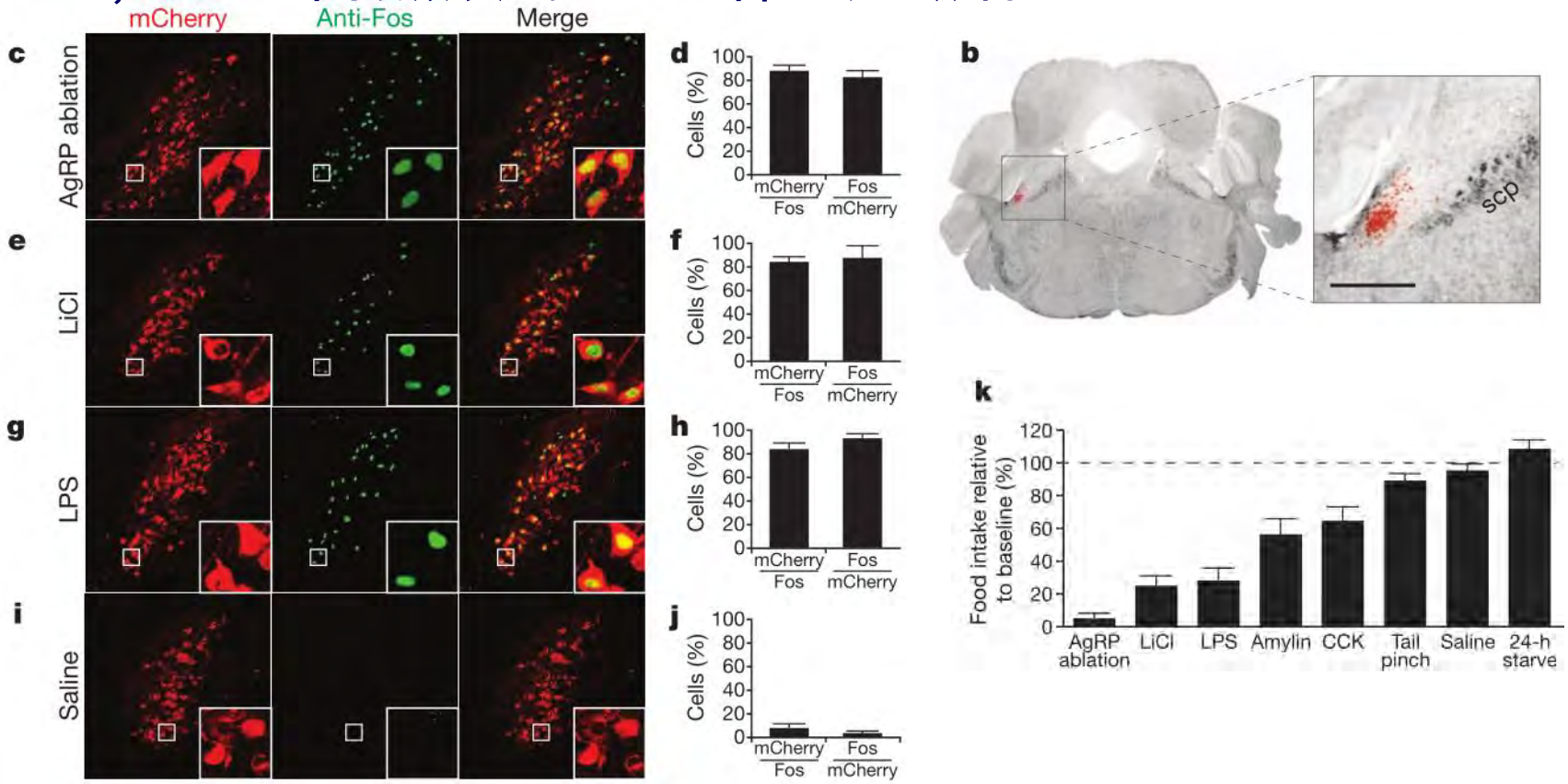

c–j,Representative histological examples and quantification of coincidence of mCherry and Fos expression. k, Degree to which various conditions reduce food. l, Appetite suppression correlates with the percentage of PBelo CGRP neurons expressing Fos.

Nature. 2013 Nov 7;503(7474):111-4.

目 录

代谢物分析

- 质谱分析 (LC/MS、GC/MS)
- NMR分析
- 生化检测
- 实时动态检测 (活体成像)

代谢物分析

➢ LC-MS简介

液相色谱-质谱联用（LC-MS）

液相色谱
Liquid Chromatography

质谱
Mass Spectrometry

分离系统

检测系统

基于LC/MS的代谢物分析

➢ 基于LC-MS的靶向与非靶向代谢物分析

✓ 靶向(Targeted)与非靶向(Untargeted)代谢组学

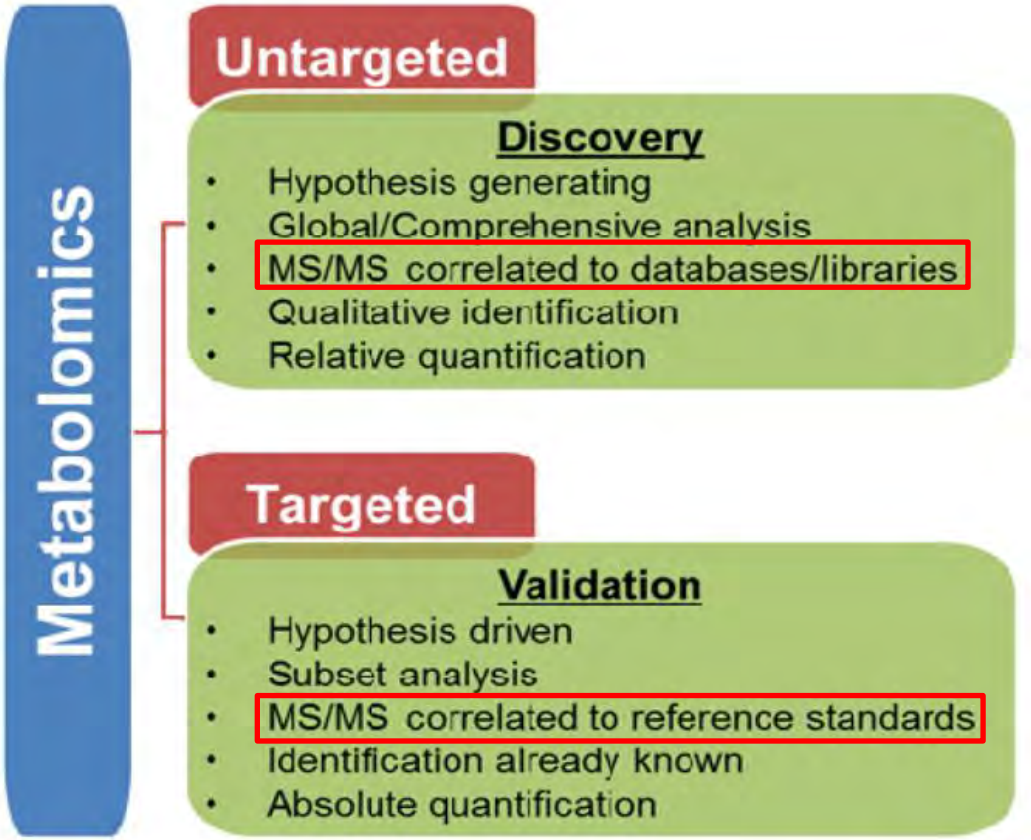

基于LC/MS的代谢物分析

- **基于LC-MS的靶向与非靶向代谢物分析**
  - ✓ 靶向代谢物分析实例

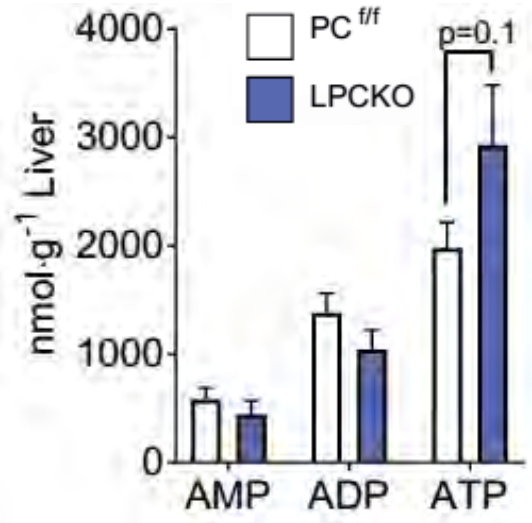

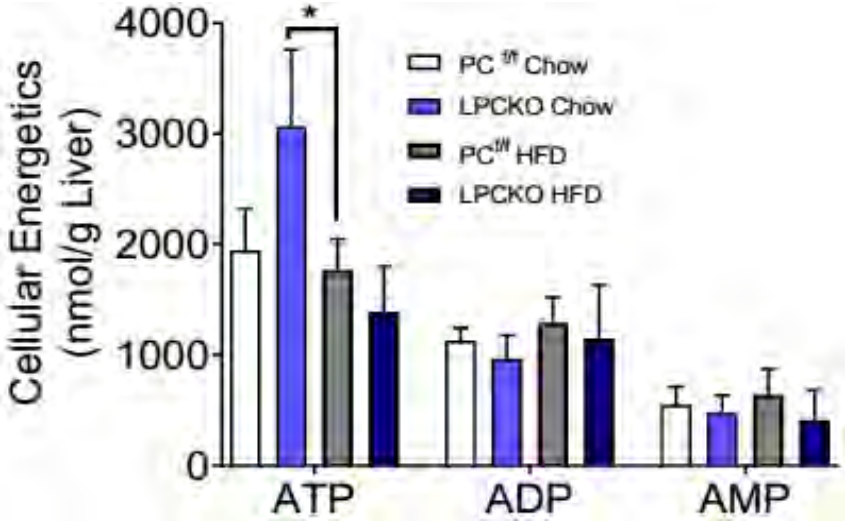

Cell Metabolism 29, 1291–1305, June 4, 2019

基于LC/MS的代谢物分析

- **基于LC-MS的靶向与非靶向代谢物分析**
  - ✓ 靶向代谢物分析实例

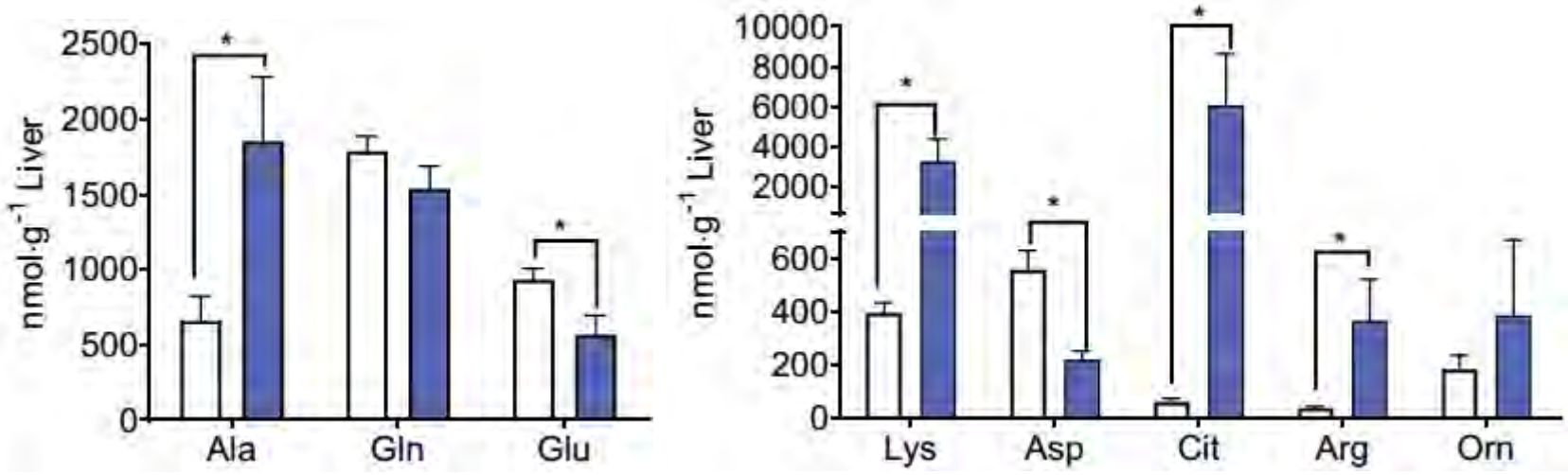

Measurement of Amino Acids in Liver： Amino acids were detected using the MRM mode by monitoring specific transitions under positive electro spray on API 3200 triple quadrupole LC/MS/MS. Quantification was done by comparison of individual ion peak areas to that of an internal standard.

Cell Metabolism *29*, 1291–1305, June 4, 2019

基于LC/MS的代谢物分析

➢ 基于LC-MS的靶向与非靶向代谢物分析

✓ 非靶向代谢物分析基本步骤

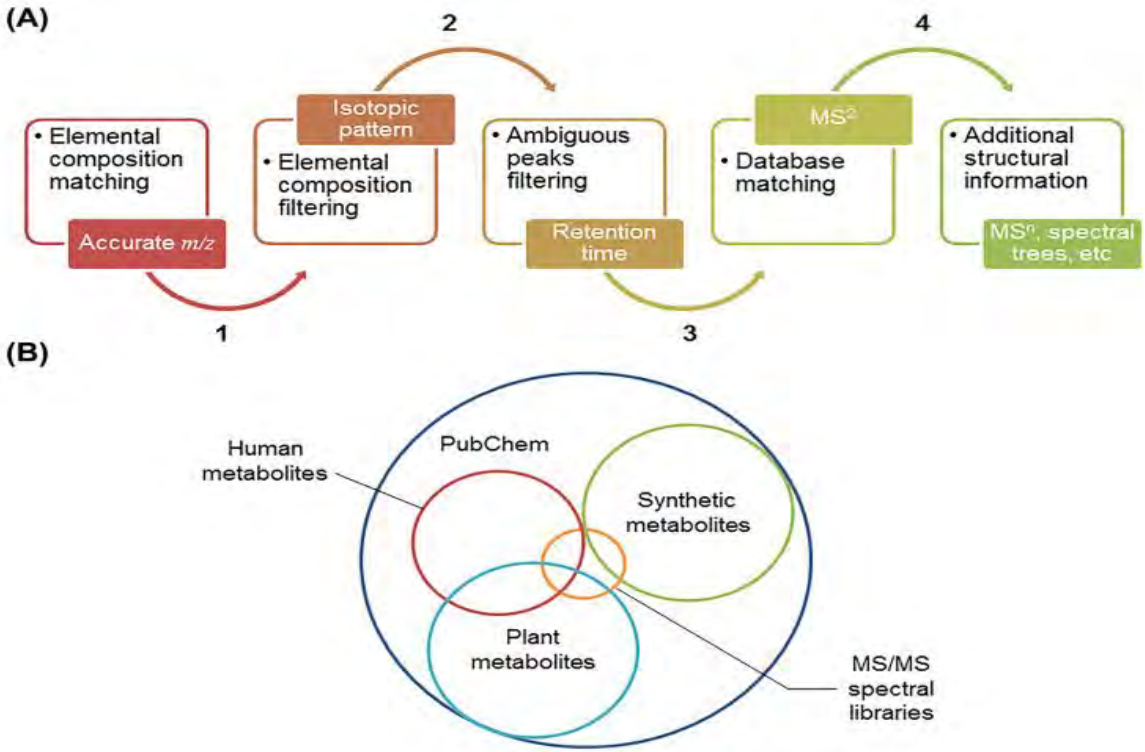

A, A typical workflow for increasing confidence in metabolite identification can be broken into 4 steps. B.Current MS/MS spectral libraries based on authenticated metabolites are small compared to the complete chemical space (PubChem)

Mass Spec Rev. 2018;1–21.

基于LC/MS的代谢物分析

- **基于LC-MS的靶向与非靶向代谢物分析**
  - ✓ 非靶向代谢物分析示例

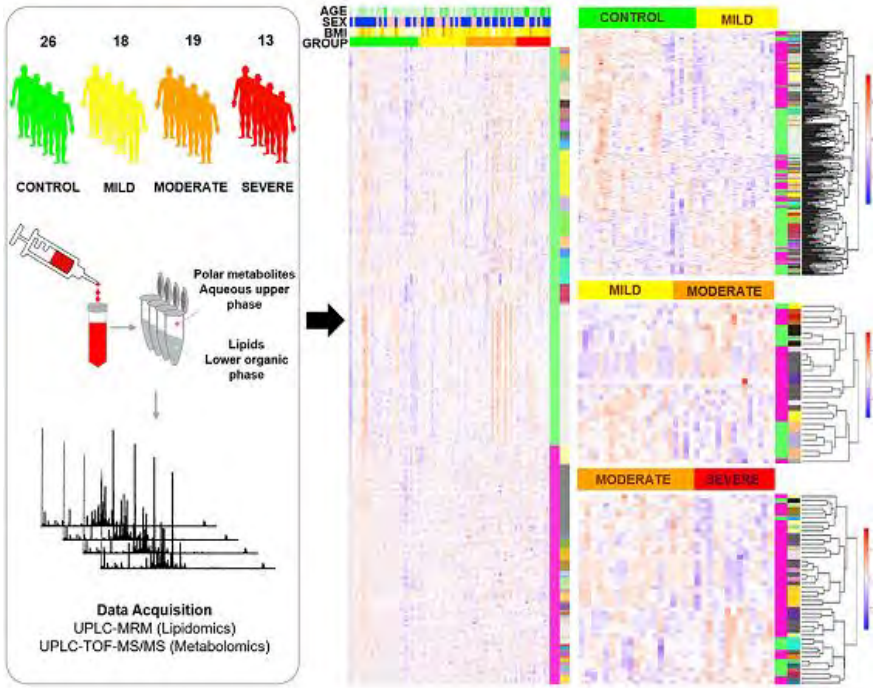

1002 identified metabolites
598 lipids & 404 polar metabolites

Omics-Driven Systems Interrogation of Metabolic Dysregulation in COVID-19 Pathogenesis

Cell Metabolism 32, 188–202.e1–e5, August 4, 2020

代谢流分析

➢ 稳定同位素代谢流分析

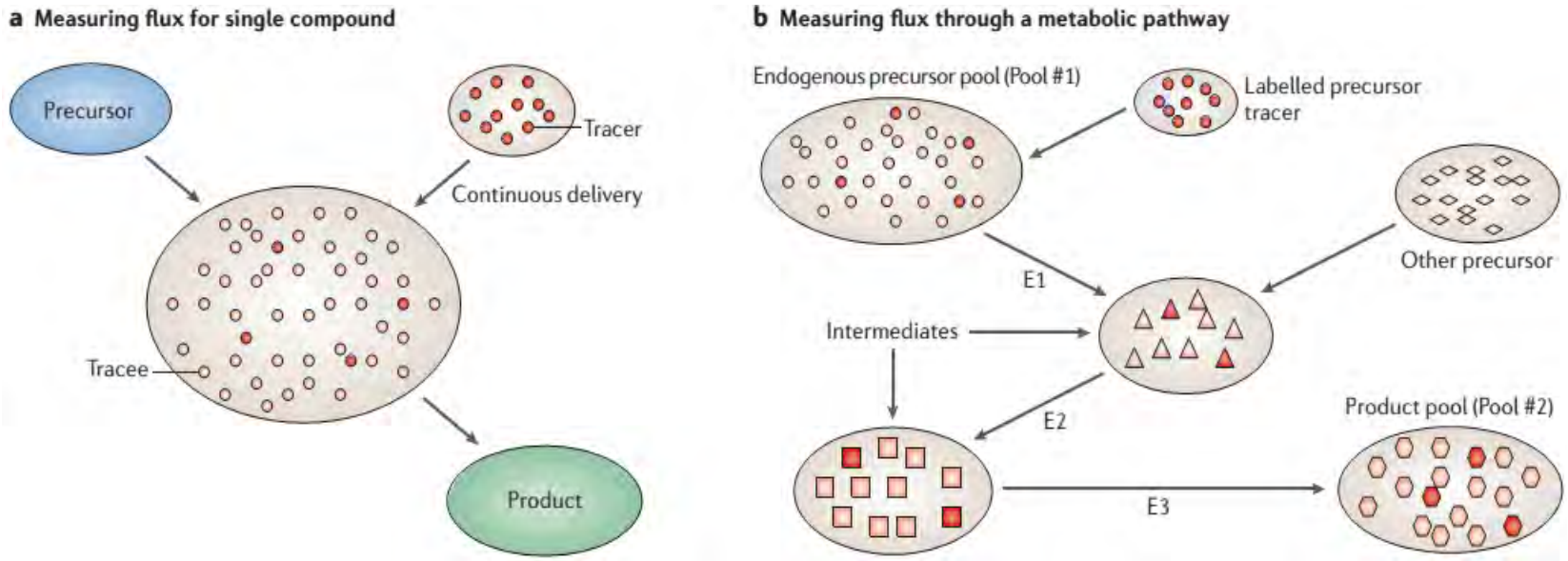

Measurement of metabolite flux using isotope tracers. A) Flux is measured as the (rate of infusion)/(isotopic enrichment of tracee). B) Labelled substrate is introduced into a precursor pool (Pool #1) in vivo. The substrate is then processed via a series of enzymatic steps (E1, E2, E3) and combined with other precursors until the final product is produced, the product pool (Pool #2). By measuring the percent enrichment of both Pool #1 and Pool #2 with the isotopic label, the fractional transfer of label from substrate (tracer) to product can be assessed. Fractional transfer from precursor to product is measured as the (isotopic enrichment of product)/(isotopic enrichment of precursor).

代谢流分析

➢ 稳定同位素代谢流分析示例

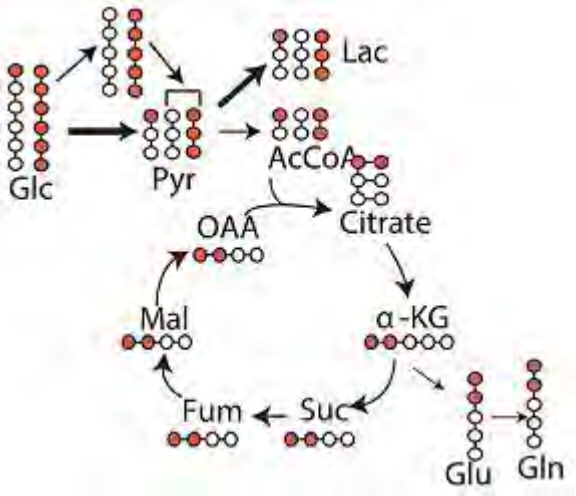

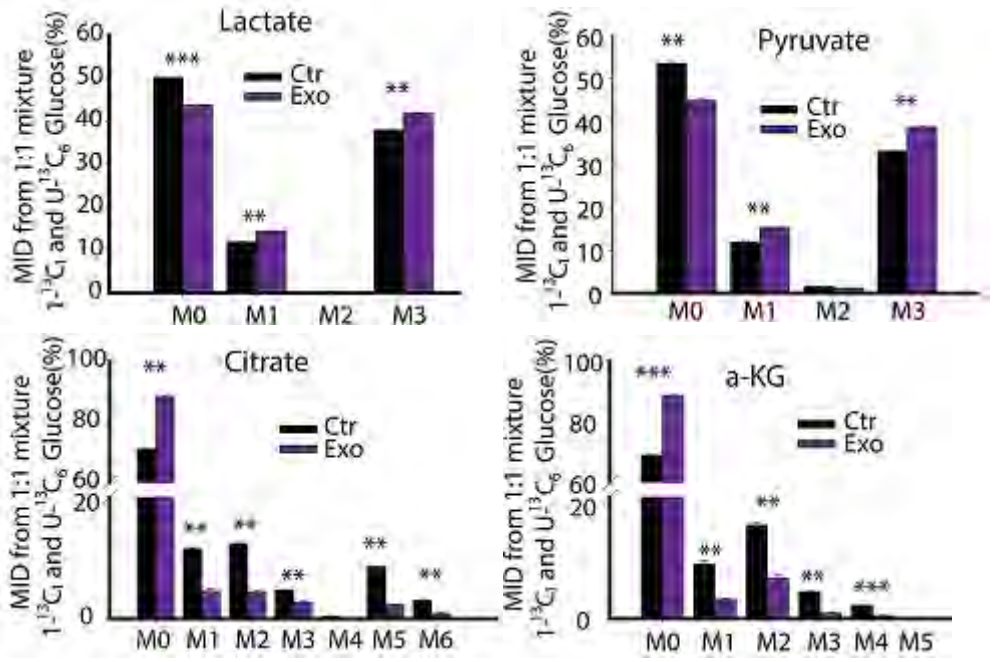

Schematic of carbon atom transitions using 1:1 mixture of $13C_6$ glucose and 1-13 C_1-labeled glucosewhere M0 refers to the isotopologue with all 12C atoms and M1 and higher refer to heavier isotopologues with one or more 13C atoms derived from the tracer.

Zhao *et al.* eLife 2016;5:e10250.

代谢流分析

➢ 稳定同位素代谢流分析示例

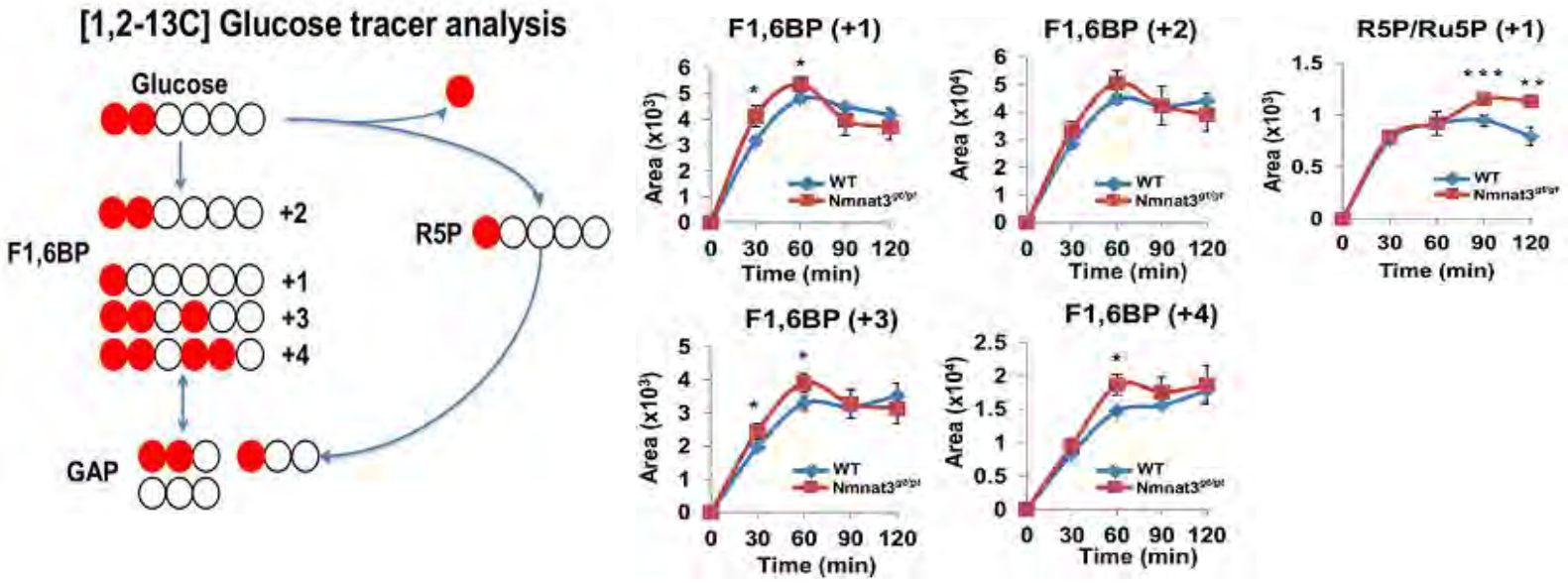

Scheme of the carbon flow by [1,2-13C]glucose tracer analysis.
White and red circles are 12C and 13C.

THE JOURNAL OF BIOLOGICAL CHEMISTRY VOL. 289, NO. 21, pp. 14796–14811, May 23, 2014

基于NMR的代谢物分析

➢ NMR谱图所包含的信息

✓ 构成有机体的1H、12C以及稳定同位素2H、13C的原子核自旋量子数不为零，在外磁场作用下这些原子核会像陀螺一样进动。此时在磁场垂直方向加一个射频电场，射频电场频率与这些原子核进动频率相同时，可出现核磁共振吸收现象，核自旋方向改变，产生向高能级的跃迁。当核再回到低能级的时候，就会放出一定的能量，使得核磁共振谱上出现峰值。对NMR谱图的解析可得到相应原子的信息。

Information:

Larmor 频率	原子核
化学位移:	结构测定(功能团)
J-偶合:	结构测定(原子的相关性)
偶极偶合:	结构测定 (空间位置关系)
弛豫:	动力学

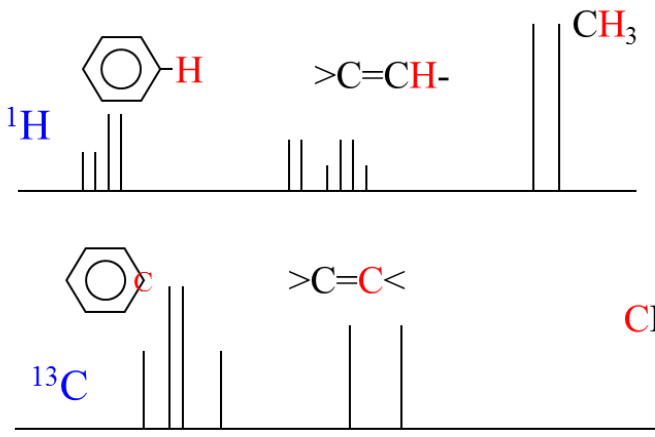

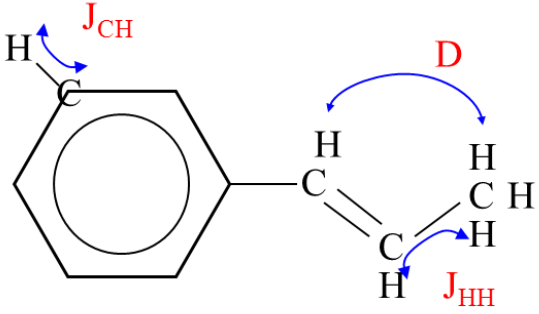

基于NMR的代谢物分析

➢ NMR分析示例

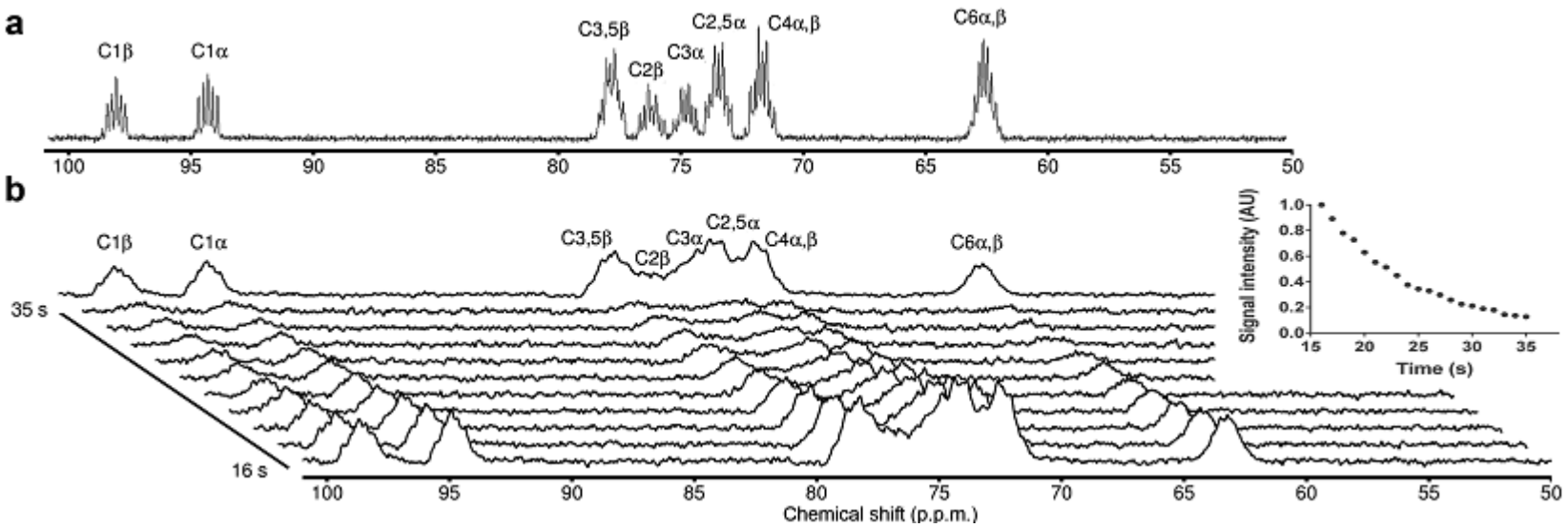

[U-2H, U-13C] glucose signals are detectable in vivo.
(a)13C NMR spectrum of [U-2H, U-13C]glucose in vitro (b)Representative 13C tumor spectra acquired between 16 s and 36 s after the intravenous injection of 0.35 mL 100 mM hyperpolarized [U-2H, U-13C]glucose.

Nat Med. 2014 January ; 20(1): . doi:10.1038/nm.3416.

基于NMR的代谢物分析

➢ NMR分析示例

Dev Cell. 2020 Apr 20;53(2):240-252.e7.

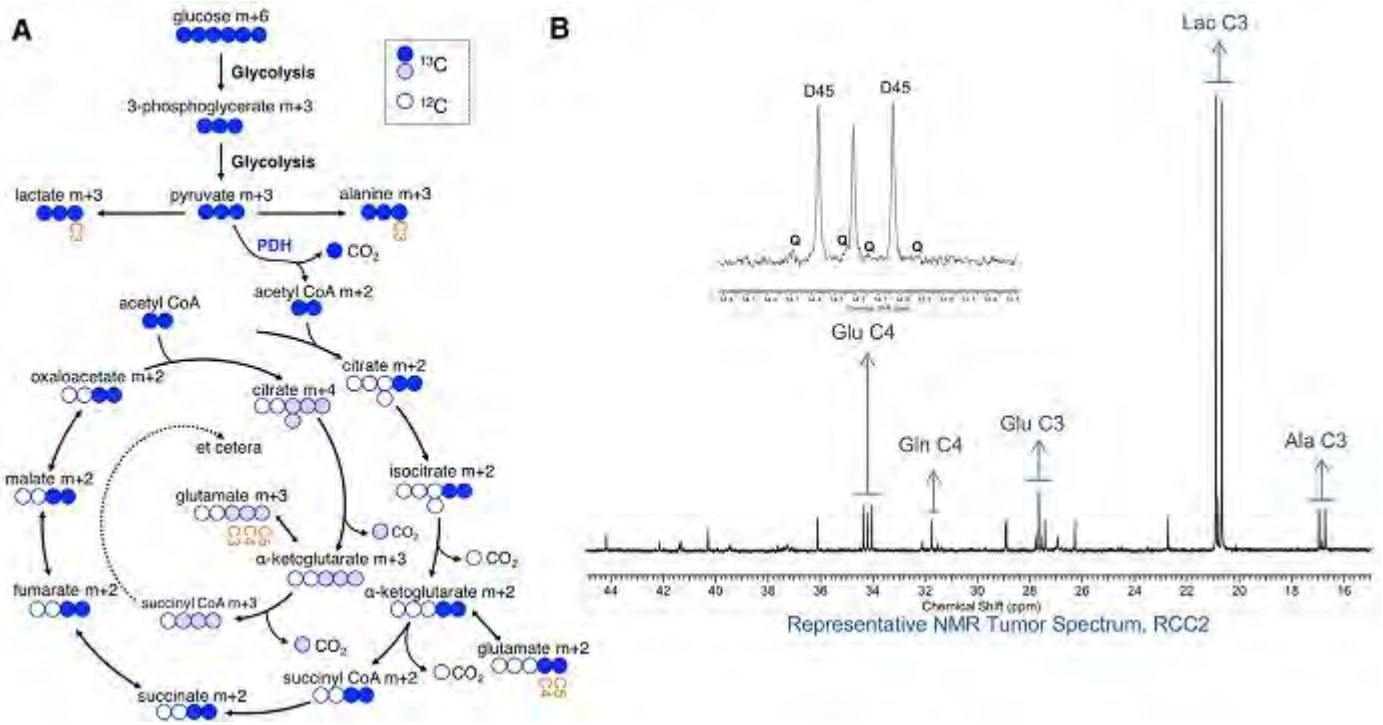

In Vivo Labeling from ccRCC Tumors and Adjacent Kidney Infused with [U-13C]Glucose
(A) Schematic for metabolism of [U-13C]glucose. ‘‘Labeled’’13C carbons are colored circles and ‘‘unlabeled’’12C carbons are white circles… . (B) Representative 1H-decoupled 13C NMR tumor spectrum from patient RCC2. The inset is a magnification of the peaks from glutamate (Glu) at carbon 4 (C4).

Courtney et al., 2018, Cell Metabolism *28*, 1–8

代谢物实时动态检测

➢ 钙离子实时动态检测

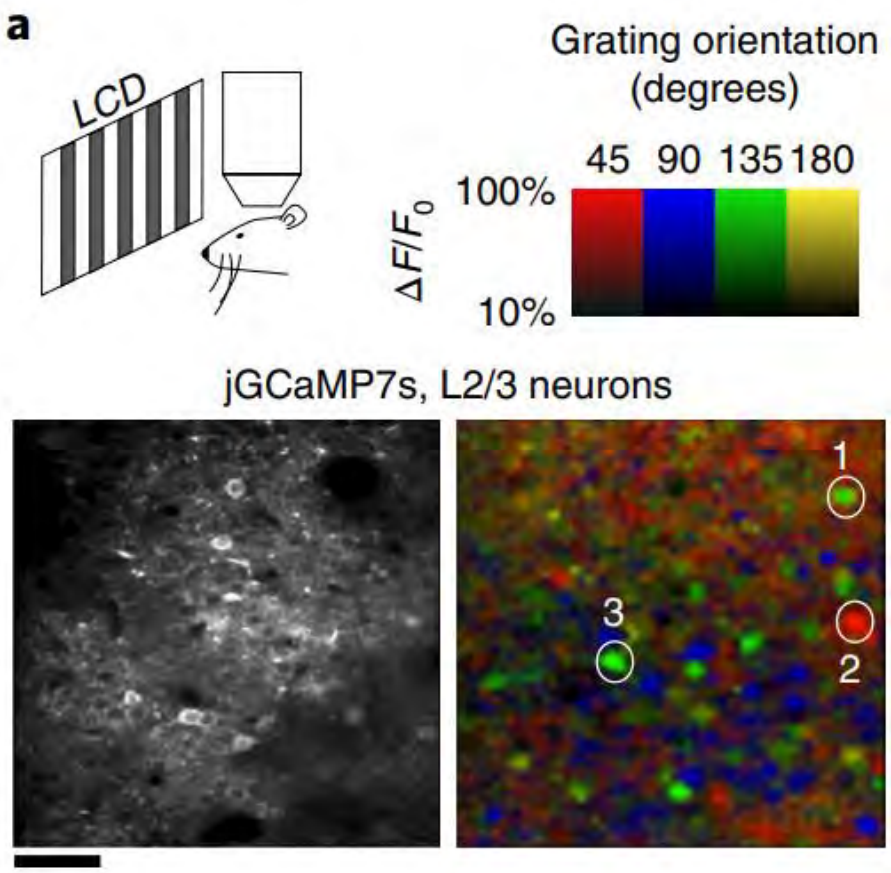

Nat Methods. 2019 Jul;16(7):649-657.

代谢物实时动态检测

- 代谢小分子实时动态检测 (FiNad检测NAD^+)

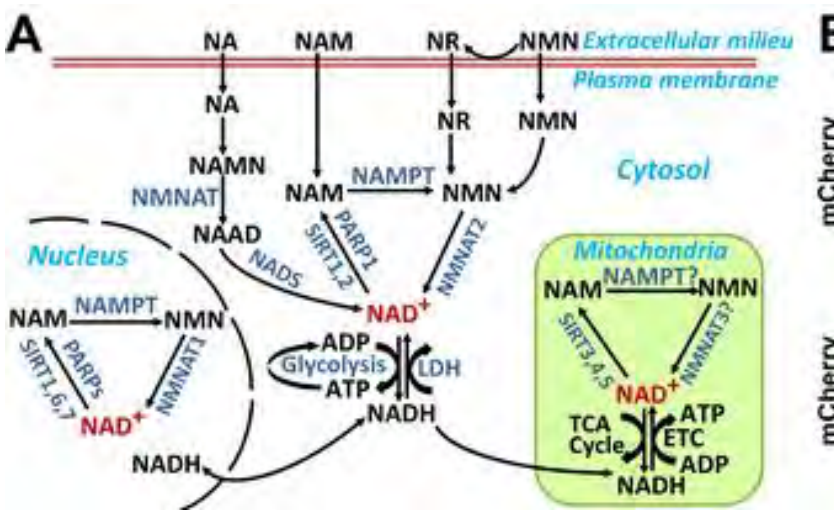

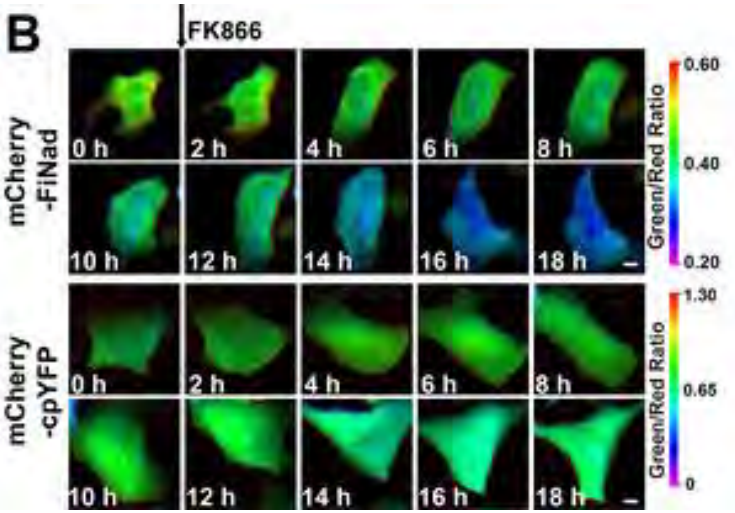

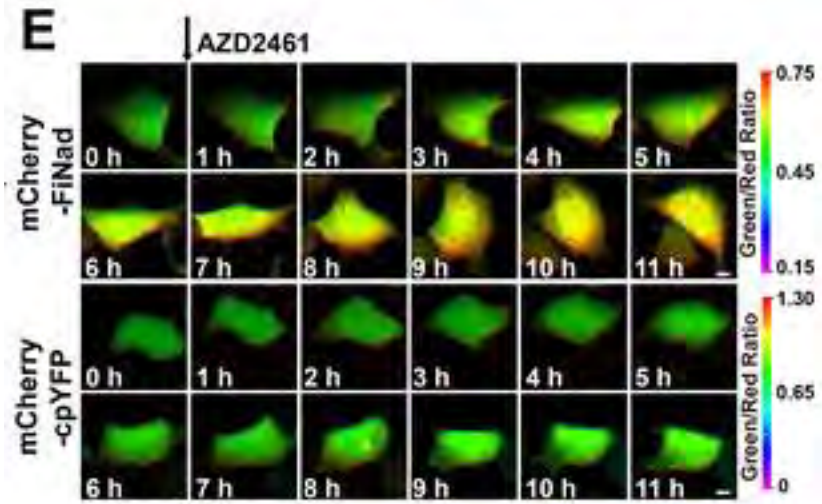

- ✓ ATP、Lactate等越来越多的代谢小分子荧光探针被开发和应用。

Dev Cell. 2020 Apr 20;53(2):240-252.e7.